THE MICROWAVE DIGESTION OF SOLIDS

Prepared by: Mr. G.A. Broomhall,
Masters student in the Department of Electrical Engineering at the University of Cape Town.

Prepared for: Professor B.J. Downing, Professor of Applied electronics in the Department Electrical Engineering at the University of Cape Town.

31 January 1990

This thesis dissertation was prepared in partial fulfillment of the requirements for the degree of MSc. in Electrical Engineering.

TERMS OF REFERENCE

This dissertation, on the microwave digestion of solids, was proposed by Professor B.J. Downing, Professor of Applied Electronics, Department of Electrical Engineering, University of Cape Town, on the 1st of August 1988.

Professor Downings specific instructions were:

1) Evaluate the requirements of a microwave digestion system and determine the factors affecting it's operation.

2) Obtain a suitable microwave cavity for use in this digestion system.

3) To gain control of the digestion heating process using an accurate computer control system.

SYNOPSIS

Microwave ovens have been available for domestic cooking since 1956. This method of heating is very efficient compared to conventional cooking methods. As a result many applications have arisen particularly in the field of analytical chemistry. Most routine analysis of biological and chemical samples by atomic absorption spectroscopy (AAS) and inductively coupled plasma atomic emission spectroscopy (ICP-AES) involves the time consuming operation of digesting the samples in acid on a hot plate. However, much time saving has been demonstrated by the use of microwave digestion, and successful digestions have been achieved in 10% of the time required for traditional methods. The first digestions using microwave heating were performed in open vessels. However many problems were identified. The development of closed teflon vessels increased the rate of reaction and efficiency of the digestion process as elevated temperatures above boiling point could be reached under an increase in pressure. This also maintained the integrity of the samples. Presently research is being conducted by two foreign companies to establish the parameters affecting the digestion process.

Mr. M.A.B. Pougnat of the Analytical Chemistry Department, U.C.T., who is currently doing a PhD on microwave digestion techniques, approached the Electrical Engineering Department with the need of a microwave digestion system for these research purposes. This dissertation was subsequently proposed by Professor B.J. Downing on the microwave digestion of solids.

This set the initial objectives of the dissertation:

1) To design and construct a microwave digestion system which can process a variety of sizes and types of chemical samples.
2) To achieve an optimum heating process where a maximum amount of microwave energy is transferred to the all the types of samples applied to the system.
3) To distribute an equal amount of power to each of the samples applied to the digestion system.
4) To control the digestion heating process using a computer control system where the heating process parameters may be specified for each sample digestion.

The conventional microwave oven was studied and tested to evaluate its operation as a digestion system. The microwave oven is an overmoded cavity whereby several modes are excited in the loaded cavity, and as the material properties change during the heating process, different electromagnetic modes take over the heating process. The microwave oven is adaptable to many types of loads but as a result has a reduced energy transfer efficiency. Testing performed using a network analyser showed no symmetry in the microwave field structure. This was verified by a change in the return loss recorded with each load position in the oven cavity. Conventional microwave ovens rotate the load inside the cavity or use mode stirrers to average the power delivered to the loads. This results in a none ideal heating process. The systems heating characteristics will be different for each load processed making it none ideal for process control.

Cylindrical resonant cavities were studied to satisfy the requirements of having a symmetrical field structure, delivering an equal power to all the loads.

Microwaves were launched in the center of the cylindrical cavity using an E-field probe which sets up a TE_{01} mode field pattern. This has a constant E-field in the azimuthal direction and the field is symmetrical about its center. The sample loads are then placed symmetrically about the center of the cavity an equal distance from the center, thus distributing equal power to all the samples. The cylindrical cavity was tested on the network analyser to determine its performance. The cavity displayed a good field symmetry when tested. The match was however very narrow band as the sample volume to cavity volume ratio was low for the small digestion samples used. As a result the cavity was very sensitive to a change in load and a match could not be achieved for all sample loads. However increasing the load of the cylindrical cavity by using a fixed water tank load produced a good energy transfer efficiency for all the applied sample loads. The cylindrical cavity was suited to the digestion of large sample loads.

A resonant horn cavity was designed and tested for a better coupling mechanism between the sample loads and the microwave field. Microwaves were launched into a rectangular waveguide which was flared as a horn antenna waveguide to accommodate the sample loads. The aperture of the horn was short circuited such that the field propagating in the horn is in phase over the area of the short circuit plate. Microwave energy is then reflected back to the source forming a resonant cavity. The sample loads were positioned equal distances from the launcher for an equal distribution of power to all the loads. Due to a change in the coupling mechanism of the microwave field with the sample loads, compared to that of the cylindrical waveguide, a stable match was achieved for all the sample loads tested. The cylindrical cavity has a high energy transfer efficiency for all the sample loads tested. When testing for wave symmetry, a good correlation was found in the matches achieved for a

sample load placed in different positions an equal distance from the center of the launcher. This was verified by performing heating tests which produced linear heating of all the sample loads. The resonant horn cavity satisfied the requirements for use in a microwave digestion system.

A need was identified from industry in South Africa for the other uses of the digestion process. These applications require further testing to determine their feasibility. An experimental microwave digestion system was designed to test these processes. Here, a single load applicator cavity was required to be adaptable for the different types of digestion tests to be performed using different material loads. In a theoretical analysis, the major factors determining the match of the loaded cavity were found to be:

1) The variety of material loads used.
2) The range of sizes of loads used.
3) The loads position in the cavity and its size and shape relative to the size and shape of the cavity.
4) The load temperature.
5) The excitation frequency.

Microwaves were launched into a rectangular waveguide setting up TE_{01} mode. This feeds the microwaves to a cylindrical waveguide, through a quarter wave transformer, setting up TE_{11} mode. Using a cross directional coupler, a measure of the reflected power can be obtained. In order to obtain a match for every loaded cavity, tuning screws were used to optimize the power transfer to the loaded cavity at resonance. Thus achieving a match for each load. After testing on a network analyser, the cross directional coupler was found unsuitable for a variably loaded transmission line. The cylindrical cavity was found to have a high

energy transfer efficiency for small loads applied to the cylindrical cavity, this was a very narrow band match. With larger loads, an extremely wideband match was achieved, thus having a high energy transfer efficiency over the complete digestion process.

A computer control system was built using an a versatile IBM compatible personal computer. A PC-26 analogue to digital converter board was used to read the thermocouple temperature measurement of the load. An AD594 IC was used to linearise the thermocouples response and to perform cold junction compensation. A turbo pascal control program was written to control the system by cycling power to the microwave magnetron through an 8255 parallel peripheral interface board. The control system was set up with the magnetron power circuitry and microwave cavity, and was seen to operate correctly over the four stages of a heating cycle. Heating tests were done using a medium sized sample load. The heating of the load to a set point temperature was achieved with accurate maintaining of that set point. A high energy transfer efficiency was obtained. Tests performed on identical loads indicated the reproducibility of the digestion process.

TABLE OF CONTENTS

Tables:

INTRODUCTION

Most routine analysis of biological and chemical samples by atomic absorption spectroscopy and inductively coupled plasma atomic emission spectroscopy involves the time consuming operation of digesting the samples in acid on a hot plate. However, much time saving has been demonstrated by the use of microwave digestion. At present, independent research in this area is being performed by two foreign companies to determine the digestion process heating parameters. Mr. M.A.B. Pougnet of the Analytical Chemistry Department, who is currently doing a PhD dissertation on microwave digestion techniques, approached the Electronic Engineering Department with the need of a microwave digestion system for these research purposes.

The objectives of this dissertation were:
1) To design and construct a microwave digestion system which can process a variety of sizes and types of chemical samples.
2) To achieve an optimum heating process where a maximum amount of microwave energy is transferred to the all the types of samples applied to the digestion system.
3) To distribute an equal amount of power to each of the samples applied to the digestion system.
4) To computer control the digestion system where the heating process parameters may be specified for each sample digestion.

Later, a real need was identified from industry in South Africa for different uses of this digestion process. As most of these processes were untested, the feasibility of each processes was undetermined. As a result this dissertation was expanded to the design and construction of an experimental microwave digestion system which would be used to determine the feasibility of each of

these processes. This system must accommodate a wider variety of sizes and types of samples, with the aid of a computer to control the digestion heating process.

The main limitations experienced in this dissertation work was a lack of funds required for process equipment.

This dissertation begins with an introduction to microwave heating, giving an account of the mechanism of microwave heating and the history of microwave digestion. The conventional microwave oven was then evaluated to determine if it satisfied the requirements for use in a microwave digestion system. Resonant cavity structures were then studied for use in an optimal digestion process. A cylindrical waveguide cavity and a resonant horn cavity were designed and tested to fulfil these requirements. Finally, an experimental microwave digestion system was built and a control system designed to set the parameters of the heating process.

CHAPTER 1

1) INTRODUCTION TO MICROWAVE HEATING

1.1) The Mechanism of Microwave Heating

1.1.1) Dielectric loss

Microwave energy is absorbed by a sample at a rate dependent on its dissipation factor. A samples dissipation factor is the ratio of its dielectric loss (ϵ'') to its dielectric constant (ϵ'); $\tan \delta = \epsilon''/\epsilon'$. Energy is absorbed and dissipated as microwaves pass into a sample, the greater the dissipation factor of a sample, the less the penetration depth of microwave energy [1]. The half-power depth is the depth at which the power density is reduced to half that at the surface.

Microwave energy is lost to a sample by two mechanisms: ionic conduction and dipole rotation.

1.1.2) Ionic Conduction

Current flows due to the conductive migration of dissolved ions in an applied electric field. This causes heat production due to I^2R losses because of resistance to ion flow. Parameters affecting ion conduction are ion concentration, ion mobility, and solution temperature. The dissipation factor will increase with increasing ion concentration and will change with temperature because temperature affects ion mobility and concentration.

1.1.3) Dipole Rotation

An electric field causes the alignment of molecules in the sample which have permanent or temporary dipole moments. As the field decreases, thermal agitation returns the molecules to disorder, in the relaxation time, τ , and energy is released. At a frequency of 2.45 GHz, the alignment of the molecules and their return to disorder occurs 4.9×10^9 times per second.

The dielectric relaxation time is the time it takes the molecules to achieve 63% of their return to disorder. The maximum energy conversion per cycle will occur at a frequency, $f = 1/\tau$, ie. a high dissipation factor. This frequency, f, for water is greater than 2.45Ghz, therefore as the input frequency is decreased energy absorption decreases and the half-power depth increases. As the water temperature is increased the dielectric relaxation time decreases resulting in a decrease in dissipation factor.

1.1.4) Relative contributions of dipole rotation and ionic conduction

For small molecules, such as water and other solvents, the dielectric loss of a sample due to the contribution of dipole rotation decreases as the temperature increases. However, dielectric loss due to ionic conduction increases as temperature increases. Therefore, in a microwave heating process, the dielectric loss to a sample is initially dominated by dipole rotation. As temperature increases, the dielectric loss is dominated by ionic conduction. The percent contribution of these two mechanisms of heating depends on the mobility and concentration of sample ions and the relaxation time of the sample.

1.2) The History of Microwave Heating

Microwave ovens for heating food have been produced since 1945. They have been available for domestic cooking since about 1956 [2]. Microwave cooking is very efficient with more than 50% of the mains power being converted to heat absorbed in the food compared to about 6% for conventional cooking.

The most common application of microwave ovens in the chemical laboratory is for sample drying. They have been used in the chemical industry for the last 30 years. One of the first applications was reported by Hesek and Wilson in 1974 [3]. Using a 550 watt oven to dry a variety of salts it was realized that great time saving could be achieved compared with traditional methods. There have also been many reported investigations on the uses of microwaves for drying of plants, coal, sludges and clays. A commercial moisture analyser (CEM Corporation) has been available for many years which automatically monitors sample drying and determines the moisture content.

In a recent study [4] minerals and chemical compounds were tested to determine their heating characteristics. It was observed that certain good microwave absorbers reached extremely high temperatures in a short time, for example magnetite (Fe_3O_4) reached 1258°C in 2.75 minutes using a 1Kw microwave oven. These selective heating characteristics have several uses in extractive metallurgical applications [4,5], melting of inorganic minerals and preparation of mixed oxides. Walkiewicz et al [5] observed the formation of microcracks in minerals subjected to microwaves which could play an important role in the efficiency of microwave acid dissolution of many minerals.

Certain ferrite materials experience a change in microwave absorption when they reach a certain temperature, the Curie point. When exposed to microwaves the material absorbs the radiation strongly and rises to the rated temperature, it then stops absorbing until it drops below the rated temperature. These materials can be used for heating objects by conduction. Beary [6] has described the use of these devices (thermopads) for drying laboratory samples. Two such available accessories are the "ashing block" and the "muffle furnace".

Atomic absorption spectroscopy (AAS) and inductively coupled plasma atomic emission spectroscopy (ICP-AES) are widely used for the determination of a large range of elements in biological and environmental samples. Both of these techniques require that the samples be in solution. This involves time consuming sample digestion procedures traditionally done using hot plate and other thermal conduction techniques [7]. Improvements in the digestion procedure using microwave ovens has been demonstrated over the last 13 years.

1.2.1) Open vessel Digestion

The first report on the use of a microwave oven for sample digestion was by Abu-Samra et al in 1975 [8]. Here a 600 watt microwave oven was used with modifications for the extraction of acid fumes. Successful digestions were achieved in 10% of the time required for traditional methods.

Many problems were identified . The acid mixture to sample ratios were critical to avoid "flashes" in the erlenmeyer flasks. The cavity required suitable protection from the highly corrosive acid fumes. The magnetron needed protection from reflected microwave power.

1.2.2) Closed Vessel Techniques

New developments in sample digestion techniques were brought about in 1983 in a report from the Chamber of Mines, USA, by Matthes et al [9]. Here, instead of using open vessels, digestions were carried out in sealed plastic containers transparent to microwaves. Teflon PFA has been found to be the most superior material for closed vessel containers used in obtaining elevated temperatures and pressures.

There are many advantages in using closed vessels rather than open vessels:

1) The rate of reaction and efficiency of acid decomposition increases greatly with temperature [10]. Reactions carried out at elevated pressures are not limited by the normal boiling point of the acids and thus require considerably less time to reach completion. This time is shortened due to a more rapid temperature rise compared with traditional heating by conduction.
2) As the reactions are more efficient, smaller acid to sample ratios can be used leading to lower reagent blanks.
3) Closed vessels maintain the integrity of the samples thus contamination from the environment or cross contamination between samples is avoided.
4) The determination of volatile elements is feasible and practical.
5) Using feedback control of temperature and pressure it is possible to automate the process.

Several parameters affect the digestion process such as the choice of acid, ratio of acid to sample, power levels and time of microwave irradiation. Due to the widely different digestion approaches used there is no consistency in the literature concerning the methods for a certain digestion procedure. In open vessel digestion the temperature is limited to the boiling point of the

acid and can be related to digestion on a hot plate. In closed vessel digestion the situation is different. Developments along these lines was brought about by Kingston and Jassie from the National Bureau of Standards in 1986 [9]. In collaboration with CEM corporation they developed a system to measure the temperature and pressure of a variety of samples and acids being digested in closed Teflon vessels. This has led to the calculation of the power absorbed by the samples. This can be derived from fundamental thermodynamic laws:

$$W = K\ c\ (T_1 - T_2)\ m/t \qquad \ldots.(1.1)$$

where: W = apparent power absorbed by the sample (watts)

K = conversion factor (calories to watts)

= 4.184

c = heat capacity (cal g^{-1} deg^{-1})

T_1, T_2 = initial and final temperature (deg C)

m = mass (grams)

t = time (seconds)

Errors in using this equation are:

1) Changes in heat capacity with temperature.
2) Heat loss will decrease the apparent power.
3) Changes in the dielectric constant cause a decrease in absorption with increase in temperature.

Using equation (1.1) to predict the time required to reach a set temperature it was found to work well for large acid samples. As this equation does not take into account the loss of heat it can only be used to estimate the initial temperature rise and is not applicable to maintaining the sample temperature.

1.2.3) Commercially available microwave digestion systems

Two microwave systems are currently available:
1) CEM MDS 81D microwave oven: This is equipped with a 600 watt magnetron which is protected from reflected power by a circulator. It has a teflon lined cavity, extraction facilities to remove corrosive fumes, accurate microprocessor controls of power levels and time of irradiation and a carousel that can accommodate twelve vessels. Temperature measurement is made using a shielded thermocouple inserted into the cavity through a rigid waveguide attenuator. Pressure measurement is done using a pressure transducer also inserted through a waveguide attenuator.
2) Microdigest A 300: This system, which was developed by a French company Prolabo [10], consists of a rectangular waveguide applicator. A port allows the vessels to be lowered inside the waveguide. A microprocessor is used to control power levels and irradiation times for the automatic treatment of 16 different sample digestions.

1.2.4) Digestion process measurements and requirements

Process parameters to be measured during closed vessel digestion are temperature and pressure. Absorbed power can be calculated using equation (1).

Requirements in the operation of a digestion system are:
1) Adequate power from the magnetron which must be protected from reflected power. Good power absorption must be achieved for all sample loads.
2) Microprocessor control of temperature and pressure by using time cycling and power variation.
3) A uniform microwave field for equal heating of all samples.

4) The cavity must be resistant to very corrosive acid fumes.
5) The cavity must accommodate many vessels of different sizes and shapes. It must have exhaust ports for the removal of acid fumes and have ease of placing and removing vessels.
6) Safe.

CHAPTER 2

2) EVALUATION OF THE CONVENTIONAL MICROWAVE OVEN

The conventional microwave oven was studied and tested to evaluate its operation, heating characteristics and microwave field structure with respect to use in microwave digestion.

2.1) Single mode and multimode microwave cavity applicators

Figure 2.1 shows the typical microwave processing system and its equivalent circuit. This basically consists of: a) the microwave energy source, usually a high power magnetron, b) transmission lines, usually waveguide or coaxial cable, c) the cavity and d) the material load. Maximum power transfer occurs when the output admittance of the microwave source, Y_g, and the input admittance of the material loaded cavity, Y_{in}, equals the transmission characteristic admittance, Y_o.

2.1.1) The multimode or overmoded cavity

Most heating processes use either nonresonant cavity applicators, in the form of single or multipass slotted waveguides, or multimode resonant cavities. The most common type used is the multimode cavity or "microwave oven". The multimode cavity is popular because of its low cost, simple construction and adaptability to all loads. The efficiency of power absorption is dependent on the materials complex dielectric constant and temperature, and the systems excitation frequency and field strength. These factors change with time during

the process. The shape and size of the cavity and the load also effects the coupling of microwave power. However multimode cavities reduce these factors to the geometry of the cavity and load. During the heating process several modes may be excited in the loaded cavity. However the material properties change and other modes will take over the heating process. This makes the multimode cavity very adaptable for many types of loads but the efficiency of power transferred to the load is low. It is also an open loop system making it none ideal for process control.

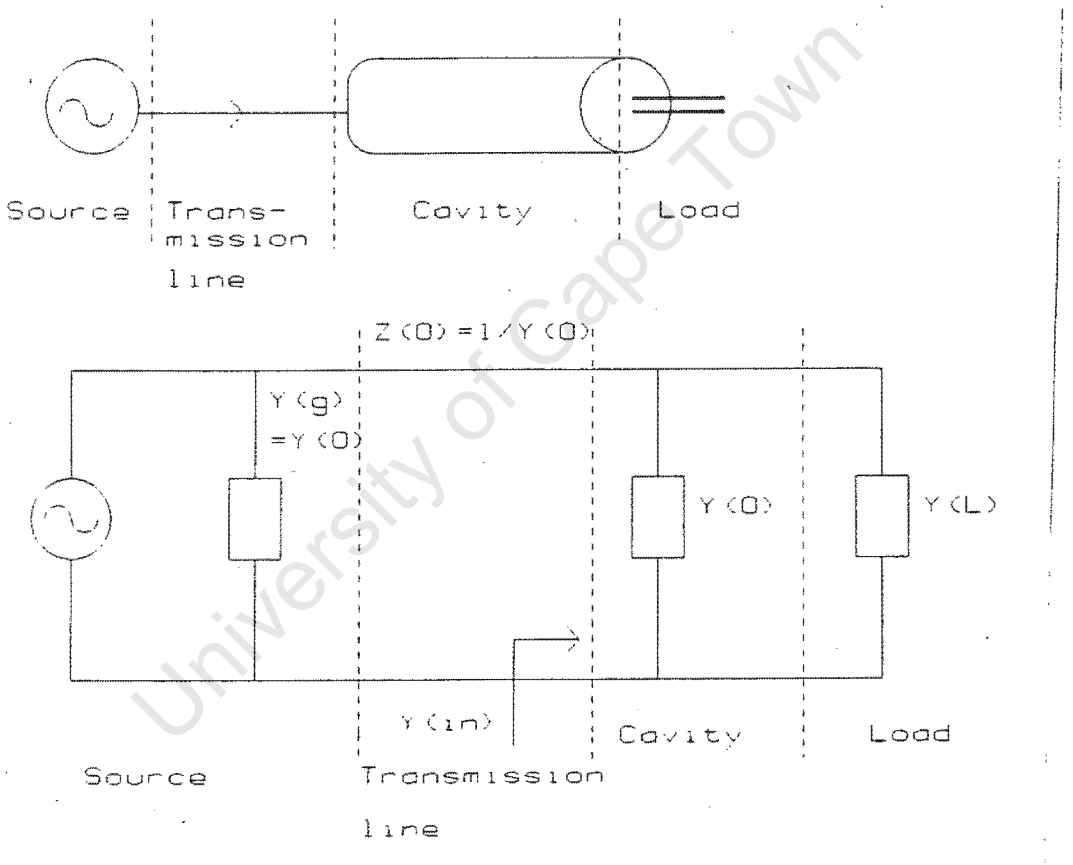

Figure 2.1: The microwave processing system

2.1.2) The single mode cavity

The single mode cavity can be tuned mechanically to select a number of different modes when it is unloaded.

When loaded, these modes are modified by the dielectric medium and become hybrid modes. New modes may be excited depending on the materials dielectric constant and its position in the cavity. Power coupled to the cavity, P_t, is absorbed by the load, P_l, and the cavity walls, P_c, in proportions dependent on the relative losses of the material versus the cavity losses; $P_t = P_l + P_c$.

The single mode cavity focuses the energy into the load depending on the cavities match for one excitation frequency. The complex input impedance of the cavity is given by: $Z_{in} = R_{in} + jX_{in}$. Thus two tuning adjustments are needed to match the cavity load to the transmission line. They must cancel the load reactance and adjust the load resistance to equal the transmission line characteristic impedance. This can be done by tuning the dimensions of the cavity and varying the length of the launching probe. Tuning screws can also be used.

Figure 2.2 shows the equivalent circuit of a loaded single mode cavity. G_c, L_c and C_c represent the conductance, inductance and capacitance at the excited frequency and jX represents the reactive effect of the evanescent modes far from resonance. At resonance the capacitive and conductive susceptance cancel giving a purely conductive impedance. When the cavity is loaded, resonance is shifted down in frequency and the Q-factor is reduced as the load increases the damping. The additional conductance, G_l, and susceptance, jB_l, added to the circuit by the load are functions of the loads position, volume, shape and composition. These factors determine the resonance shift and the resultant match.

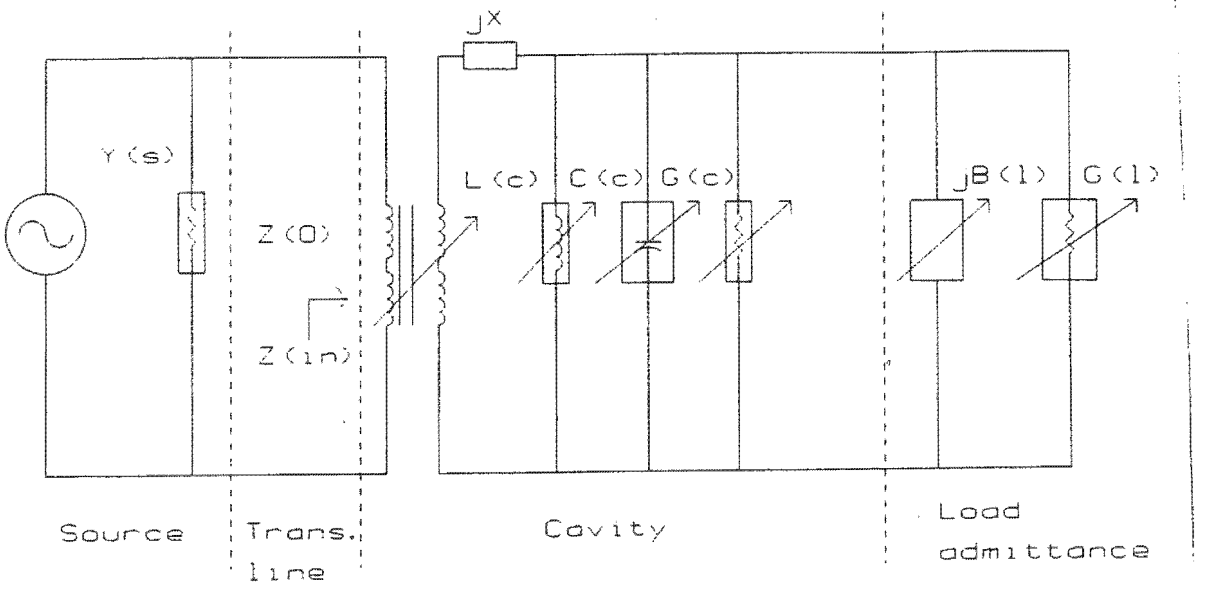

Figure 2.2: Single mode cavity equivalent circuit

Single mode cavities have a high energy transfer efficiency and show good potential for process control [12]. Experiments are repeatable, thus the heating cycles and tuning can be experimentally determined to process loads optimally.

2.2) The commercial microwave oven

2.2.1) Microwave oven power output

Gerling [13] reported the testing of various microwave oven models to form an accurate procedure to measure the power output. Using caliometric computations, equation 1.1, the power output to four different sized loads was calculated and compared to the measured mains power. Average power was calculated for two different types of loads. Comparing the two heating curves over time showed very little variation in the heating process. The measured power output of seven ovens was lower than that rated by an average of 20 %, with an average efficiency compared to mains power of 38%. The power output of all the microwave ovens increased with increase in load. There was, however, a slight drop in power with loads above 500 grams.

2.2.2) Microwave oven construction

Commercial microwave ovens all launch microwave energy into a waveguide which feeds into the cavity. The waveguide is designed so as not to cause a mismatch. As shown in figure 2.3, microwaves are fed into the cavity either from the side or from above. Due to the cavities field being nonuniform and multimoded, the load is either rotated on a carousel or a mode stirrer is used to average the power to the load. The mode stirrer is a fan shaped blade that redistributes the electromagnetic energy around the cavity so that the heating of the load is less dependent of position.

a) Mode stirrer

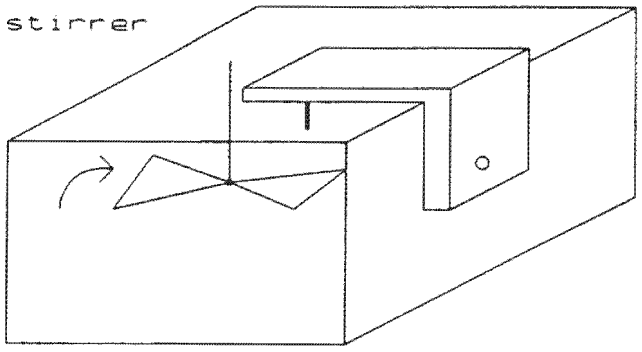

b) Carousel

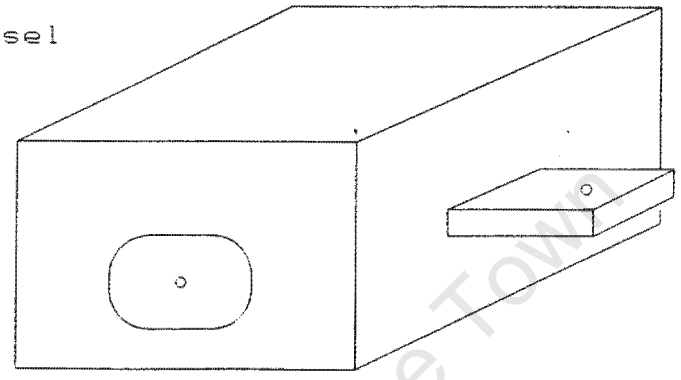

Figure 2.3: The commercial microwave oven construction

2.2.3) Microwave oven components

A commercial microwave oven was bought for testing of its cavities field structure. The microwave ovens microwave parts and power supply were also used in later high power tests. The internal circuitry is shown in figure 2.4.

The oven comprised of the following parts:

a) Three door switches are a necessary safety requirement.
b) Heat switches are placed on the cavity wall and the magnetron, which open circuit when the system over heats.

c) A timer and power meter are used for control of the heating process. Power control is achieved through time cycling, duty cycles of ten seconds are usually used.
d) A RC filtering circuit is used at the input of the mains to smooth the supply.
e) The magnetron is the source of microwave power, it converts DC power to AC power. A high DC voltage (4000 V) is connected to the anode and cathode and a low AC voltage (3.1 V) is used to heat the cathode heater filament. The output frequency is 2.45 GHz.
f) A transformer is used to step up the 220 AC mains voltage to 2500 AC volts
g) A voltage doubler is used to supply the magnetron voltage. Figure 2.5 shows its operation. The transformer supplies approximately 2500 AC volts which charges up the capacitor. When the current flows in the opposite direction, the diode prevents the voltage in the capacitor from being discharged back through the diode. This voltage is added to the approximately 2500 volts produced on the transformer winding on the negative side of the AC wave. This raises the circuit voltage to approximately 4000 volts peak. The diode is thus a one way current limiting device and a rectifier.
h) The magnetron is heated up during operation. This is a result of heat generated from within the magnetron and by power being reflected back to the magnetron from the oven cavity. Cooling is achieved by using a blower motor feeding air past its cooling fins.

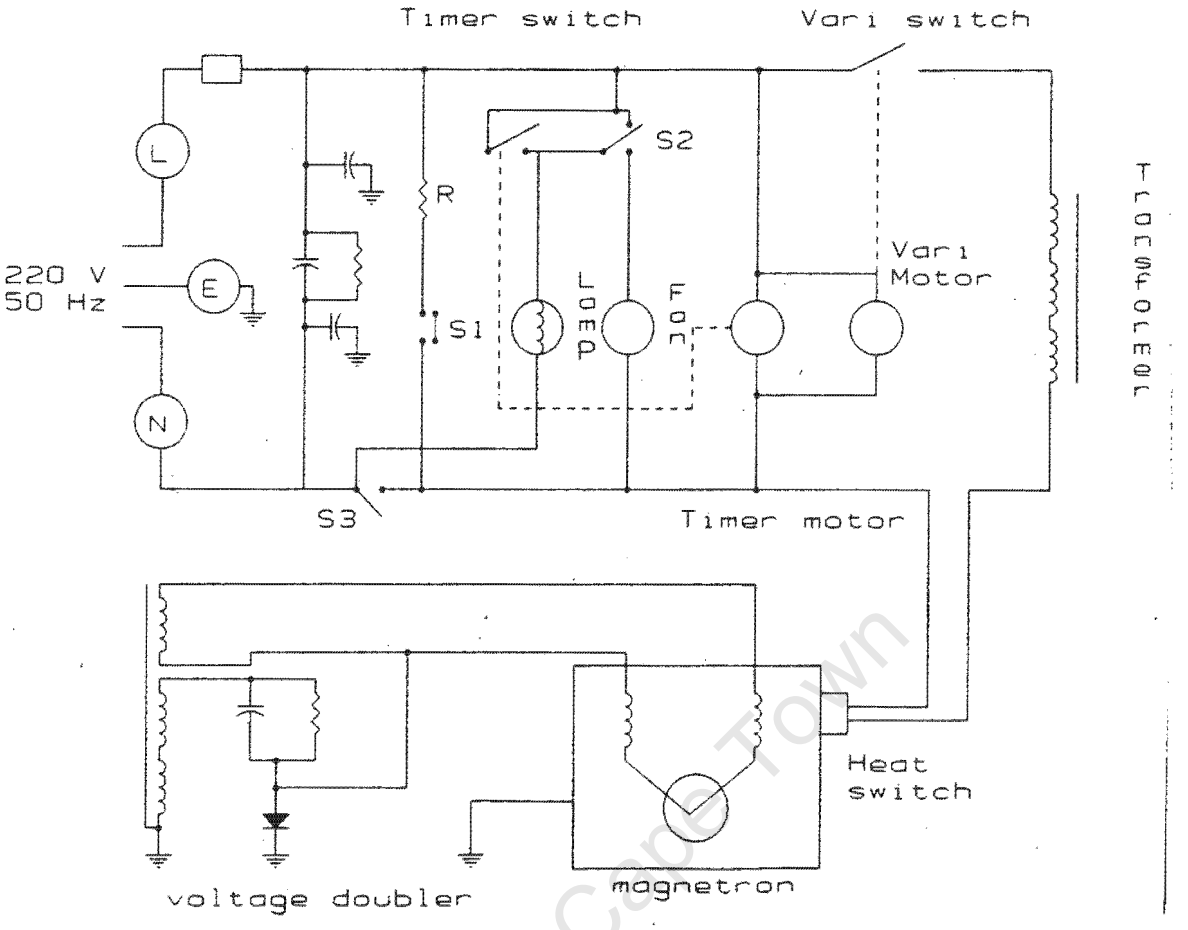

Figure 2.4: Microwave oven circuitry

When the door is closed switch S1 opens and switches S2 and S3 close. The timer motor now cycles power to the transformer through the vari switch. The blower and the lamp remain on through the timer switch over the whole heating process. When the door is opened the power is cut but as a safety precaution switch S1 short circuits the primary coil of the transformer discharging it through resistor R.

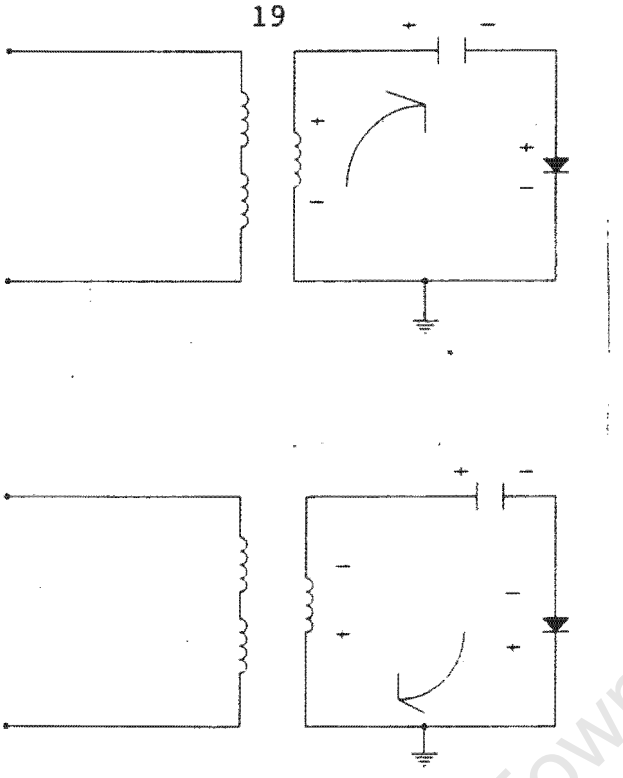

Figure 2.5: The voltage doubler

2.3) Microwave oven tests on the network analyser

2.3.1) Test setup and procedure

The oven tested launched the microwaves from a waveguide through the side wall of the cavity. The magnetron was removed so that tests could be carried out at low power on a network analyser. Microwaves were now launched using an SMA dipole antenna inserted into the waveguide, in place of the magnetron. The network analyser was used to measure the reflection coefficient or return loss directly for different loads placed in the cavity, so that the ratio of power reflected to power absorbed for each load could be calculated. First the SMA probe was matched to the waveguide. Filling the cavity with a carbon microwave absorbant sponge matched the waveguide to the cavity. Now measuring the return loss on the network analyser a match of -32 dB was obtained at a

frequency of 2.45 GHz by adjusting the probes length and position. The frequency was swept from 2.4 to 2.5 GHz to cover the magnetron RF frequency of 2.45 GHz. Different numbers and sizes of water loads were placed in the cavity using 100 ml and 400 ml erlenmeyer beakers. Water volumes were measured out with a pipette. Figure 2.6 shows the different positions tested on the carousel. By rotating the carousel of a loaded cavity the maximum and minimum return loss could be observed for a change in position.

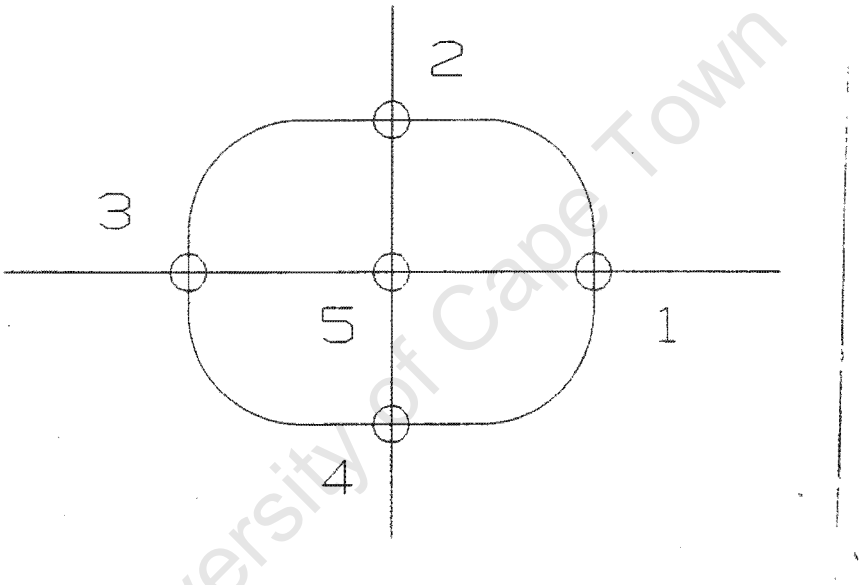

Figure 2.6: The test load positions in the microwave oven

2.3.2) Microwave oven test results

Firstly tests were done using a single water load to observe the change in return loss with the loads position and size. The size of water load was varied from 0 ml to 300 ml. Table 2.1 shows the recorded return loss measured for the load size and position indicated.

Load volume (ml)	Return loss (dB) at position:				
	1	2	3	4	5
0	-3.1	-3.4	-2.6	-2.8	-2.8
25	-7.0	-7.9	-5.9	-4.6	-6.8
50	-10.4	-9.2	-4.8	-6.8	-8.0
75	-18.0	-16.0	-8.8	-10.2	-11.5
100	-22.0	-4.0	-8.0	-4.5	-9.4
125	-21.0	-5.2	-12.0	-5.8	-13.8
200	-10.2	-13.2	-17.0	-9.0	-19.5
300	-23.2	-5.2	-12.0	-6.8	-13.8

Table 2.1: Return loss tests using a single load

At no load, an empty beaker is transparent to microwaves, the return loss was roughly -3 dB, or 50 % of the power being reflected. This power is divided between the power absorbed by the cavity halls and that returned to the magnetron. A load of constant water volume resulted in a wide variation of return loss with a variation of positions in the cavity. A variation of load volume with a fixed position produced no correlation with the return loss results of any of the other positions. Different modes are excited within the cavity with each load size and position, with a different standing wave pattern resulting in different heating characteristics in each case. The average return loss for each size load tends to increase, as expected, with an increase in load volume. An increase in load increases the circuit losses and thus the return loss.

Tests were then carried out using two and three water loads, the load size and position was then varied to determine any wave symmetry. The loads were placed symmetrically on the carousel and rotated from 0 degrees

to 180 degrees. The load size was varied from 15 ml to 150 ml each. The carousel was turned on to observe the maximum and minimum return loss for a rotation of the load. Table 2.2 shows the return loss results for each position and load size.

No	load volume (ml)	Return loss (dB) at position:					
		0^0	90^0	45^0	-45^0	max	min
2	15	-10.2	-11.8	-13.7	-11.5	-26	-6
2	20	-14.1	-17.8	-14.0	-12.7	-34	-10
2	25	-11.0	-14.5	-15.3	-15.5	-23	-8
2	100	-14.2	-7.5	-12.8	-19.6	-35	-8
2	150	-10.0	-12.5	-31.3	-15.8	-28	-12
3	10	-6.0	-14.5	-6.6	-10.3	-26	-4
3	15	-7.0	-13.8	-8.5	-9.2	-22	-6
3	20	-6.0	-12.0	-8.5	-15.3	-36	-6
3	25	-22.1	-8.9	-9.0	-24.6	-42	-6.5

Table 2.2: Test results using multiple loads

There appears to be no symmetry in the cavity wave structure. There is again a wide variation of return loss with the loads position and the size of the load. The number of loads, all holding the same total volume, also varies the return loss of the system, eg. the results from two 15 ml loads and three 10 ml loads were different because of position. There is a great difference between the maximum and minimum return loss for each load placed in the cavity on rotation of the carousel. These values vary between 100 % and 60% of the power being absorbed. The microwave oven rotates the load, continually varying the wave structure inside the cavity, thus averaging out the power delivered to each load.

The microwave oven is a nonresonant, multimode system with a resulting standing wave pattern dependent on the loads size, position and composition. The systems heating characteristics will be different for each load processed making it non ideal for process control. Uneven heating results, separate loads placed in the oven will heat up at different rates and so rotation is necessary. The microwave oven is not optimum for a heating process as power is lost when the load moves through maximum and minimum return loss positions. It is often difficult or inconvenient to rotate the loads in a microwave digestion system as the samples require ventilation to the atmosphere. The ventilation tubes, therefore, rotate with the samples resulting in a complex mechanical structure. Resonant cavity structures, with symmetrical wave properties to deliver equal power to all the loads, were then studied for use in an optimal power transfer system with control of the heating process. These structures enable the separate loads to be vented to the atmosphere without the need to rotate the loads within the field structure.

CHAPTER 3

3) THE EVALUATION OF THE CYLINDRICAL WAVEGUIDE CAVITY FOR USE IN A DIGESTION SYSTEM

As the microwave oven is not ideal for use in a digestion system, cylindrical resonant cavities were studied. These structures were chosen as they satisfy the requirements of having a symmetrical wave structure, delivering equal power to all the loads. The cavity must have a good energy transfer efficiency for all the possible sizes of load. That is, there must be a good match for all loads.

3.1) Cylindrical waveguide theory and transverse electric and magnetic modes

The electromagnetic fields within the waveguide are formulated as a set of mode functions indicative of the possible transverse field distribution in the waveguide [16]. Transverse electric and transverse magnetic modes propagate in waveguide. Solving Maxwell's equations using the standing wave solution of Helmholtz's equation, in cylindrical coordinates, produces the electric and magnetic components of the propagating mode as functions of Bessel's function. Satisfying the boundary conditions for the waveguide sets the requirement:

$$J_n'(k_c a) = 0 \qquad \ldots.(3.1)$$

Where J_n' is the first derivative of the n^{th} order Bessel function of the first kind, J_n. Values of $k_c a$, which satisfy this requirement, for the different TE_{np} and TM_{np} modes are tabulated in the literature. This sets the propagation constant, cutoff frequency, waveguide wavelength and waveguide impedance for each mode (see appendix B). The dominant mode is the mode of

TE_{11} as it has the lowest cutoff frequency in circular waveguide.

3.2) Resonant cavity equivalent circuit and Q-factor

The quality factor, Q, is a measure of the energy storage property (reactance) in relation to the energy dissipation property (resistance) in a circuit. It is thus a measure of the frequency selectivity of a resonant circuit and is defined as:

$$Q = 2(\text{max energy stored})/(\text{energy dissipated per cycle})$$
$$= wW/P \qquad \ldots.(3.2)$$

where: W = maximum stored energy

P = average power loss

At resonance, the electric and magnetic energies are equal and in time quaderature. The total energy stored is calculated by integrating the energy density over the volume of the resonator. The average power loss is calculated by integrating the power density over the inner surface of the resonator. Substituting these into equation 3.2 and simplifying gives the Q-factor of a cavity resonator as approximately:

$$Q = w(\text{volume})/2R_s(\text{surface area}) \qquad \ldots.(3.3)$$

An unloaded resonator can be represented by either a series or parallel resonant circuit. figure 3.1 shows the equivalent circuit of a cavity coupled through a N:1 transformer and a series inductor, L_g, to a generator with internal impedance, Z_g. Figure 2.2 shows the equivalent parallel circuit of a loaded single mode cavity. The resonant frequency and the unloaded Q-factor are:

$$f_o = 1/2(LC) \qquad \ldots.(3.4)$$

$$Q = w_oL/R \qquad \ldots.(3.5)$$

Resonance occurs when the capacitance and conductance are equal and cancel, giving a real impedance R. However, loading the cavity introduces extra resistance and reactance. This causes resonance to shift down in frequency and lowers the Q-factor.

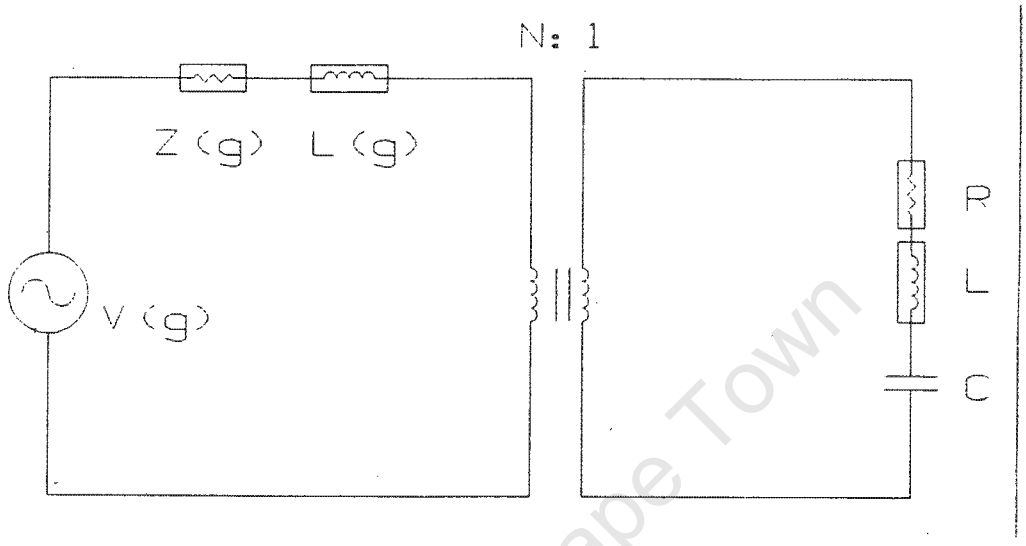

Figure 3.1: Equivalent circuit of a cavity coupled to a generator.

3.3) Power combiner theory

The need of high power microwave amplifiers has lead to the development of high power combiners which combine the output power of many low power devices. A resonant cavity type power combiner has a high efficiency and a narrow bandwidth [17]. The TM_{0p0} modes are used in the resonant cavity combiner/divider as it is easy to separate the associated mode from the other undesirable resonant modes. Multiple ports can be used because this mode has a constant electromagnetic field in the azimuthal direction. A double tuned cavity composed of TM_{010} and TM_{0p0} mode cavities can be used to achieve a broader bandwidth. These two cavities are coupled with a disk type probe. The peripheral ports are coupled with loops to the TM_{0p0} mode cavity. Figure 3.2 shows the equivalent circuit of this divider/combiner. The

unloaded Q-factor of the cavity is found by calculating the stored and dissipated power, and substituting these into equation 3.2 gives:

$$Q_0 = nak/2R_s(a/h + 1) \quad ....(3.6)$$

$$= f_0/BW \quad ....(3.6b)$$

where: n = intrinsic impedance

a = radius of the cavity

k = wave number = X_{np}'/a

R_s = surface resistivity

h = height of the cavity

BW = band width

It has been shown experimentally [18], that the accuracy of equation 3.6 is within 40 to 200 percent and thus is not very reliable. The reason for this is the surface roughness of the cylindrical cavity walls.

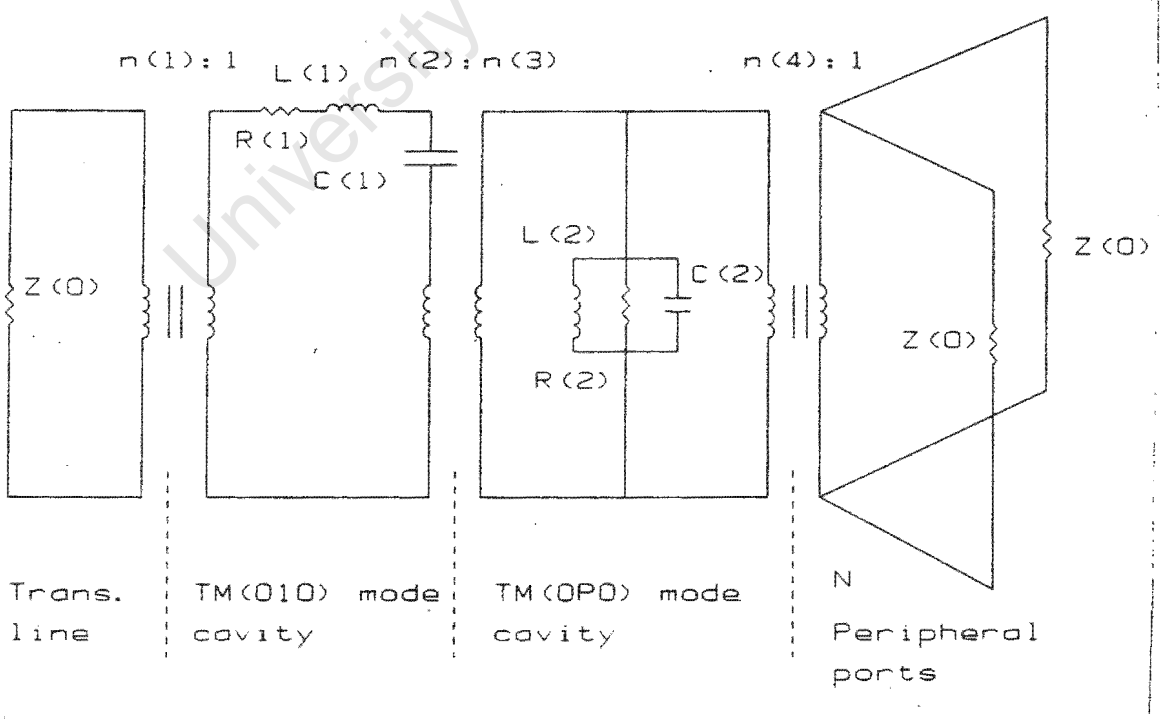

Figure 3.2: Power combiner equivalent circuit

3.4) The cylindrical cavity field characteristics and design

Now with a grounding in cylindrical waveguide theory, the cylindrical resonant waveguide could be evaluated to determine if it will fulfil the requirements of a digestion system with multiple loads requiring equal microwave power.

3.4.1) The cylindrical resonant cavity characteristics

For a high energy transfer efficiency, the cavity must be matched to all possible loads. A high return loss, at least -10 dB, must be achieved for all loads. The cavity must have a wide enough bandwidth to achieve this requirement for all possible shifts in resonance frequency when it is loaded. This is shown in figure 3.3. Here the unloaded cavity is matched at f_0 with a return loss of -25 dB. However when loaded, resonance shifts down in frequency to f_0', now with an insufficient bandwidth a match of only -3 dB is achieved at f_0.

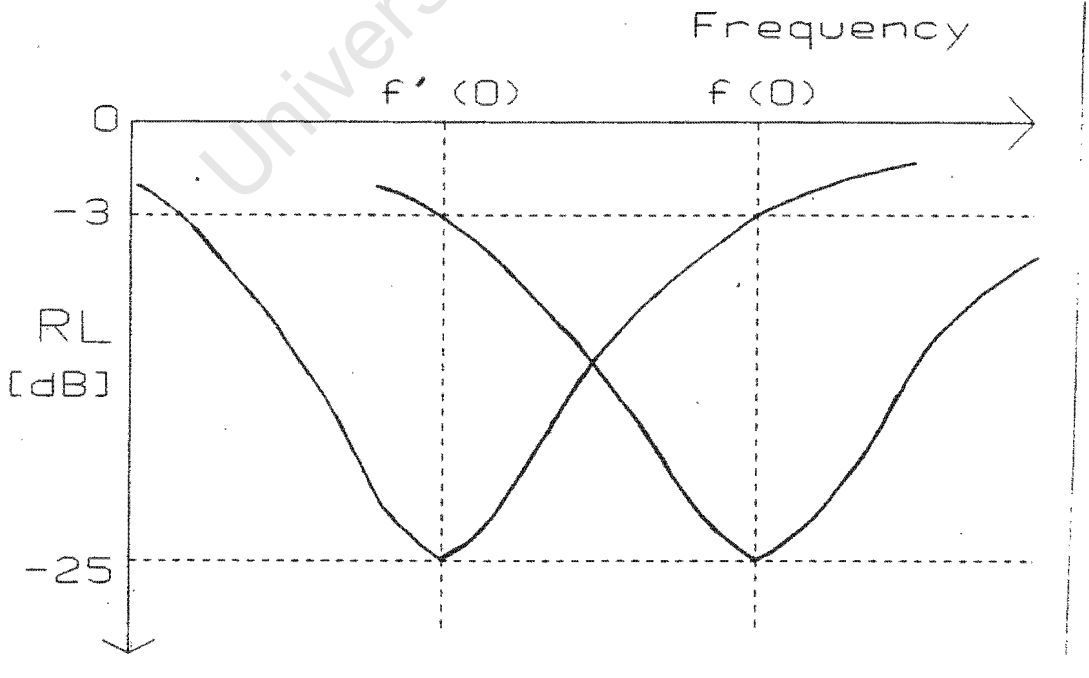

Figure 3.3: Cavity return loss requirements

As discussed earlier, a symmetrical field distribution is required in the cavity for equal distribution of power to all the loads. Figure 3.4 shows the field pattern of the TE_{01} mode in cylindrical waveguide. This mode has a constant E-field in the azimuthal direction and the field is symmetrical around the center. The field distributions of the other TE_{op} modes are similar to that of the TE_{01} mode. They have the same field symmetry but extra zero E-field values along the radius of the waveguide. The subscript p indicates the number of zeros of E_{ϕ} along the radial of the waveguide. These modes can be excited by launching the microwaves with a monopole antenna or E-field probe positioned at the center of the cavity. The sample loads can then be positioned symmetrically around the center of the cavity, thus not degrading the unloaded wave symmetry. This has a similar geometry to the cavity power combiner [17]. The low power FET amplifiers are replaced with the sample loads and coupling is through the E-field. The loads must be placed at equal distances from the center ensuring that each load sits in an equal E-field intensity. This is shown in figure 3.5.

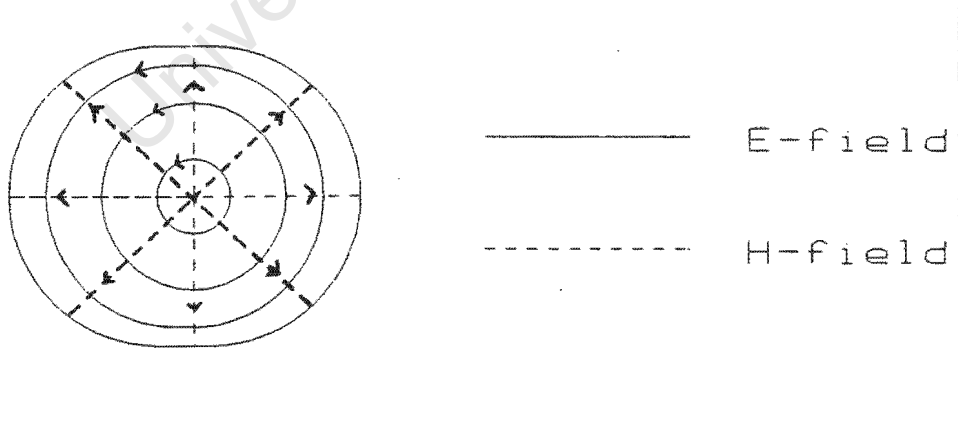

Figure 3.4: TE(01) mode in a cylindrical cavity

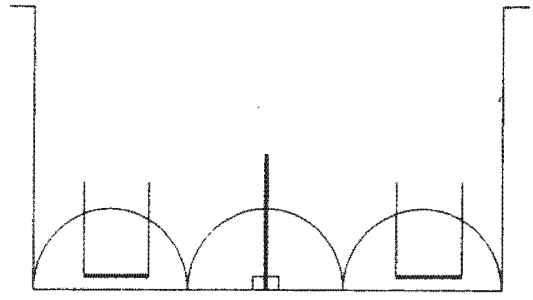

Figure 3.5: E-field distributions for TE(0P) modes

3.4.2) Cylindrical resonant cavity design and construction

For TE_{op} modes, the electromagnetic field in cylindrical coordinates is given by:

$E_{\phi} = E_{o\phi}J_o'(X_{op}'r/a)$ in the azimuthal direction

$H_z = H_{oz}J_o(X_{op}'r/a)$ along the axis of the waveguide

Now using a cutoff frequency of 2.45 GHz with the correct roots of $J_o'(k_c a)$, ie. X_{op}', in equation B.5 (appendix B), the required diameter of the cylindrical cavity is calculated. Table 3.1 shows the calculated values for the modes indicated. These are the minimum size diameters that will allow the corresponding modes to propagate. The size of the cavity will determine which modes are propagated.

mode:TE_{np}	01	02	03	04
X_{np}'	3.832	7.016	10.173	13.324
a [cm]	7.5	13.7	19.8	25.9
diam [cm]	15.0	27.4	36.6	51.8

Table 3.1: Critical cavity diameters

From a practical consideration of the size of the cavity, it was decided that it must be large enough to accommodate eight sample loads. It must be able to house both open and closed vessel digestions. The dimensions

of the closed teflon PFA vessels set the minimum height of the cavity at 20 cm. The cavity must wide enough to hold the largest open vessels, these are 250 ml erlenmeyer flasks, 9 cm in diameter. Figure 3.6 shows the top view of the cavity with the symmetrical load positions from which the required cavity size is calculated:

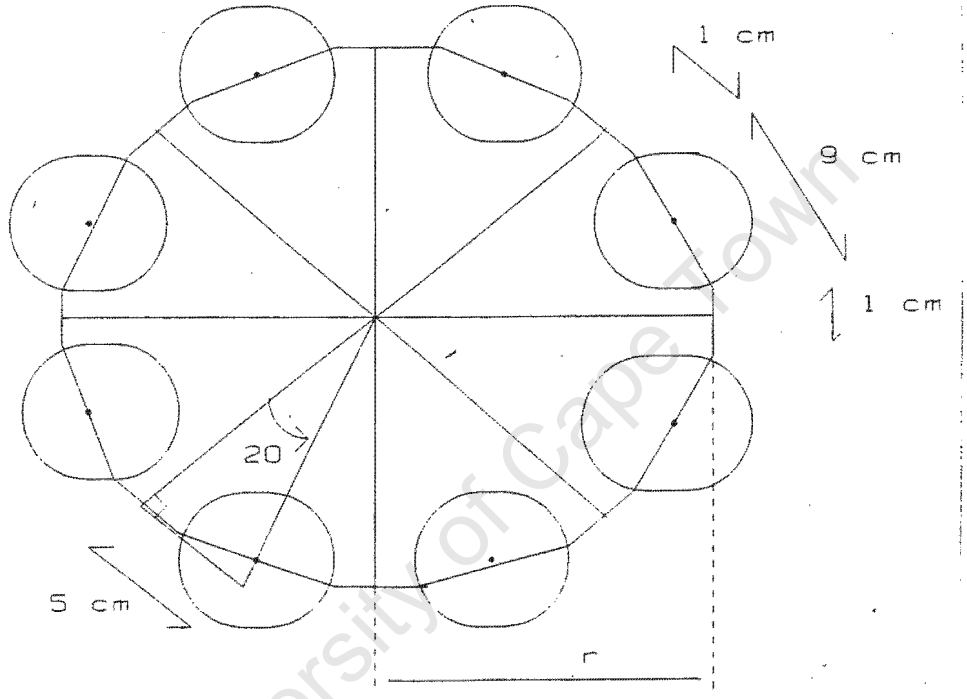

Figure 3.6: Practical cylindrical cavity design

Minimum diameter: circumference = 8 x (9 + 1) = 80 cm

$r = 80/2\pi = 12.7$ cm

$d = 2(12.7) + 2(10/2) = 35.5$ cm

Maximum diameter: $r = 5/\sin(20) = 14.6$ cm

$d = 2(14.6) + 2(10/2) = 39.2$ cm

The diameter of the cavity was chosen to be 40 cm, This would allow TE_{01}, TE_{02} and TE_{03} modes to exist in the cavity. When the sample loads are inserted in the cavity, hybrid modes are excited. However the distortion

in the field symmetry is equal on all the loads, due to their symmetrical positioning, thus heating each load equally. Higher order modes can propagate in the load as the cutoff wavelength is increased by the square root of the loads dielectric constant.

Appendix C shows a picture of the constructed cylindrical resonator cavity. The cavity is made out of stainless steel for its strength, and is 40 cm in diameter and 20 cm high as designed. Easy access to the interior of the cavity is made available through a removable lid on the top. Extra modifications will be needed when it is used to do digestions. It must be teflon lined and must have exhaust ports drilled through the cavity lid above the position of the sample loads. It must also have a window for viewing the samples and a duct for cooling the samples and extracting the acid fumes using a fan.

3.5) Testing and results of the cylindrical resonant cavity

3.5.1) Cavity test setup

Typical sample loads in a digestion process vary between 3 and 7 ml each. Tests were done using these volumes of water load and the number of sample loads in the cavity was varied. A fixed polypropylene base was made to fit in the cavity on which the load positions were set. This reduces the number of variables that can effect the results. Polypropylene is transparent to microwaves and will not affect the electromagnetic field.

The network analyser was used to measure the return loss for each load at 2.45 GHz. The frequency was swept to cover 2.45 GHz and microwaves were fed into the cavity using an N-type probe. The size of the launcher antenna was adjusted until a good match was obtained for the cavity. The match was obtained for a fully loaded cavity, then sample loads could be removed and the resonant shift and return loss recorded for each. Now the cavity is being effectively unloaded and the resonance shifts up in frequency, but the effect is the same. This was done as the cavity matching was very sensitive at no load, showing a high Q-factor. A match could be more easily obtained with a loaded cavity where the Q-factor has been reduced. The symmetrical property of the field was also tested by rotating the load positions by either 90^0 or 45^0 around the center of the cavity. For good symmetry the return loss for each angle should be the same. The cavity was tested for leakage. If leakage is substantial, this could affect the field structure inside the cavity and become a health hazard.

A Hewlett Packard data logger was connected to the network analyser for plotting of the resultant resonance curves. These plots are shown in appendix I. This also

calibrated the network analyser using manufactured short and open circuit loads.

3.5.2) Results of testing by varying the cavity load

Tests were done using sets of 3, 5 and 7 ml sample loads. The cavity was initially matched to eight of these loads, the number of loads were then reduced and the results documented. Table 3.2 shows the return loss and resonance shift recorded for the set of 7 ml loads. The loaded cavity was initially matched with a return loss of -23.7 dB at 2.45 GHz. Figures I.1a to I.1e show the plotted return loss over the swept frequency for each load tested in the 7 ml set.

no. of loads	f_0 [GHz]	RL [dB]
8	2.45	-23.7
6	2.48	-14.4
6 (90^0)	2.48	-14.2
4	2.49	-7.1
2	2.50	-6.0
2 (90^0)	2.50	-7.2

Table 3.2: Return loss results for 7 ml loads

A shift up in the resonant frequency resulted with each reduction in the number of loads. The maximum shift of 50 MHz resulted at the smallest of the two 7 ml sample loads. Each shift in the resonance frequency corresponded to a reduction of the return loss at that frequency. The return loss at 2.45 GHz decreased from a good match at -23.7 dB to a mismatch of 0 dB at smaller loads. The cavity showed good symmetry properties as the return loss for two and six sample loads rotated by 90^0 were similar in size. Discrepancies could result from load positioning after rotation and the launcher centering. The plotted return loss curves before and after rotation are of the same shape showing the same

characteristic resonant peaks over the swept frequency range.

Table 3.3 shows the cavity test results for the set of 5 ml loads. An initial match of -17.5 dB was obtained for the maximally loaded cavity. Figures I.2a to I.2h show the plotted return loss over the swept frequency for each load tested in the 5 ml set.

no. of loads	f_0 [GHz]	RL [dB]
8	2.45	-17.5
6	2.47	-18.0
4	2.49	-6.1
4 (45^0)	2.49	-6.8
2	2.50	-4.9
2 (90^0)	2.50	-4.7
2 ($+45^0$)	2.50	-4.9
2 (-45^0)	2.50	-5.2

Table 3.3: Return loss results for 5 ml loads

Here again resonance shifted up in frequency with each load removed, corresponding to a decrease in the return loss. Again a mismatch resulted when the load was varied. Good field symmetry was seen in comparing the plots of figure I.2c and I.2d and the plots of I.2e, I.2f, I.2g and I.2h. The rotation of two 5ml loads in the cavity gave the same resonance characteristics over the sweep range for all the angles.

Table 3.4 shows the test results for the set of 3 ml sample loads. The cavity is initially matched to -16.2 dB for the maximally loaded cavity. Figures I.3a to I.3g show the plots of return loss for each load.

no. of loads	f_0 [GHz]	RL [dB]
8	2.45	-16.2
6	2.47	-8.0
6 (90^0)	2.47	-9.4
4	2.49	-5.0
4 (45^0)	2.49	-5.4
2	2.49	-6.1
2 (90^0)	2.49	-6.1

Table 3.4: Return loss results for 3 ml loads

These are similar to those results of the 5 ml and 7 ml sets of loads. As can be seen from the plots before and after rotation of the same load, the resonance curves are almost identical for the same size load. The return loss at the resonant peak of each of these plots compare very well. This indicates the cylindrical cavity has good symmetry properties. However, due to the cavities narrow bandwidth and high Q-factor the cavity becomes mismatched when the load is varied and the resonant peak shifts. This will result in the cavity only having a high energy transfer efficiency for some loads, and the process will not be optimal.

From equation 3.6 it can be seen that reducing the height, h, of the cavity will lower the Q-factor and thus broaden the bandwidth. The cylindrical cavity height was then reduced to 7.5 cm, the maximum height of the open vessel flasks. Now only open vessel digestions can be processed as it cannot fit the closed vessels. Similar tests were then performed to establish if this had produced the desired results of a good loaded cavity match for all loads. The cavity Q-factor was determined and compared with the theoretical value calculated. The bandwidth of the antenna or E-field launcher was also determined to establish if it was limiting the bandwidth of the cavity.

3.5.3) Results of testing the cavity with a reduced height

Table 3.5 shows the return loss and resonant frequency results from the reduced height cavity with 3 ml and 5 ml sets of loads. Figures I.4a to I.4c show plots of the 3 ml load tests and figures I.5a to I.5c show plots of the 5 ml load tests.

load vol.	no. of loads	f_0 [GHz]	RL [dB]
5 ml	8	2.45	-14.0
5 ml	6	2.46	-8.1
5 ml	4	2.49	-6.0
5 ml	2	2.49	-5.9
3 ml	8	2.45	-18.3
3 ml	6	2.46	-12.0
3 ml	4	2.49	-6.0
3 ml	2	2.49	-4.8

Table 3.5: Return loss results for 3 ml and 5 ml loads in the reduced height cavity

Comparing these plots of figures I.4, for the 3 ml loads, and figures I.5, for the 5 ml loads, with the corresponding figures I.2 and I.3 respectively, shows that the bandwidth for the reduced height cavity is larger than that of the original height cavity. This increase in bandwidth is still not sufficient to prevent a mismatch for all loads. For example, consider the figures I.4a to I.4c. The cylindrical cavity is originally matched to eight 3 ml loads, with a return loss of -18.3 dB at 2.45 GHz. When the number of loads are reduced to six, figure I.4a, the resonance frequency has shifted to 2.46 GHz and the match has been reduced to approximately -5.5 dB at 2.45 GHz. This is still a reasonably sufficient match and specifies 28 % of the power being reflected. When the number of loads are reduced to four, figure I.4b, the resonance shifts again reducing the match at 2.45 GHz to approximately 0 dB.

This is a total mismatch with 100 % of the power being reflected. These are still inadequate conditions for use in a digestion process.

The Q-factor of the cylindrical cavity was then experimentally determined for comparison with the theoretical Q-factor. The bandwidth was measured as the frequency difference between the points on the resonance curve at which the power is half the peak power value. This is the -3 dB return loss level. The Q-factor was then calculated from:

$$Q = f_0/BW$$

The unloaded cavity was matched with a return loss of -22.3 dB at 2.45 GHz, the load was then gradually increased with the bandwidth and resonant frequency measured for each load. The experimental Q-factor was calculated from these values. Table 3.6 shows the results obtained. As expected, the Q-factor decreased and the bandwidth increased with an increase in load.

volume of load	f_0 [GHz]	BW [MHz]	Q_{exp}
no load	2.45	65.4	37.5
2x3 ml	2.44	66.5	36.7
2x5 ml	2.44	69.7	35.0
4x3 ml	2.43	71.9	33.8
4x5 ml	2.41	76.2	31.6
6x5 ml	2.40	82.2	29.2
8x5 ml	2.40	87.3	27.5

Table 3.6: Experimental Q-factors

Before using equation 3.6 to calculate the theoretical Q-factor, the possible electromagnetic modes that can propagate in the cavity must be determined. For TE_{np} modes, the roots of Bessel's function ,X_{np}', are used in equation B.7 (appendix B) to find the cutoff frequency for each mode in the waveguide. Only modes with a cutoff frequency less than 2.45 GHz can propagate in the

cavity. Using equation B.5 calculates the cutoff wave number for each mode. These wave numbers are used in equation 3.6 to determine the Q-factor of each mode. Setting the conductivity of steel equal to $2x10^6$ mhos/meter [15], the surface resistivity of the cavity was calculated using equation A.5 (appendix A):

$$R_s = \sqrt{(w\mu/2\sigma)} = \sqrt{(2\pi x 2.45x10^9 x 4\pi x 10^{-7}/2x2x10^3)}$$
$$= 2.2\ \Omega/m^2$$

Other constants used are: a = 20 cm

n = 377 Ω

h = 7.5 cm

Table 3.7 shows the electromagnetic modes that may propagate in the cavity and their cutoff frequency and Q-factor.

mode: TE_{np}	11	01	21	12	22	02	03
X_{np}'	1.841	3.832	3.054	5.331	6.706	7.016	10.17
f_c[GHz]	0.44	0.91	0.73	1.27	1.60	1.67	2.43
k_c	9.205	19.16	15.27	26.66	33.53	35.08	50.87
Q_{th1}	43.0	89.5	71.4	124.6	156.7	164.0	237.7

Table 3.7 : Theoretical Q-factors for propagating modes

The Q-factor can also be calculated using equation 3.3, using the same surface resistivity value:

cavity volume = $\pi r^2 h = 0.01 m^3$
cavity surface areas = $2x\pi r^2 + 2\pi rh = 0.345\ m^2$

giving: $Q_{th2} = 20.3$

The Q-factors calculated using the first method are much larger than the unloaded cavity Q-factor measured. Mode TE_{03} is the expected propagated mode in the unloaded cavity, but its Q-factor is 237.7. Considering these Q-factors, TE_{01} is the most likely excited mode, however there are expected errors of up to 200 % using this

method. The second method produced results of a much more comparable nature to the Q-factor measured experimentally and is considered more realistic.

A monopole antenna was constructed on a base the same size as the cavity diameter, and was matched to free space. The Q-factor of the antenna was then measured to determine if it was limiting the bandwidth of the cylindrical cavity. Figure I.6 shows a plot of the return loss over the swept frequency range. The bandwidth is much larger than that of the cavity with a Q-factor of approximately 3.7. The antenna is not limiting the cavity bandwidth.

The reason for the cavities low bandwidth and sensitivity to load variation is the large cavity volume to load volume ratio. If the load in the cavity is increased the bandwidth will increase accordingly, producing a better match for the load variations. For this reason a water tank load was constructed to fit inside the cavity and increase the load volume.

3.5.4) Results of the cavity tests with a water tank load

The idea behind the water tank is to increase the cavities fixed load which will increase its bandwidth. Additional sample loads now added to the cavity will not cause a significant shift in the resonant frequency, thus ensuring a good match. The water tank, which was constructed out of a material transparent to microwaves, fitted neatly on the floor of the cavity, distributing its water load evenly across the cavities floor. This maintains the symmetry of the electromagnetic field in the cavity. The water tank was fitted with two ports so that cool water could be passed through the tank as it heats up during the digestion process.

The load volume of the tank was set at 150 ml and the tank then inserted inside the cavity. A match was obtained for the loaded cavity with a return loss of -30 dB at 2.45 GHz and the Q-factor measured to be 27.9. Now sample loads were added and the resultant match, resonant shift and Q-factor recorded. Table 3.8 shows the recorded results using the fixed water tank load.

volume of load [ml]	RL [dB]	Q_{exp}	f_0 [GHz]
tank:150	-30	28.8	2.450
2x3 + 150	-24	27.9	2.4471
4x3 + 150	-23	27.4	2.4465
4x5 + 150	-24	27.5	2.4460
8x5 + 150	-20	26.8	2.4462

Table 3.8: Results of cavity tests with a fixed water tank load

The shift in resonant frequency has been reduced significantly from 50 MHz, seen in previous results, to 3.8 MHz. As a result a good match is maintained for all the extra sample loads placed in the cavity. The power transferred to the cavity will be divided between the sample loads and the water tank load. The cavities Q-factor is now lower than that without the water tank load, and it decreases accordingly, with each sample load added. This decrease in Q-factor, as with return loss, is much smaller than that recorded in the previous tests without the water tank load

3.6) Conclusions

The cylindrical resonant cavity showed a good symmetrical field distribution. However the shift in resonant frequency resulting from the cavity being loaded, resulted in a mismatch and a low energy transfer efficiency. This is due to the high Q-factor and low bandwidth of the cavity, which has a high cavity volume to load volume ratio even with the cavities height reduced. The cavity worked well with the fixed water tank load giving a good match for all sample loads inserted. The cylindrical cavity is thus more suited to the digestion of larger sample loads. A further disadvantage of this cavity results from the requirement for the energy to be launched into the cavity through a coaxial launcher. The power from a low power magnetron is 450 watts while the commercial N-type coaxial launcher are only rated to 50 watts.

A microwave horn type cavity was designed to fulfil the requirements for use in the digestion of these small loads. This has the added advantage that microwave energy could be launched into the cavity using a waveguide launcher thus avoiding the power limitations of coaxial launchers. This cavity is reported in chapter 4.

CHAPTER 4

4) THE RESONANT HORN CAVITY

4.1) Transverse field modes in rectangular waveguide

An electromagnetic plane wave propagating in a rectangular waveguide forms a standing wave pattern which can be represented as a set of mode functions. Both transverse electric, TE_{np}, and transverse magnetic, TM_{np}, can propagate in rectangular waveguide. The electric and magnetic field components of these modes are found by substituting Helmholtz's equation, in rectangular coordinates, into Maxwell's equations for plane waves and solving for the boundary conditions.

The propagation is assumed to be in the positive z direction, with the waveguide walls lying in the x and y planes, see figure 4.1. The propagation constant in the waveguide, γ_g, differs from the intrinsic propagation constant, γ:

$$\gamma_g^2 = \gamma^2 + k_x^2 + k_y^2 = \gamma^2 + k_c^2$$

where k_c is the cutoff wave number.

$k_x = m\pi/a$

$k_y = p\pi/b$

m and p denote the number of half wave lengths of electric or magnetic intensity in the x and y directions respectively.

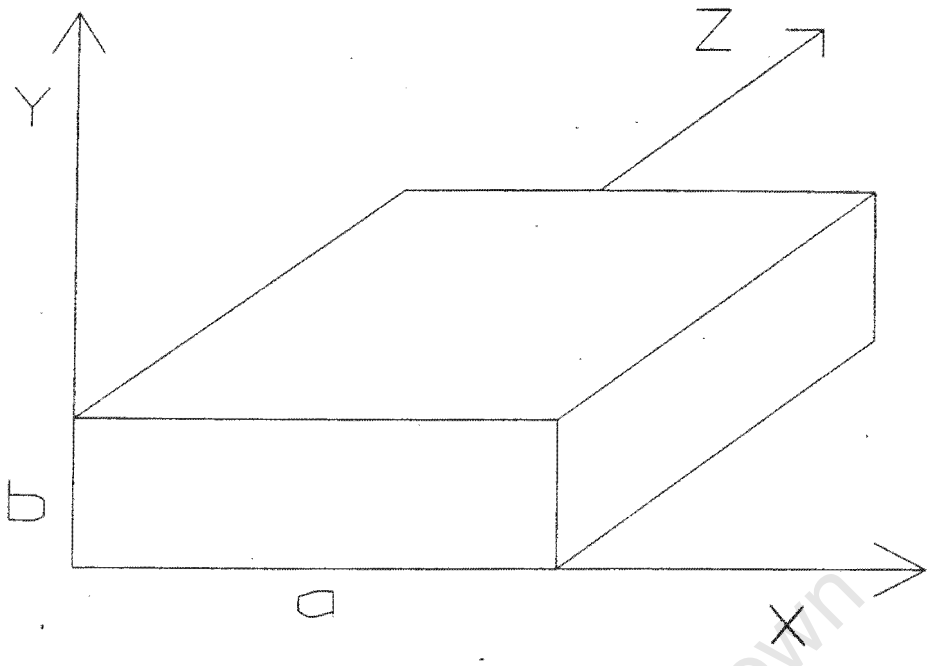

Figure 4.1: Rectangular waveguide coordinates

Using equation A.1 for a loss-less dielectric, $\sigma = 0$, gives:

$$\gamma_g = +/-j\sqrt{(w^2\mu\epsilon - k_c^2)} \qquad ....(4.1)$$

There will be no propagation if $w_c^2\mu\epsilon = k_c^2$ and $\gamma_g = 0$. This determines the cutoff frequency:

$$f_c = 1/(2\pi\sqrt{(\mu\epsilon)})\sqrt{(k_x^2 + k_y^2)} = k_c/2\pi\sqrt{(\mu\epsilon)} \qquad ....(4.2)$$

If $w^2\mu\epsilon > k_c^2$, the wave will propagate. If $w^2\mu\epsilon < k_c^2$, the wave will be attenuated. The dimensions, a and b of the waveguide determine which modes will propagate and which modes will be attenuated. The propagation constant (the phase constant in a loss-less dielectric), characteristic impedance and waveguide wavelength can now be expressed in terms of the cutoff frequency for each mode:

$$\beta_g = w\sqrt{(\mu\epsilon)}\sqrt{(1 - (f_c/f)^2)} \qquad ....(4.3)$$

$$Z_g = n/\sqrt{(1 - (f_c/f)^2)}, \text{ where } n = \text{free space impedance} \qquad ....(4.4)$$

$$\tau_g = \tau/\sqrt{(1 - (f/f)^2)}, \text{ where } \tau = \text{free space wavelength}$$
$$= \tau/\sqrt{(1 - (\tau/2a)^2)} \qquad ....(4.5)$$

The dominant mode is TE_{01} which has the lowest cutoff frequency. This mode is degenerate with the transverse magnetic mode TM_{np}.

4.2) Theory of the horn resonant cavity

4.2.1) The horn antenna

The horn antenna consists of a flared section on the end of a rectangular waveguide. It is used as a means of matching the rectangular waveguide to free space. The rectangular waveguide can be flared in the E-field plane or the H-field plane or both, producing the E plane sectoral, H plane sectoral and pyramidal horns respectively. Figure 4.2a shows the field distribution of the rectangular waveguide in TE_{01} mode. For propagation in this mode $a > \tau/2$, where τ is the free space wavelength. One half wavelength of E-field intensity exists over the aperture of the waveguide, with the maximum E-field intensity in the middle of the waveguide.

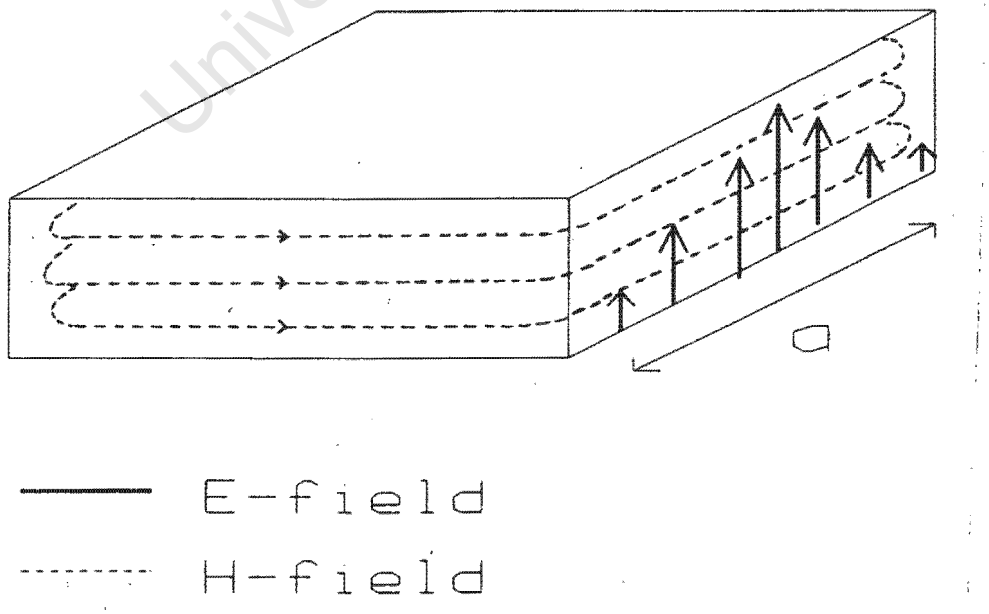

Figure 4.2a: TE(01) mode in rectangular waveguide

Figure 4.2b shows a diagram of the H plane sectoral horn

and its field distribution. The field distribution is the same as that for the rectangular waveguide in TE_{01} mode however the H-field is spread over the flared section of the horn.

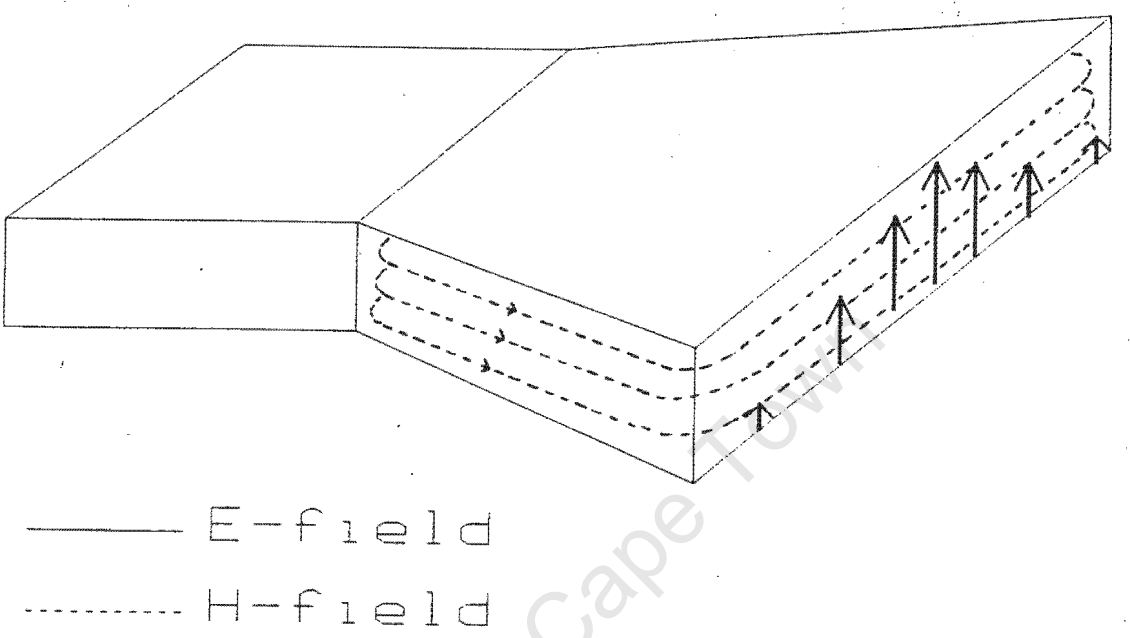

Figure 4.2b: H plane sectoral horn

Similarly for the E plane sectoral horn of figure 4.2c, the E-field distribution remains unaltered after it is flared in the E-field plane.

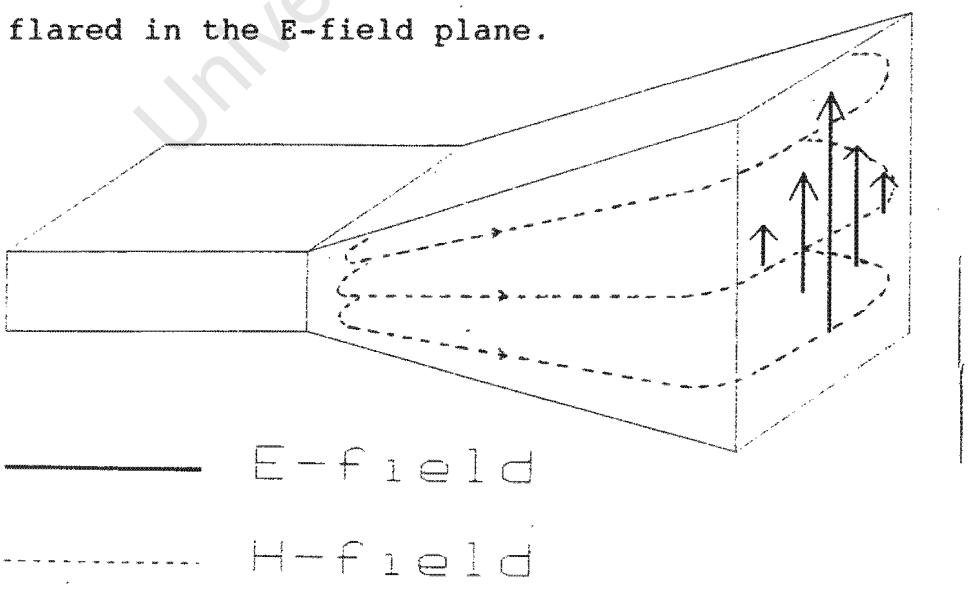

Figure 4.2c: E plane sectoral horn

The pyramidal horn is the result of the combination of the E plane and H plane sectoral horns. In antenna theory, the flared horn increases the directionality of the antenna in the flared plane according to:

$\theta = \tau/a$, where: θ = the antenna beamwidth in that plane

a = length of the horn antenna in that plane

4.2.2) The resonant horn cavity

The principle behind the resonant horn cavity is as follows. Microwaves are launched into a rectangular waveguide setting up TE_{01} mode. As the rectangular waveguide does not have the volume to accommodate the sample loads to be digested, this waveguide feeds into a pyramidal horn section which is large enough to hold the sample loads. The aperture of the horn cavity is then terminated in a short circuit such that the field propagating in the horn is in phase over the horn aperture short circuit section. This requires that the horn aperture be curved such that the electromagnetic waves propagating down the horn have all travelled an equal distance from the launcher. The microwaves are reflected back to the source setting up a standing wave pattern and a resonant cavity is formed.

The resonant horn cavity must fulfil the field requirements for its use in a digestion system. Figure 4.3 shows the horn cavities field distribution and sample load positions. For equal distribution of power to all the loads, the loads are positioned at equal distances from the launcher across the E plane flared section of the horn. The short circuit is applied a quarter waveguide wavelength away from the sample load positions for superposition of the forward and reflected waves at the sample loads. The electric field is thus symmetrical in this axial direction.

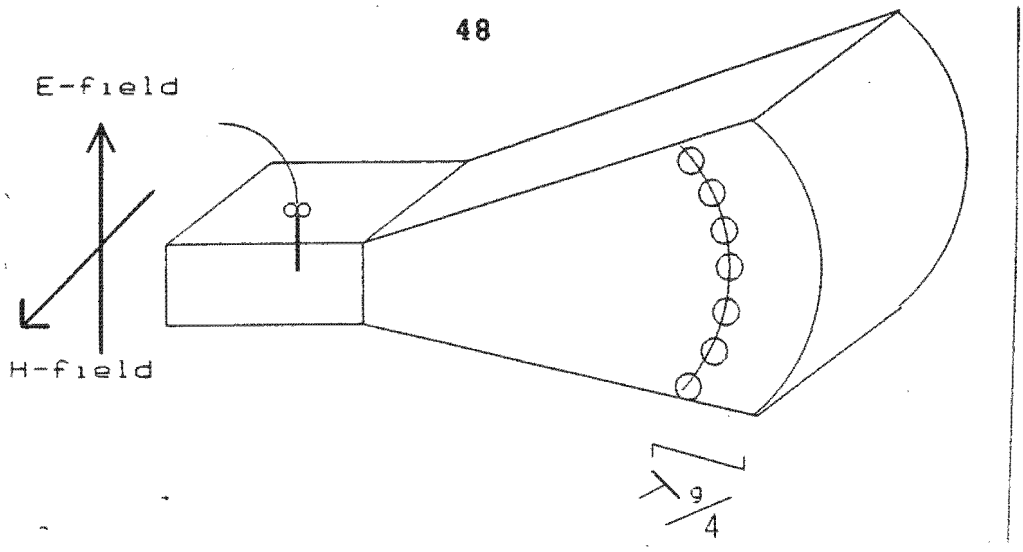

Figure 4.3: Resonant horn cavity design and load position

Compared to the cylindrical waveguide, where the loads are placed on the cavity floor at a position where the E-field is at its minimum, the sample loads are now placed in the center of the H plane flare where the E-field is at its maximum. The E-field couples to the surface area of the sample load, as shown in figure 4.4. Both of these factors will increase the coupling mechanism of the E-field with the sample loads, producing a higher energy transfer efficiency and a less sensitive match for the different loads applied to the cavity.

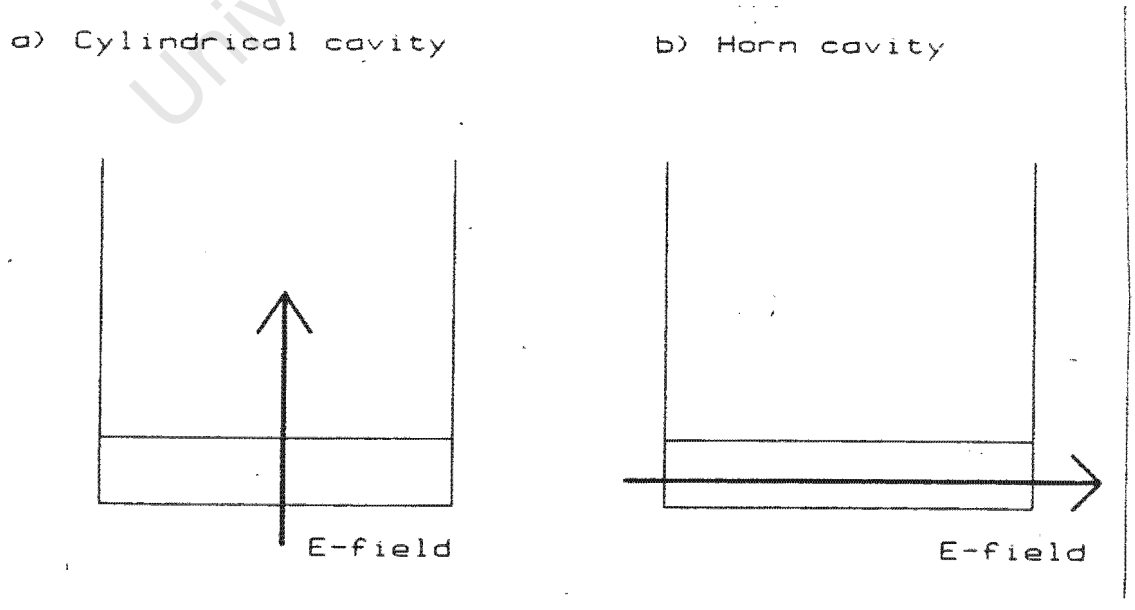

Figure 4.4: E-field coupling mechanism

4.3) Resonant horn cavity calculations and design

4.3.1) Calculations for the rectangular waveguide

The rectangular waveguide must be designed for the propagation of TE_{01} mode only. Considering that a high power magnetron must eventually be used to deliver microwave power, the dimensions of the microwave oven rectangular waveguide were used. These dimensions will have been chosen for the best match between the magnetron and the waveguide. These were measured to be:

$$a = 8 \text{ cm}$$

$$b = 3.5 \text{ cm},$$

with a length of 8 cm. Using these dimension in equation 4.5 sets the waveguide wavelength at:

$$\tau_g = 12.2/\sqrt{(1 - (12.2/16)^2)} = 18.9 \text{ cm}$$

The cutoff frequency for each TE_{np} mode can now be calculated, using equation 4.2, to determine which modes will propagate in the rectangular waveguide. Table 4.1 shows the cutoff wave numbers and cutoff frequencies for each TE_{np} mode. Only TE_{01} mode will be propagated as it is the only mode with a cutoff frequency below 2.45 GHz.

mode:TE_{np}	01	11	02
k_c	39.8	98.0	119.4
f_c [GHz]	1.9	4.7	5.7

Table 4.1: Calculated cutoff frequencies in the rectangular waveguide for TEnp modes

4.3.2) Calculations for the horn cavity

The horn cavity must accommodate eight 250 ml erlenmeyer flasks, 9 cm in diameter and 7.5 cm high. The horn flare angle and length will be set by this physical requirement. The flare in the E plane will determine the number of flasks the cavity can accommodate, while the H plane flare will determine the maximum height of the flasks to be used.

a) E plane flare calculation:

Eight sample loads placed side by side with a 1 cm spacing in between requires a flare length of 80 cm, see figure 4.5. Setting the flare angle to 75° requires that the horn be cut from a disk of circumference equal to:

$80 \times (360/75)$ cm = 384 cm

Thus: $2\pi r$ = 384 cm

r = 61 cm

An extra quarter waveguide wavelength section must be added giving:

$r_1 = r + \tau_g/4 = 61 + 4.7 = 65.7$ cm

This horn section must be connected to the rectangular waveguide with a width of 3.5 cm. The horn cavities E plane flare length must be reduced by:

$r_2 = (3.5/2)/\sin(75/2) = 2.9$ cm

The length of the E plane flare is now:

$R = r_1 - r_2 = 62.8$ cm

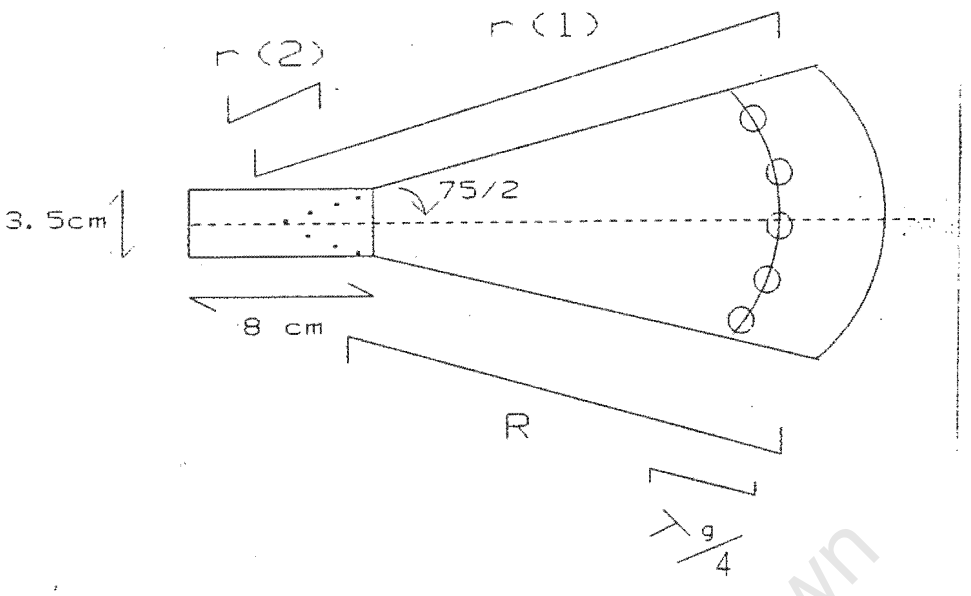

Figure 4.5: E plane flare calculation

b) H plane flare calculation:

The H plane flare length must also be 62.8 cm but with a different flare angle to accommodate the sample load flasks height, see figure 4.6. A height of 20 cm was chosen at the sample loads position as the flasks must be positioned such that the load is in the middle of this section of the flare, in the maximum E-field. The flare angle is:

$2\pi r_1$ = F(20), where: F is the fraction of the disk from which it must be cut.

Therefore: F = 20.7

Flare angle = 360/20.7 = 17.4°

Now, the radius from which the H plane flare section is cut is given by:

$r_1 = r_2 + R = (8/2)/\sin(17.4/2) + 62.8 = 89.2$ cm

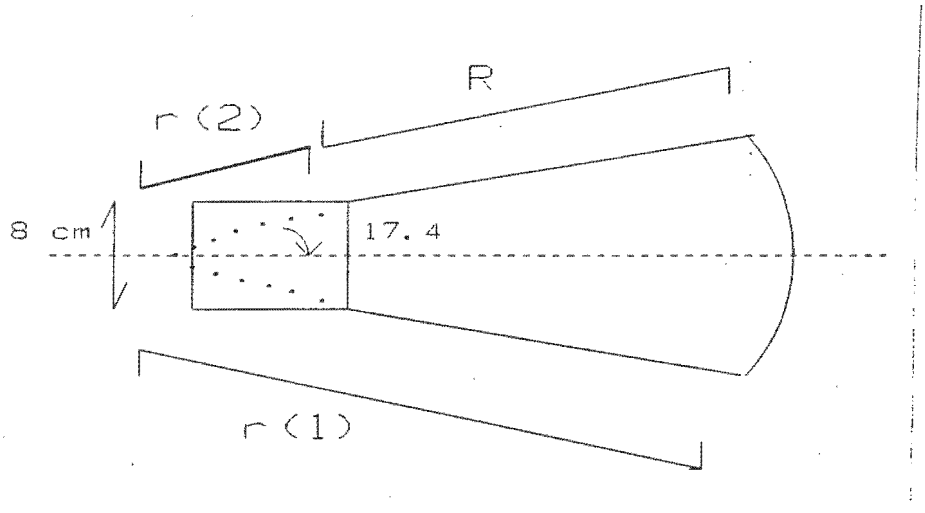

Figure 4.6: H plane flare calculation

4.4) The resonant horn cavity testing and results

4.4.1) Horn cavity test setup and procedure

The resonant horn cavity was fabricated from aluminium sheeting and constructed using pot rivets. Pictures of the constructed resonant horn cavity are shown in appendix D. The rivets were filed down to prevent any obstacles disturbing the electromagnetic field. Any cracks that could be potential leakage areas were sealed with conductive tape. The upper E plane wall was cut to form a removable lid, for easy placement of the sample loads, which could be screwed into position when under going tests. A flask shelf was made, transparent to microwaves, with the correct height to ensure the sample loads sit in the maximum E-field position. The eight sample positions were marked on the shelf to prevent any variations in the results occurring from a change in sample positions. These marked positions all lie an equal distance from the source, a monopole launcher, on the arc of a circle, as shown in figure 4.7.

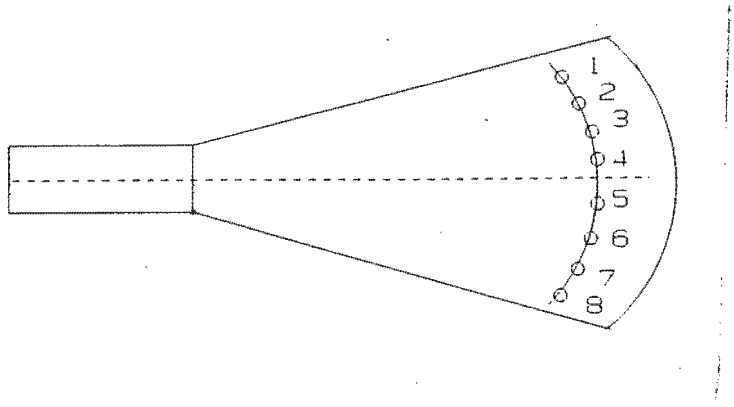

Figure 4.7: Symmetrical test load positions

Low power microwaves were excited in the rectangular waveguide by the network analyser through a N-type probe. The launcher's length was adjusted until a good unloaded cavity match was achieved, -30 dB return loss at 2.45 GHz. Tests were then carried out using the network analyser to determine the symmetry of the microwave field and the return loss for the different loads placed inside the cavity. The Hewlett Pachard data plotter was again used to calibrate the network analyser and plot the resonance curve over the swept frequency range. Later, the magnetron was connected to the cavity and a heating test was performed to test the linearity of the power absorbed by the sample loads.

4.4.2) Symmetrical field tests

The sample positions were marked symmetrically about the center of the flask shelf, see figure 4.7. The cavity was then loaded and the return loss measured, at 2.45 GHz, for different numbers of sample loads placed symmetrically inside. Table 4.2 shows the return loss results recorded for the various loads and positions indicated.

	POSITIONS			
1x10 ml	1	3	6	8
RL [dB]	-34	-36	-34	-36
2x10 ml	3,6	1,8	2,7	4,5
RL [dB]	-28	-30	-27	-30
4x10 ml	3,4,5,6	1,2,7,8	3,4,6,7	1,3,6,8
RL [dB]	-20	-22	-18	-18
6x5 ml	1,2,3,6, 7,8	1,3,4,5, 6,8	1,2,4,5, 7,8	1,2,3,4, 5,6
RL [dB]	-16	-15	-14	-14

Table 4.2: Return loss results for symmetry tests

A good match was obtained for all the sample loads inserted in the horn cavity. There was no resonance shift as the resonant frequency remained at 2.45 GHz for all the loads applied. For each set of loads applied to the cavity, there was a good correspondence between the return loss recorded for each position of the same load. There was a decrease in return loss as the cavity was increasingly loaded but not significant enough to change the percentage of power absorbed by the total load. This cavity displays good wave symmetry for all the tests undergone.

Anti-symmetrical tests were performed to see the extent to which the cavity could be loaded. Here two tests were carried out using two 10 ml loads, they were placed on positions 1,3 and 5,8 and a return loss of -32 dB and -28 dB was measured. A further test with four 10 ml loads was done. They were placed anti-symmetrically on positions 1,2,3 and 4 resulting in a return loss of -18 dB. The resonant peak shifted slightly to 2.447 GHz. This shows the cavity has an excellent ability to maintain a good match when loaded.

4.4.3) Resonant cavity return loss and Q-factor test results

The resonant horn cavity was re-matched with a return loss of -45.8 dB at a frequency of 2.45 GHz. The cavity was increasingly loaded using sets of 3, 5 and 10 ml sample loads. The corresponding resonant frequency shift, return loss, and bandwidth were recorded. The experimental Q-factors were calculated from these results using equation 3.6b and are found tabulated with the corresponding sample loads in table 4.3. Figures J.1 to J.8 of appendix J show the plotted resonance curves for these sample load volumes.

LOAD	RL [dB]	f_0[GHz]	BW[MHz]	Q
no load	-45.8	2.450	22.2	110.3
2x3 ml	-39.9	2.450	24.8	98.8
4x3 ml	-32.7	2.450	27.4	89.4
6x3 ml	-29.8	2.450	30.1	81.4
4x5 ml	-30.4	2.449	33.1	74.0
8x3 ml	-27.5	2.449	31.8	77.0
6x5 ml	-28.2	2.448	34.1	71.7
4x10 ml	-27.5	2.447	36.3	67.5
6x10 ml	-36.6	2.446	37.2	65.8

Table 4.3: Return loss results and Q-factors for an increasingly loaded horn cavity

The range of sample load volumes tested in the horn cavity exceeded the volume that would ever be used in a digestion system. The resonant horn cavity remained in match for all the loads applied. There was the characteristic downward shift in the resonant frequency with increasing load, but only slightly and not significantly enough to cause a mismatch. The good match was obtained for each load placed in the cavity, the resultant change in the power transferred to the load was less than 0.01 %. The plotted resonance curves of the results are very stable, maintaining the resonant

frequency with extreme loading, with an increase in bandwidth and decrease in return loss with increasing load as expected.

The unloaded Q-factor could be approximated using equation 3.3 for comparison with the experimental value. The surface resistance was calculated using a conductivity of 3.5×10^7 mΩ/m:

$$R_s = \sqrt{(w\mu/2\sigma)} = 0.695\ \Omega$$

The cavity volume was estimated at 8×10^{-3} m^3 and the surface area was calculated to be 1.197 m^2. This gives a theoretical Q-factor of:

$$Q_{th} = 2\pi(2.45 \times 10^9)(4\pi \times 10^{-7})/(2(0.695)(1.197) = 99$$

This compares favourably with the measured unloaded Q-factor. The experimentally measured Q-factors decreased as the load was increased. Although the Q-factor values measured for the horn cavity were larger than those measured for the cylindrical cavity, the shift in resonant frequency and the change in match with increasing load volume is much less for the horn cavity. This is due to the change in E-field coupling and the position of the samples in the horn cavity. The sample loads of the resonant horn cavity couple to the maximum E-field over a large sample area, making this coupling much more efficient. The resonance curves of figures J.1 to J.8 are very stable, the resonance pattern of the cavity over the sweep frequency used is constant for all the loads but with a characteristic broadening of the bandwidth.

4.4.4) Horn cavity heating tests

A magnetron rated at 500 watts was connected to the mains supply through a transformer and voltage doubler. The high power microwave field was excited in the cavity using the magnetron which was launched into the rectangular waveguide. Five 25 ml water samples were placed in the cavity at positions 2,3,4,5 and 6 in figure 4.8 for heating.

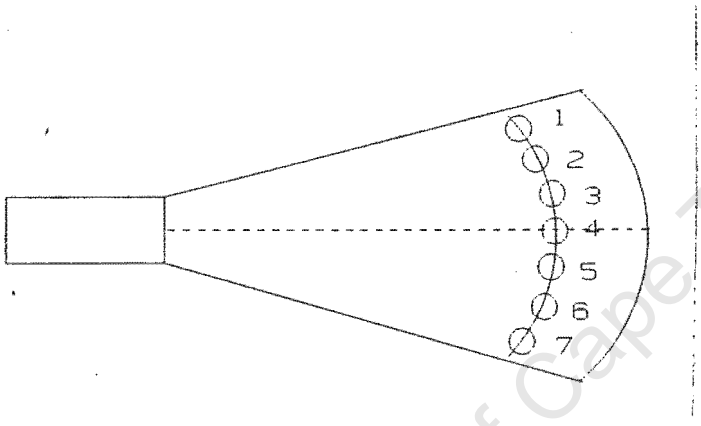

Figure 4.8: Heating test load positions

Small holes were drilled in the horn cavity lid for access to the samples for temperature measurement. Temperature measurement was performed using a Fluke digital temperature meter. A J-type thermocouple was used as the transducer. The thermocouple was cold junction compensated and linearised by the temperature meter from 0°C to 1000°C. Microwave power was applied at 30 second intervals, the power was then switched off and the temperature measured in each sample load. Some stirring of the samples was necessary to reduce the effects of localized heating. Table 4.4 shows the results from this heating test. The average temperature was calculated at each time interval, and using equation 1.1, the average power absorbed by the total load was calculated. These results are tabulated in table 4.5.

TIME: [min.sec]	TEMPERATURE at position: 2	3	4	5	6
0.0	17.3	17.2	17.2	17.4	17.3
0.45,3	26.9	27.0	31.5	27.3	25.1
1.10,6	32.0	35.0	38.4	31.5	31.0
1.40,4	39.9	40.9	46.8	39.2	36.0
2.10,4	44.2	44.2	52.7	43.0	42.1
2.45,3	49.4	49.5	56.7	48.6	47.2
3.15,3	55.7	51.6	58.6	52.1	50.3
3.40,7	57.6	54.3	60.0	55.7	52.6
4.10.6	62.9	57.3	63.5	59.2	55.6
4.40,4	65.5	59.6	65.8	61.7	57.1
5.10,2	67.0	62.4	67.1	64.0	59.4
5.40,6	68.7	64.2	68.6	65.6	61.6
6.10,3	69.9	64.9	68.9	66.4	62.1
6.40,4	71.5	67.5	70.4	68.3	63.3

Table 4.4: Hearting test for the horn cavity

TIME	T_{av}[°C]	P_{av} [w]
0.0	17.2	--
0.45	27.6	239.2
1.10,6	33.6	245.7
1.40,4	40.6	244.2
2.10,4	45.2	161.8
2.45,3	50.3	151.0
3.15,3	53.7	117.1
3.40,7	56.2	104.8
4.10,6	59.7	122.0
4.40,4	61.9	78.6
5.10,2	64.0	73.0
5.40,7	65.7	59.8
6.10,3	66.4	26.1
6.40.4	68.2	63.0

Table 4.5: Average power absorbed in the heating test

The sample loads have an initial average temperature of 17.2°C. An average temperature of 68.2°C was reached in a time of 6 minutes and 40 seconds. The maximum deviation between the sample temperatures at this point was 8.2°C. Initially, the sample load placed in the center (position 4) absorbed the most power and heated up faster than the other sample loads. However, during the process the distribution of power to each sample load changed and the temperatures of each sample evened

out. It was necessary to cool the magnetron with a fan due to it heating up during the process, this is from locally generated heat and reflected microwave power. The initial transfer of power to the loads was 239.2 watts, which slowly increased to 245.7 watts when the sample temperature was an average of 33.6°C. However, as the sample temperature increased its dielectric constant changed and the effective match of the cavity to the magnetron was degraded. Apart from two exceptions in the results of table 4.5, the power absorbed by the samples at each time interval gradually decreased to 26.1 watts when the average sample temperature was 66.4°C. It was considered that the main source resulting in uneven power to the separate loads was multimoding or generation of higher order modes within the horn cavity section. However, the power distribution and heating of the separate loads was acceptable and removed the need to rotate the loads.

4.5) Conclusions

The microwave resonant horn cavity provided an effective coupling mechanism between the sample loads and the E-field. This lead to a stable resonance curve for the loaded cavity, providing a good match for all the sample loads tested. The cavity thus has a high energy transfer efficiency for all the sample loads tested. Good correlation was found in the matches achieved for a sample load placed in different positions in the cavity. This is verified by the heating test performed, where the sample loads heated up uniformly to an average temperature of 68.2°C in 6 minutes and 40 seconds. A good initial match was achieved at a low sample temperature, 246.7 watts of energy transferred to the sample loads in 30 seconds. But as the sample temperature increased, changing the loaded cavity impedance, the match was degraded resulting in 26 watts of power transferred to the sample loads in 30 seconds.

The resonant horn cavity satisfied the requirements for use in a microwave digestion process. A good energy transfer efficiency is achieved for all loads applied to the cavity, thus producing an optimum heating system. Linear heating of all the sample loads resulted from the heating test, but the effective cavity match is reduced as the sample temperature increased.

At this point in the research, a need was identified from industry in South Africa for other uses of the digestion process. These processes still required verification of their feasibility. As a result it was decided to produce an experimental microwave digestion system with a computer control system to test the feasibility of these new digestion processes. This is reported in chapter 5.

CHAPTER 5

5) THE EXPERIMENTAL MICROWAVE DIGESTION SYSTEM

5.1) Introduction

A very real need was identified from industry in South Africa for different uses of the digestion process. Portland cement (PPC) required an on line digestion system, for use in its mines, for the determination of calcium in its ore deposits. The digestion system would allow for tests to be carried out immediately on site, on medium sized samples, giving quick, accurate results. This will save time taken to transport the samples to the laboratory, where tests are performed on a hot plate before mining can be continued. Debeers consolidated mines required a microwave digestion system for the digestion of kimberlite ore. This will possibly produce great time saving in the extraction of diamonds. This process is still in its developmental stage and requires further research to determine its feasibility. Eventually the digestion of large 20 to 50 liter samples is required for this application.

At this stage in the project it was decided to design and construct an experimental microwave digestion system which could be used to determine the feasibility of these processes. Here, a single load applicator cavity is needed which must be adaptable to the different types of digestion tests to be performed using different material loads. It must also be able to accommodate a wide variety of load sizes. Thus a good match of the magnetron power to the load must be established for all the applied loads with computer control of the heating process.

This chapter investigates the behavior of a dielectric material in an electric field and the matching considerations of a waveguide terminated in a dielectric medium. This is followed by the design and testing of the microwave digestion system parts and its overall operation. Finally details of the temperature measurement and the computer control system is given.

5.2) The behavior of dielectric material in an electric field

5.2.1) Polarization

Dielectric materials (non-conducting) do not have free mobile charge carriers. These charges are displaced under an electric field. This is known as dielectric polarization. There are dipoles that need a finite time for alignment and thus the polarization is time dependent. In an alternating (time dependent) electric field the dielectric displacement vector, D, will be out of phase with the electric field vector, E, and displaced by the angle ø:

$$E = E_o.\mathrm{Cos}(wt)$$

$$D = D_o.\mathrm{Cos}(wt - ø)$$

$$D = \epsilon.\ E$$

The dielectric constant is complex and the ratio of D_o/E is usually frequency dependent, thus two frequency dependent dielectric constants are needed, $\epsilon'(w)$ and $\epsilon''(w)$:

$$\epsilon = \epsilon' - j\epsilon'' \qquad \ldots.(5.1a)$$

$$\mathrm{Tan}(\delta) = \epsilon''/\epsilon' \quad \text{where } \mathrm{Tan}(\delta) \text{ is the loss factor} \qquad \ldots.(5.1b)$$

5.2.2) Types of polarization

There are different kinds of polarization in a dielectric with high frequency heating [19].

a) Electron polarization:
This occurs when an external electric field deflects the electrons in an atom and induces a dipole moment, μ. There is however no phase displacement with respect to the electric field and so dielectric loss does not occur. This polarization has its resonant frequency in the ultra-violet and visible spectrum area.

b) Atom polarization:
The individual ion pairs in a molecule are highly polar entities and are displaced from their positions of equilibrium under an external electric field. The ions are elastically joined and can be excited into oscillation by an alternating electric field. These are comparable with high frequency resonators known in v.h.f. technique.

c) Dipole polarization
This type of polarization occurs in dipole molecules which have a natural dipole moment. An electric field causes rotation of the dipole moment. This form of polarization occurs in the meter wave range and shorter.

5.2.3) Dielectric properties of dipole molecules

The dipole needs time to go from an unregulated thermal agitation to an oscillating condition. This is given by:

$a(t) = k.e^{-(t/\tau_0)}$ where: k = constant

τ_0 = relaxation time

and $w_m = 1/\tau_0$ is the natural frequency

The electric displacement vector differs from its value in free space by the polarization, P:

$$P = D - \epsilon_0.E = (\epsilon - \epsilon_0)E$$

If N molecules exist of electric moment μ, the mean electric moment, m, in an applied electric field, F, is:

$$m = \mu^2.F/(3.k.T)$$ where: k = Boltzmann's constant

T = Temperature (degrees K)

The total average moment per molecule is given by [20]:

$$m = (\alpha_1 + \mu^2./3.k.T)F$$ where: α_1 = polarizability of the molecule

Assuming the dipole is a small spherical cavity in the medium yields:

$$(\epsilon/\epsilon_0 - 1)/(\epsilon/\epsilon_0 + 2) = N/3.E_0(\underset{(1)}{\alpha_1} + \underset{(2)}{\mu^2/(3.k.T)})...(5.2)$$

Thus the polarization depends on two parts:

(1): The first is independent of temperature and depends on the shift of charge within the molecule.
(2): The second decreases its contribution with increasing temperature.

The effect of frequency on polarizability is two fold:
a) In the microwave region: If the natural frequency is much greater than the frequency of radiation then α_1 is independent of frequency
b) When the radiation frequency tends to the natural frequency, α_1 changes. The effect of rotation of the electric moment is strongly dependent on frequency. It has been noted by Debye [21] that at high frequencies the transient collisions between molecules would be so

high that molecules would effectively be prevented from aligning, and the dielectric constant would be low.

Debye [21] first advanced a theory which gives the relation between the real and imaginary parts of the dielectric constant and the frequency of the alternating electric field by solving equation 5.2.

$$\epsilon'(w) = \epsilon'_\infty + (\epsilon'_s - \epsilon'_\infty)/(1 + w^2.\tau^2_0) \quad ....(5.3)$$

$$\epsilon''(w) = (\epsilon'_s - \epsilon'_\infty)w.\tau_0/(1 + w^2.\tau^2_0) \quad ....(5.4)$$

$$Tan(\delta) = (\epsilon'_s - \epsilon'_\infty)w.\tau_0/(\epsilon'_s - \epsilon'_\infty.w^2.\tau^2_0) \quad ....(5.5)$$

The curves of these equations are shown graphically in figure 5.1. The curve of ϵ'' increases from zero, reaches a maximum at $w = 1/\tau_0 = w_m$ of value $\epsilon'' = (\epsilon'_s - \epsilon'_\infty)/2$, and returns to zero with increasing frequency. The curve of ϵ' decreases monotonically from ϵ'_s to ϵ'_∞ and with $w = 1/\tau_0$ reaches a value $(\epsilon'_s + \epsilon'_\infty)/2$.

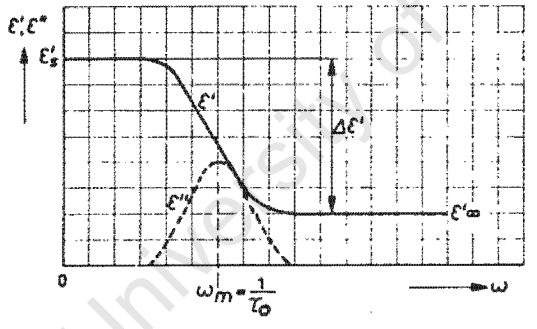

Figure 5.1: The behavior of the complex dielectric constant in the vicinity of the natural frequency

A model of the dipole molecules complex dielectric constant and its behavior has been produced by Cole-Cole [22] as shown in figure 5.2. The dipole molecule is represented by a damped resonant circuit. The imaginary part ϵ'' reaches its maximum value at the natural frequency $w = 1/\tau_0 = 1/R_2.C_2$. Figure 5.3 shows the temperature dependence of ϵ' and ϵ'' by which the natural frequency, w, increases with increasing

temperature. This too shows the decrease of ϵ'' with temperature.

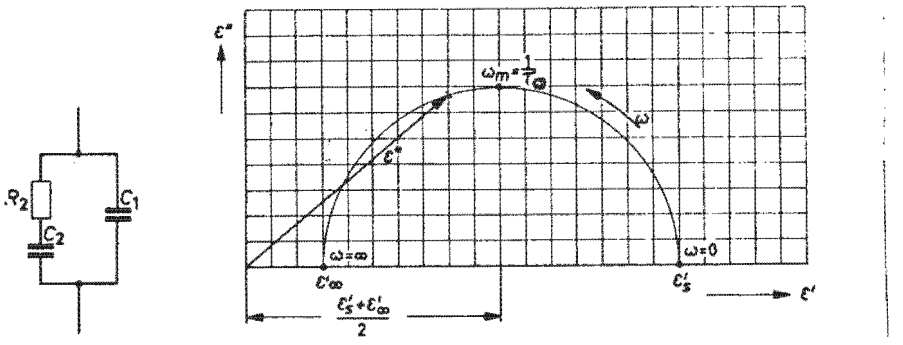

Figure 5.2: The model of the dipole molecules dielectric constant

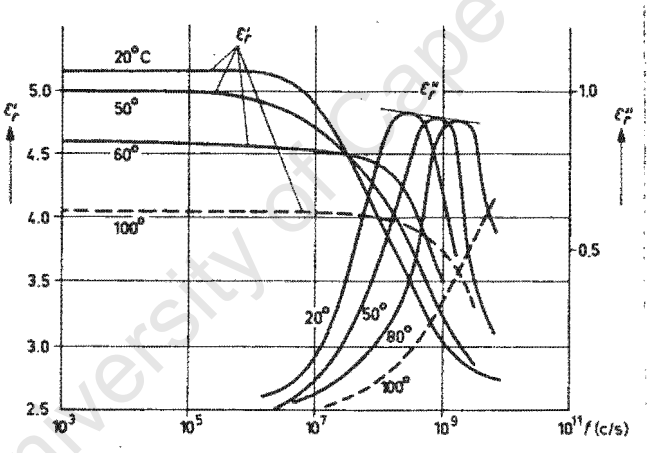

Figure 5.3: The temperature and frequency dependence of the dipole molecules complex dielectric constant

5.3) Dielectric medium in a microwave waveguide

5.3.1) Uniform transmission lines with complex parameters

The presence of a dielectric medium in a waveguide modifies the transmission line characteristic equations by taking into account a complex propagation constant. Thus the transmission line equations are complex:

$$dV/dz = - Z.I$$

$$dI/dz = - Y.V$$

$$\gamma = \alpha + j\beta = \sqrt{(k^2_c - k^2)} \qquad ....(5.6)$$

The attenuation constant, α, and the wave number, $\beta = 2\pi/\tau_g$, are determine by the type of dissipation, the mode in question and the geometry of the waveguide. Similarly the characteristic impedance is also complex, and is given by:

$$Z = 1/Y = \begin{cases} j\omega\mu/\gamma & \text{for M-modes} \qquad ....(5.7) \\ \gamma/j\omega\mu & \text{for E-modes} \qquad ....(5.8) \end{cases}$$

By using the complex relative dielectric constant of equation 5.1a, with a relative permeability of unity, in equation 5.6 gives the propagation constant of:

$$\gamma = \sqrt{((2\pi/\tau_c)^2 - (2\pi/\tau_0)^2 \epsilon/\epsilon_0)}$$

In a waveguide with cutoff wavelength $\tau_c > \tau_0$ the attenuation constant is [23]:

$$\alpha = \pi.\tau_{g0}.\epsilon''/\tau_0^2(1 - x^2/8 \ldots) \quad \text{for } x << 1 \quad ....(5.9a)$$

$$\alpha = 1/\delta.(1 - 1/(2x) \ldots) \quad \text{for } x >> 1 \quad ....(5.9b)$$

and the wave number is:

$$\beta = 2\pi/\tau_{g0}(1 + x^2/8 \ldots) \qquad \text{for } x << 1 \quad \ldots.(5.10a)$$

$$\beta = 1/\delta.(1 + 1/(2x) \ldots) \qquad \text{for } x >> 1 \quad \ldots.(5.10b)$$

where: $\tau_{g0} = \tau_0/(\sqrt{(\epsilon' - (\tau_0/\tau_c)^2)})$ ....(5.11)

$$x = \epsilon''\tau^2_{go}/\tau^2_0 \qquad \ldots.(5.12)$$

$$1/\delta = \pi/(\tau_{g0}.\sqrt{(2x)}) = \sqrt{(w.\mu_0.\sigma/2)} \qquad \ldots.(5.13)$$

Now the characteristic admittance of a propagating mode in a dissipative waveguide is determine using equations 5.9 and 5.10. For H-modes this is given by:

$$Y = \sqrt{(\epsilon_0/\mu_0)}.\tau_0/\tau_{go}.[1 - j(\tau_{go}/\tau_0)^2\epsilon''/2] \quad \text{for } \epsilon''/\epsilon'<<1 \quad \ldots.(5.14)$$

$$Y = \sqrt{(\epsilon_0/\mu_0)}.\tau_0/(2\pi.\delta)\{1 - j\} \qquad \ldots.(5.15)$$

Theses are approximations and hold true for the case of $\epsilon''/\epsilon' << 1$ and τ_0 not too close to τ_c.

5.3.2) Matching considerations

As discussed, the efficiency of energy transfer is a function of many variables. Some of these are related to the material and are included in the load admittance, Y. The material dielectric constant is a function of material type and density, excitation frequency, w, and load temperature, a non linear function of the electric field strength, E(r), and is also dependent on the time history of the material temperature and electric field:

$$\epsilon = f(w,E,T,r)$$

During the microwave heating process both the real and imaginary parts of the complex dielectric constant may change because of their dependency on temperature, chemical composition and electric field. Thermal runaway, hot spots within the material, and reduced heating can occur depending on the nature of this

change. These effects cause the material admittance to be nonlinear and variable and results in a mismatched, inefficient processing system.

Electromagnetic coupling depends on the cavity size and geometry, material size and shape, the position of the load in the cavity and the relative size and shape of the material and the cavity. The frequency of the microwave energy also influences the coupling. For a high energy transfer efficiency, with constant or controllable heating, the magnitude of the electric field must be varied as a function of position to compensate for the change in ϵ.

5.4) Microwave digestion system design

5.4.1) Digestion system description

An experimental digestion system was desired as a processing system, to digest all types of loads. Due to many types and sizes of loads to be digested and the different factors affecting the dielectric loads match, a method was needed to adjust the loaded cavities admittance and obtain a good match for all loads over the entire heating process. This can be accomplished by using capacitive tuning screws. A small metal post inserted into a waveguide parallel to the E-field forms a shunt reactance. The tuning screw is thus a variable reactance which increases as the screw is inserted. With a measure of the amount of power being absorbed by the load, the match can be adjusted so that a high energy transfer efficiency can be obtained. The load containers, chosen for their resistance to acids and transparency to microwaves, are teflon vessels. They are generally closed vessels which can digest small samples up to a liter in volume. These have two exhaust ports on the lid for the extraction of acid fumes. These closed vessels will determine the size of the cavity.

High power microwaves are launched into a rectangular waveguide and fed into a loaded cylindrical cavity through a quarter wave transformer. The quarter wave transformer uses the reflections produced at a change in waveguide cross section to match the cylindrical cavity to the rectangular cavity, as shown in figure 5.4a. The return power is measured by using a cross coupler attached to the rectangular wave guide. This consists of a rectangular waveguide section which couples some of the forward and reflected electromagnetic energy down the two different arms of the coupler waveguide. One arm of the coupler is terminated in a resistive card. The

other arm is used to couple a fraction of the reflected energy to a waveguide to coaxial line transformer, and using a detector, a measure of the reflected power can be obtained. Thus, tuning the screws, on line adjustment of the load match can be achieved.

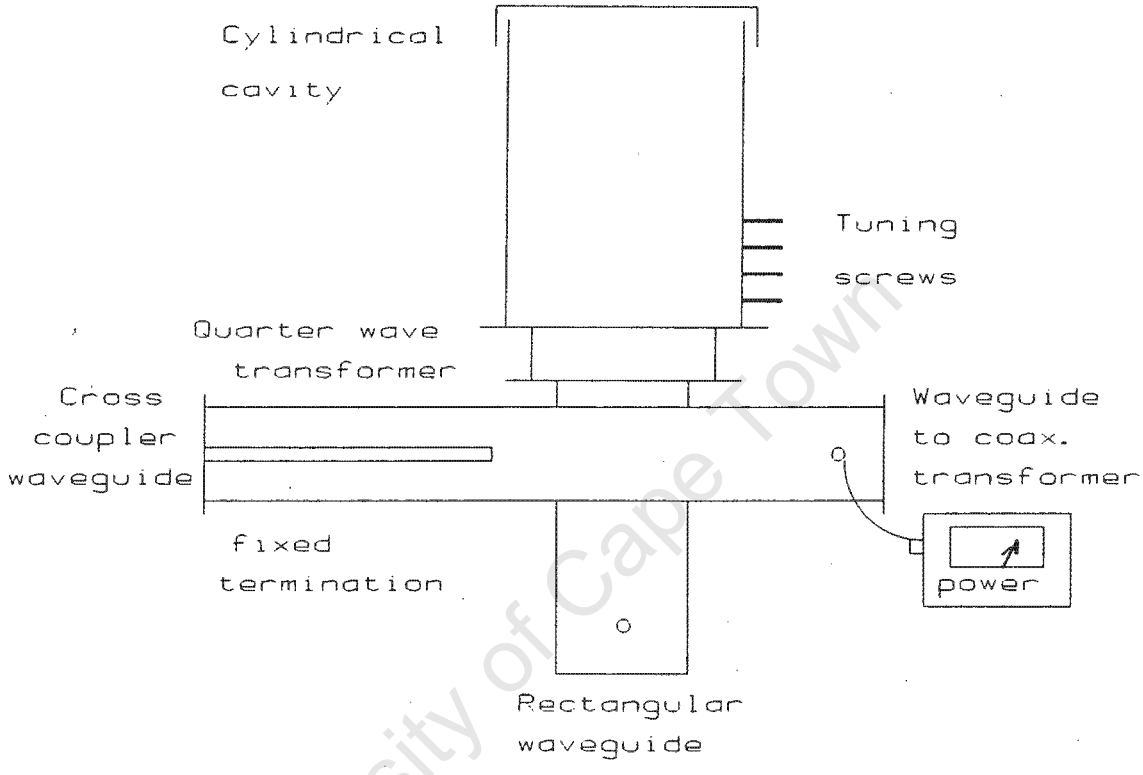

Figure 5.4a: The experimental microwave digestion system

The process will be controlled using a personal computer. For each heating process, the heating parameters can be fed to a control program, which will monitor each digestion process. This requires the measurement of the load temperature and the ability to cycle power to the magnetron. The advantages in using a PC over a microprocessor run system is that there is easy access to the control program for modifying and updating the control process and easy manipulation of the process data for viewing the entire heating process graphically.

5.4.2) Rectangular launching waveguide

The rectangular waveguide will be used to launch the microwaves using a 500 watt magnetron. This magnetron was acquired from a commercial Kenwood microwave oven. The dimensions of the waveguide were chosen to be the same as the original launching waveguide in the Kenwood microwave oven. These dimensions are set for the best match between the magnetron and the waveguide. The sides are 8cm by 4cm as shown in figure 5.4b and figure E1 of appendix E. The free space wavelength at a frequency of 2.45 GHz is 12.2 cm. Thus the waveguide can only house one half wavelength and TE_{01} mode is setup, this is the dominant mode in rectangular waveguide. The cutoff frequency for this waveguide is determined from the cutoff wavelength:

$$\tau_c = 2.a = 2.8 \text{ cm} = 16 \text{ cm}$$

$$f_c = c/\tau_c = 1.88 \text{ GHz}$$

The waveguide wavelength is calculated using equation 4.5:

$$\tau_g = \tau_0/\sqrt{(1 - (\tau_0/2a)^2)} = 12.2/\sqrt{(1 - (12.2/16))}$$
$$= 18.9 \text{ cm}$$

The characteristic impedance of this waveguide is:

$$Z_0 = Z_w.(\tau_g/\tau_0).b/a \qquad \ldots.(5.16)$$
$$= \sqrt{(4\pi x10^{-7}/8.854x10^{-12})}.(1.554).4/8$$
$$= 292.7\ \Omega$$

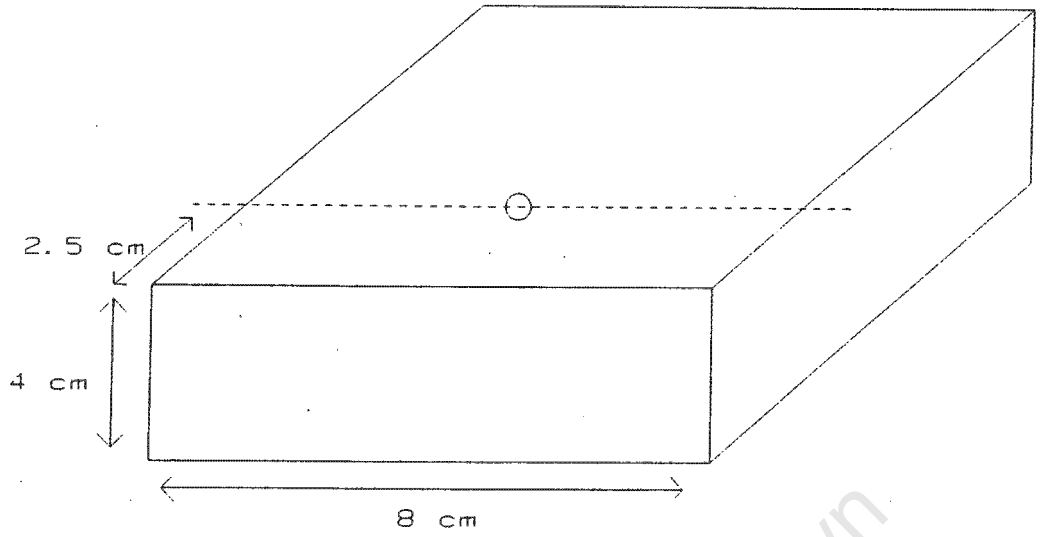

Figure 5.4b: The rectangular launching waveguide

5.4.3) The cylindrical waveguide cavity

The microwaves are fed from the rectangular launching waveguide to the cylindrical cavity which houses the load. The largest closed vessel to be used for digestions has a one liter volume with a diameter of 11 cm and a height of 14 cm. This determines the minimum size of the cylindrical cavity. TE_{11} mode is the dominant mode in cylindrical waveguide and, due to the similarity in E-field and H-field distribution with the TE_{01} mode in the rectangular waveguide, is the most probable mode excited in the cylindrical cavity, see figure 5.5. This mode is desirable as a thermocouple inserted into the cavity will be perpendicular to the E-field and will not couple onto the electromagnetic energy in this mode.

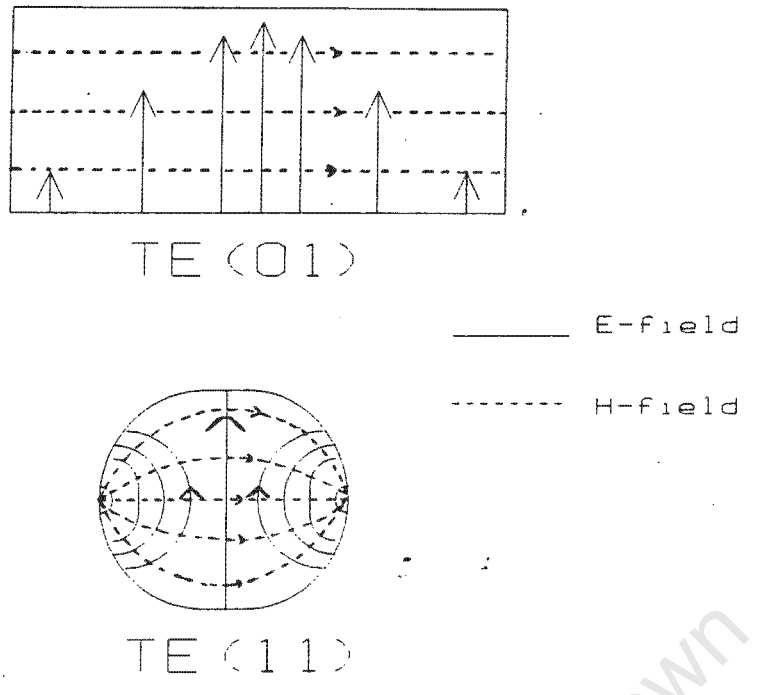

Figure 5.5: Mode transformation between rectangular waveguide, TE(01), and cylindrical waveguide, TE(11)

It would be mechanically difficult to roll a cylindrical cavity of these dimensions from durable, strong metal sheeting. Any imperfections in the tubing or bends introduce other components of polarization, which introduce out of phase components and could result in elliptical polarization. The most convenient size of cylindrical piping was acquired with a diameter of 14 cm. This determines the propagation constant, waveguide wavelength and waveguide impedance for the cavity . Using equation B.6 for the TE_{11} mode, X'_{np} = 1.841, and an excitation frequency of 2.45 GHz:

$$\beta_g = \sqrt{(((2\pi f)^2.\mu\epsilon - (X'_{np}/a)^2)} \quad \text{where: } a = \text{cavity radius}$$

$$= \{(2\pi.2.45\times10^9)^2 - (1.841/0.07)^2\}^{-0.5}$$

$$= 44.1$$

From equation B.7 and B.8 the cutoff frequency and waveguide wavelength are calculated respectively:

$$f_c = X'_{np}/(2\pi.a.\sqrt{(\mu\epsilon)}) = 1.841/(2\pi a.\sqrt{(\mu\epsilon)})$$

$$= 1.26 \text{ GHz}$$

$$\tau_g = \tau/\sqrt{(1 - (f_c/f)^2)} = 14.3 \text{ cm}$$

Finally, the cylindrical cavity impedance is calculated using equation B.9:

$$Z_g = 2\pi f.\mu/\beta_g = 438.7\ \Omega$$

The tuning screws must be positioned below the load in the cylindrical cavity. The screw forms a shunt reactance when inserted in a waveguide. As its length is varied inside the waveguide a variable reactance is created. Four tuning screws were used along the base of the cylindrical cavity each one eighth of a wavelength apart. This will ensure that the load is matched to the magnetron. The height or the cylindrical cavity was set at 36 cm to allow 13 cm for the tuning screws positions and for the load vessel height of 14 cm. The cylindrical cavity is shown in figure E5 of appendix E.

Above the load the cavity was short circuited with a metal lid. This can be twisted and removed for placing a new load for digestion. The lid has a quarter wave flange covering the top of the cylindrical cavity, as shown in figure E6. This prevents any microwaves from escaping the cavity as an open circuit at the end of the flange will be transformed to a short circuit at the cavity lid a quarter wavelength, 3.6 cm, away.

A theoretical analysis was done to determine what other modes could be excited in the cavity, and to calculate the extent to which the load could be expected to change. As the waveguide dimensions and the frequency of the wave do not change, the product (k_c/a), equation B.5, is constant.

$X'_{np} = k_c.a$ where: k_c = the mode wave number

$= (w\sqrt{(\mu\epsilon)}).a$ a = cavity radius

$= 3.59$

Thus in order for a mode to propagate it must have a product $(k_c.a)$ less than or equal to 3.59. The only other electromagnetic modes, besides TE_{11}, which satisfy this requirement are TE_{21} and TM_{01}:

TE_{11}: $k_c.a = 1.841$

$f_c = 1.256$ GHz

TE_{21}: $k_c.a = 3.054$

$f_c = 2.083$ GHz

TM_{01}: $k_c.a = 2.045$

$f_c = 1.395$ GHz

However if a waveguide is filled with a dielectric, the cutoff wavelength in the dielectric is increased by the square root of the relative dielectric constant, $\epsilon_{r(1)}$,

$$\tau_{c(1)}/\tau_{c(air)} = \sqrt{(\epsilon_{r(1)})},$$

and the attenuation and waveguide wavelength are altered. For water $\epsilon = 80$:

$\tau_{c(air)} = \tau_c/\sqrt{80} = 1.743(a)/\sqrt{80}$

$= 1.3$ cm

$f_c = 21.99$ GHz

Now using equation B.7 the product $(k_c.a) = X'_{np}$ can be calculated:

$k_c.a = 2\pi.a.f_c/\sqrt{(\mu\epsilon)} = 32.2$

Modes which propagate in the dielectric medium must have a (k_c.a) product less that or equal to 32.2. Under these conditions any TE_{np} and TM_{np} modes can be excited in the dielectric medium. Higher order modes are also set up at the discontinuities of a dielectric and with its change in shape. There are problems resulting from the excitation of these higher modes:

a) Power is transferred from the main mode to the higher order modes, which not being matched to the load and below cutoff of the launching rectangular waveguide, would set up standing waves in the cylindrical waveguide.

b) The thermocouples could couple onto the higher order modes, any mode with an E-field component parallel to the thermocouple, and yield erroneous readings.

Using the derived equations of a dielectrically loaded waveguide in section 5.3, the complex impedance can be calculated for each electromagnetic mode. Values of the complex dielectric constant of water at temperatures of 1 to 95 degrees celsius were obtained in [19] and were used to determine the extent to which the dielectric constant of water changes with temperature. The results of a water load impedance at 25 °C and 85 °C follow:

a)Water load at 25 °C:

Tan(δ) = 0.157 radians, and ϵ' = 76.7, therefore ϵ'' = 11.94. The impedance of the water loaded cylindrical waveguide represented to the different modes at this temperature is shown in table 5.1.

Mode: np	TE_{11}	TM_{01}	TE_{21}	TE_{33}	TE_{14}
α	35.1	35.1	35.2	37.5	38.6
β	451.6	451.1	450.3	422.6	410.7
Z [Ω]	29.5 - j20.8	29.4 - j20.1	29.4 - j20.2	30.1 - j22.0	30.3 - j22.8

Table 5.1) Complex impedance for modes in a water loaded cavity at 25 °C

b) Water load at 85 °C:

Tan(δ) = 0.047 radians, and ϵ' = 56.5, therefore ϵ'' = 3.08. Table 5.2 shows the impedance of the water loaded cavity for each mode at 85 °C.

Mode: np	TE_{11}	TM_{01}	TE_{21}	TE_{33}	TE_{14}
α	10.6	10.6	10.6	11.6	12.1
β	386.0	385.4	384.4	351.4	337.0
Z [Ω]	48.3 + j9.93	48.3 + j9.96	48.5 + j10.0	52.6 + j11.89	54.6 + j12.88

Table 5.2: Complex impedance for modes in a water loaded cavity at 85 °C

Both the above tables of results are listed in order of increasing (k_c.a) product values. The impedance of the loaded waveguide varied only slightly with each mode. For both temperatures, the calculated attenuation constant increased and the phase constant decreased as the modes became closer to cutoff. There was a small change in the complex impedance of the loaded waveguide as seen by the different modes at the same temperature.

The impedance tended to increase as the mode approached cutoff. This increase was more marked at the higher temperature. The effects of a change in load temperature were more marked. There was a large decrease in the attenuation constant and the phase constant for each mode at a higher temperature. The change in the complex impedance with temperature was also quite large. Here the real part of the impedance increased and the imaginary part of the impedance decreased with temperature. Thus the effect of a change in temperature has a greater effect on the match of microwave power than does a change in electromagnetic mode.

5.4.4) The quarter wave transformer

As discussed, the quarter wave transformer matches the microwaves from the rectangular waveguide to the cylindrical cavity. The dimensions of the transformer are chosen to provide the correct impedance to match rectangular waveguide to the cylindrical cavity. Figure 5.6 shows the transmission line schematic diagram of this load transformation. The transmission line equation is:

$$\frac{Z_{in}}{Z_0} = \frac{\{Z_L.\mathrm{Cos}(wL/c) + jZ_0.\mathrm{Sin}(wL/c)\}}{\{Z_0.\mathrm{Cos}(wL/c) + jZ_L.\mathrm{Sin}(wL/c)\}}$$

where: L = electrical length of the transmission line

Z_L = load impedance

Z_0 = waveguide characteristic impedance

If $L = \tau_g/4$ then $wL/c = 2\pi.f.L/c = \pi/2$

$$\frac{Z_{in}}{Z_{01}} = \frac{\{Z_L.\mathrm{Cos}(\pi/2) + jZ_{01}.\mathrm{Sin}(\pi/2)\}}{\{Z_{01}.\mathrm{Cos}(\pi/2) + jZ_L.\mathrm{Sin}(\pi/2)\}}$$

$$= Z_{01}/Z_L$$

Now a match is required such that: $Z_{in} = Z_0$:

$$Z_{01} = \sqrt{(Z_0 . Z_L)}$$

For the quarter wave transformer with $Z_L = 438.7\ \Omega$ and $Z_0 = 292.7\ \Omega$:

$$Z_{01} = \sqrt{\{(438.7).(292.7)\}} = 358.3\ \Omega$$

Using equation 5.16 the dimensions of the quarter wave transformer are found. The width, a, and height, b, of the transformer must be chosen to be the best intermediate waveguide step transition between the rectangular waveguide and cylindrical cavity. After some trial and error these were found to be:

$$Z_{01} = Z_w . (\tau_g/\tau) . b/a = 358.3\ \Omega$$

$$b/a = 0.612$$

Therefore: a = 11.0 cm

b = 6.7 cm

$L = \tau_g/4 = 4.74$ cm

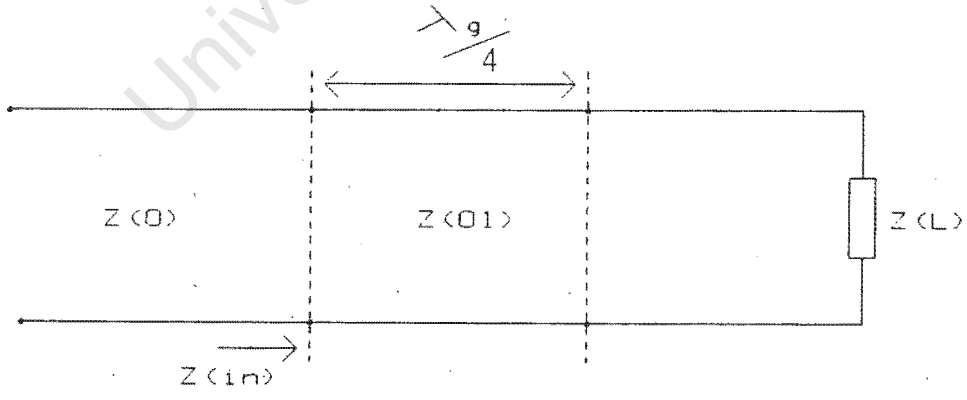

Figure 5.6: Schematic diagram of a quarter wavelength transformation

5.4.5) The directional cross coupler

a) Introductory theory to directional couplers

A directional coupler is defined as a junction of four transmission lines, (1), (2), (3) and (4), such that all the lines are terminated in their characteristic impedances, see figure 5.7 [20]. The terminals are matched and there is negligible coupling between (1) and (3) and (2) and (4). A wave incident on line (1) leaves by lines (2) and (4). A wave incident on line (2) leaves by lines (3) and (1). Thus the powers absorbed by matched loads on arms (3) and (4) indicate the microwave power travelling past the coupling junction in line (1) and (2) in the two directions.

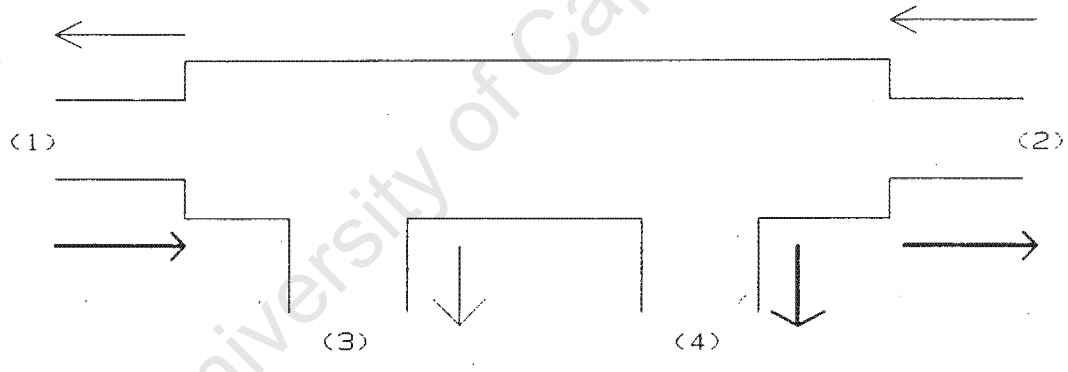

Figure 5.7: Four junction directional coupler

The characteristics of a directional coupler are described using the terms "coupling" and "directivity", and the standing wave ratio in the main transmission line [24]. The coupling and directivity are shown schematically in figure 5.8. The coupler is designed so that ideally $P_b = 0$, but it will have a some value which is small compared to P_f. The coupling is:

$$C = 10.\log_{10}(P_i/P_f)$$

The quality of the coupler is measured by its directivity. This is a measure of amount of power coupled to the detector from a wave travelling in the opposite direction to that of the desired coupled wave. The directivity is defined as:

$$D = 10.\log_{10}(P_f/P_b)$$

The standing wave ratio, which is measured in the main line, looking in the direction of the wave to which the coupler is sensitive (with the other end matched), is also defined as a characteristic of a directional coupler.

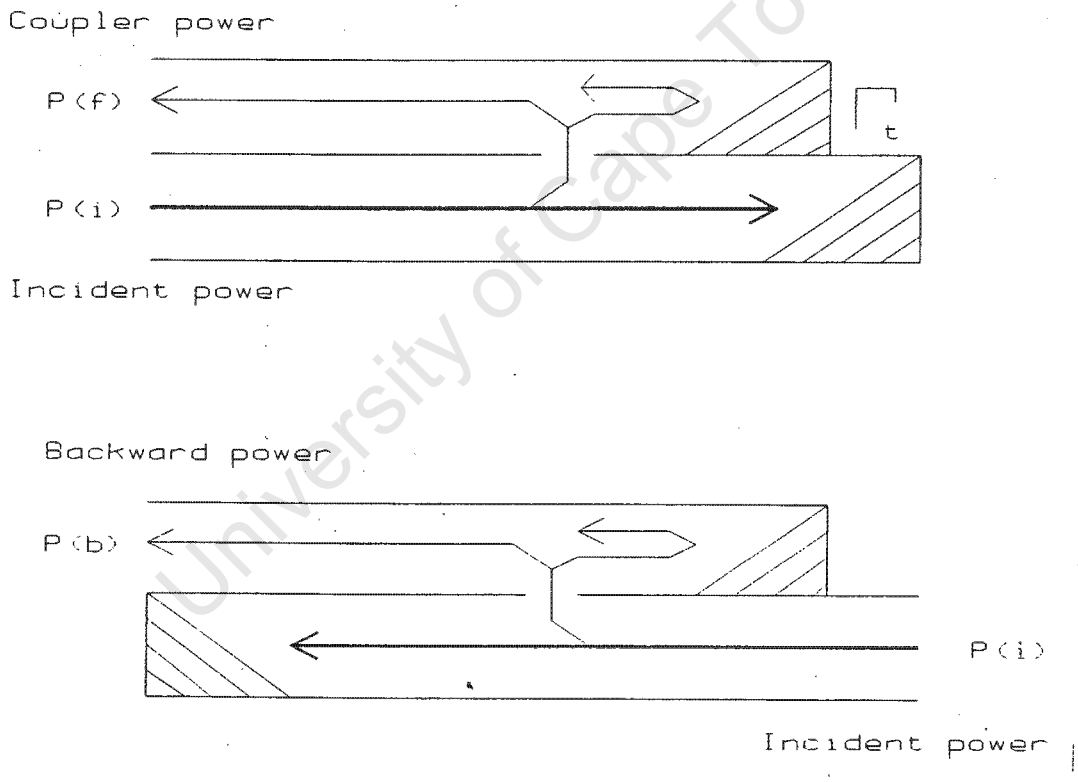

Figure 5.8: Definition of coupling and directivity

A microwave system often needs to monitor the amount of power being transferred down the transmission line or waveguide. A directional coupler measures the forward going wave or reflected wave power using a single detector. The directional coupler couples onto a

fraction of the wave power in the preferred direction, to a detector, through a waveguide to coaxial transformer. The power coupled from the wave travelling in the other direction propagates down the second directional coupler arm which is terminated in a matched impedance. This fixed termination reduces the directional coupler to a three terminal pair network. The backward coupled power, P_b, is made up of two components. The directional element of the coupler contributes an amount P_0, caused by the backward wave. The termination also receives an amount of power equal to P_f as the directional element is a symmetrical structure. This is large compared to P_0. Any reflection from the fixed termination will go largely to the output terminal and will contribute to P_b. If Γ_t is the terminations reflection coefficient then the backward wave will be the vector sum of these two sources, with $e^{j\phi}$ being the possible phase relationship. Defining the reflection coefficients:

$$\Gamma_d = \sqrt{(P_b/P_f)}$$

$$\Gamma_0 = \sqrt{(P_0/P_f)}$$

Then: $$\Gamma_d = [\Gamma_0 + \Gamma_t . e^{j\phi}]$$

$$D = -20.\log(\Gamma_d)$$

The directional cross coupler was designed for the microwave digestion system to measure the amount of power being reflected from the load back to the magnetron.

b) The two hole cross coupler

This coupler consists of a rectangular waveguide connected across the launching rectangular waveguide by means of a coupler plate. It has the same dimensions as the launching waveguide giving it the same waveguide wavelength and cutoff frequency. Figure 5.9 shows a diagram of this coupling mechanism. The coupler plate

consists of a conductive metal plate inserted between the two waveguides. Microwaves are coupled to the auxiliary guide through two coupling holes displaced a quarter wavelength apart in the horizontal and vertical directions. Power coupled to the auxiliary guide from a wave travelling in the forward direction of the main guide, P_i, can propagate to the left and to the right. The two coupled waves propagating to the left will be in phase and constructively interfere. However, the two waves travelling to the right will be 180° out of phase and cancel giving no microwave propagation. The coupling and directivity of the cross coupler are determined experimentally by varying the size of the coupling holes, and the frequency of operation is determined by the position of the coupling holes. A coupler plate was used as it can easily be removed to change these variables.

For the detection of reflected power the waveguide to coaxial line transformer must be situated to the right of the auxiliary guide (1). The fixed termination is positioned on the left arm of the auxiliary guide to absorb the power coupled from a wave travelling in the forward direction of the main guide, the undesired direction. For a good quality directional coupler a high directivity is required, +/- 20 dB, and good fixed termination is needed to prevent any power being reflected to the detector.

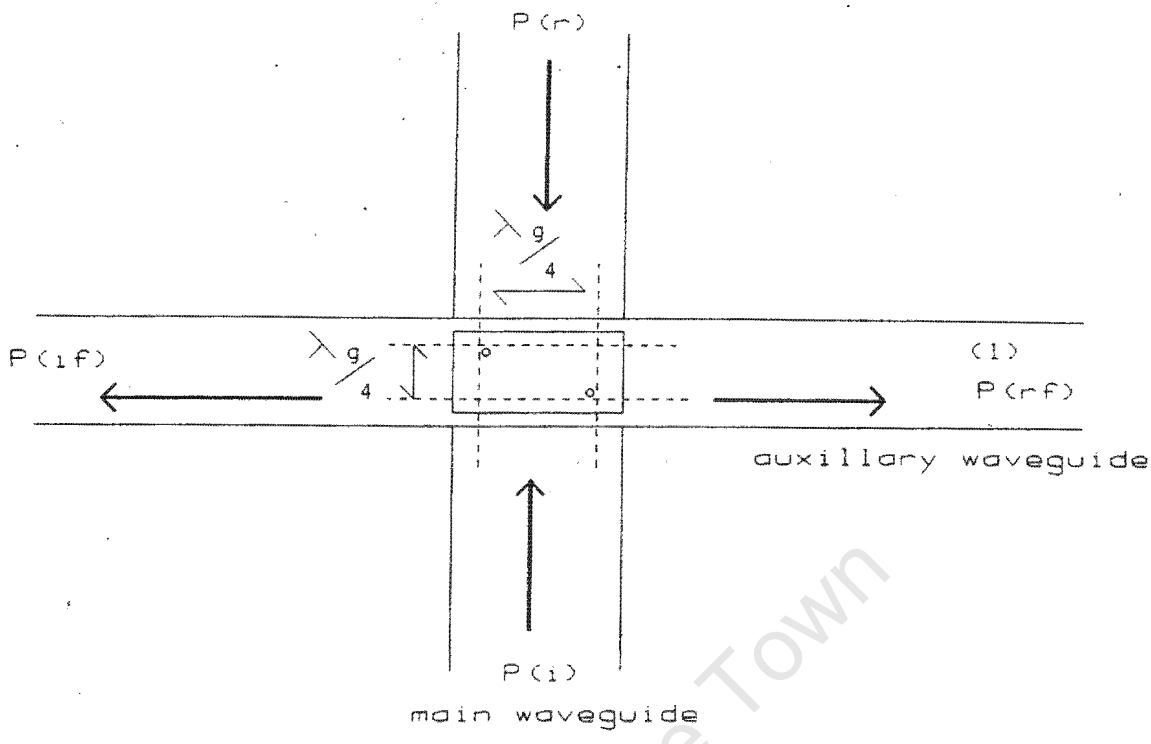

Figure 5.9: The coupling mechanism of the two hole cross coupler

c) The fixed termination

This terminates the unused port of the cross coupler into a matched load. The termination is made using a tapered strip of resistance card placed in the center of the waveguide, in the direction of the E-field, and touches the two broad walls of the waveguide. This ensures that the resistance card couples onto the maximum E-field component in the guide. For a broader band match, double tapered strips can be used which can be placed side by side and shifted with respect to each other. This is then supported by a short circuit block at the end of the waveguide.

The tolerance of the match increases as the taper length increases. The angle of the taper should be as flat as possible to reduce reflections caused by a mismatch. A taper length of half a wavelength is usually adequate

for single taper design. The attenuation per unit length, A, of a resistance strip in a rectangular waveguide decreases linearly with increasing resistivity, Ω, measured in ohms per square. The following formula has been worked out empirically [25]:

$$A = 5.0 - 0.38.\Omega/100 \quad [dB/in.]$$

for: $\tau_0 = 10$ cm

$a = 7.5$ cm, $b = 3.8$ cm

Mylar resistance card was used with a resistivity of 100 Ω/in.

$$A = 5.0 - 0.38 = 5.62 \quad [dB/in.]$$

Thus for 30 dB attenuation the resistance card must have a length of 16 cm. To be certain of a good termination the card was made to be 25 cm with a tapered section of one waveguide wavelength, 19 cm. The unnecessary card can be trimmed experimentally. Figure 5.10 shows a diagram of the fixed termination.

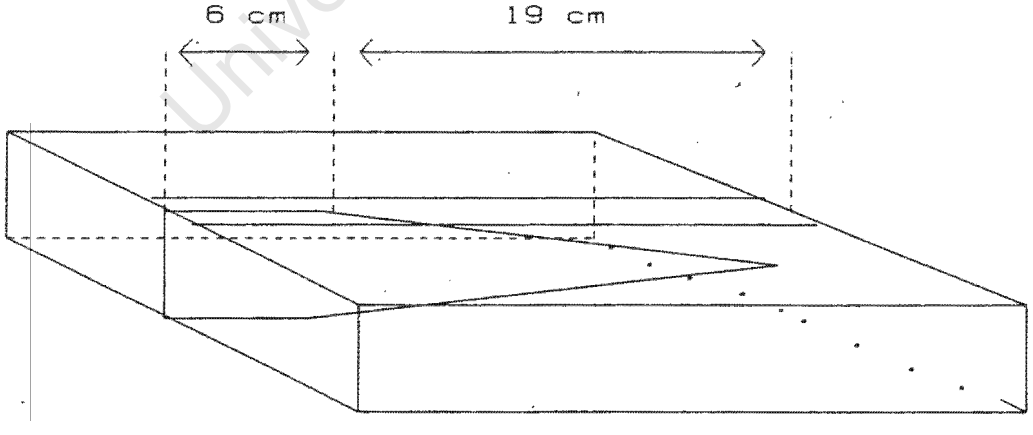

Figure 5.10: The fixed termination

d) The waveguide to coaxial line transformer

This consists of a short circuited rectangular waveguide with an E-field probe centered in the maximum E-field position (the center of the broad side of the waveguide), and positioned approximately a quarter wavelength, 4.7 cm, from the short circuit plate. At this position, the reflected wave from the short circuit plate is lagging in phase by 360°, and the forward and reflected waves add forming a peak in the standing wave.

It has been shown by Slater [25], that a match between the coaxial line and the waveguide can be achieved by varying the length of the probe and its distance from the end plate. The coaxial stub acts as a variable reactance in series with a waveguide antenna. By varying the length of the short circuited section the radiation resistance of the antenna is varied . It is, therefore, possible to make the reactance of the antenna zero and the resistance Z_0.

5.4.6) Final digestion system construction

The rectangular waveguide, cross coupler and quarter wave transformer were constructed from brass sheeting. Figure E1 of appendix E shows the design of the rectangular waveguide. The launching probe position is marked 2.5 cm from the bottom of the waveguide. The guide was raised 7 cm on a base to allow for the positioning of a fan duct for the cooling of the magnetron. The front view shows two side flaps were fitted to hold the magnetron in place. The waveguide extends 20 cm in length, the upper part is used for the positioning of the cross coupler. A window was cut in the top of the waveguide to fit the coupler plate. The side view of figure E1 shows two side flaps at the top of the guide for the fitting of the cross coupler

waveguide over the coupler plate. A round flange was soldered to the top of the waveguide (see the top view) to attach the quarter wave transformer.

The cross coupler design is shown in figure E2. The top view shows the terminated arm, 25 cm in length, with a slot on the broad waveguide face and a removable back plate for the positioning of the resistance card. The other coupler waveguide arm houses the waveguide to coaxial line transformer. This has a removable back plate for the insertion of brass washers which are used to vary the short circuit position from the E-field probe. The position of the SMA launcher is marked in the center of the guide, 4.5 cm from the short circuit plate. A window was cut on the broad face of the waveguide to fit over the coupling plate. The front and side views show the side flaps used to attach the coupler waveguide to the rectangular waveguide. Figure E3 shows the design of the coupler plate.

The design of the quarter wave transformer is shown in figure E4. This has a height, width and length of 6.7 cm, 11 cm and 4.7 cm respectively, as designed. Two circular flanges were soldered to the top and bottom of this transformer to attach it to the rectangular and cylindrical waveguides.

Figure E5 shows the design of the cylindrical cavity. This cavity was constructed from stainless steel piping 14 cm in diameter, with a height of 36 cm. The tuning screws are set 1.8 cm apart, 2 cm from the bottom of the guide. Copper screws, 5 cm long, were used each with a nut to set the individual screw positions. Two brass ledges were soldered to the top of the cavity for the housing of safety switches. These switches are closed circuited when the cavity lid is in place. The cylindrical cavity lid is shown in figure E6. The

quarter wave flange of the lid, used to ensure no microwaves escape, can be seen in the side view. The top view shows two side flaps which close the safety switches of the cylindrical cavity when the lid is twisted into position.

These parts were constructed and the system assembled in the university engineering workshop. Appendix E shows a picture of the assembled digestion system. Microwave testing was performed using a scalar network analyser in the laboratory. The results follow in section 5.5.

5.5) Digestion system microwave testing

5.5.1) The cylindrical cavity match

Low power microwaves were fed into the waveguide using the network analyser. An N-type launcher was fitted to the rectangular waveguide for this purpose. The size of the E-field probe was adjusted until a good unloaded match was achieved. The unloaded cavity was short circuited using the lid. Now the tuning screws depth can be varied to see the effect on the cavity match. The unloaded cavity match displayed a return loss of - 26 dB, this was very high Q and consequently had an extremely narrow band match. Adequate variation of the frequency of the match was achieved by tuning the screws depth in the cavity. This unloaded narrow band match was in contrast to the match obtained once the cavity was loaded. Here, the maximum load of one liter was positioned in the cylindrical cavity. An excellent wide band match was achieved for this loaded cavity and a return loss of - 28 dB was observed at a frequency of 2.45 GHz. The resonant curve fall off was extremely shallow with an observed match of - 20 dB and - 22 dB at 2.40 Ghz and 2.50 GHz respectively. Thus with extreme loading of the cylindrical cavity a very wide band, low Q, match was obtained.

5.5.2) The waveguide to coaxial line transformer matching

The waveguide cross coupler was tested on the network analyser to match the coaxial line to the waveguide via an E-field launching probe. The window of the cross coupler was sealed with a solid brass plate and a tapered piece of resistance card, as designed, was placed in the termination arm to match the opposite side of the coupler waveguide. Figure 5.11 shows this experimental setup. The SMA launcher was initially positioned a quarter wavelength away from the end plate, $D = \tau_g/4 = 4.7$ cm. However, inserting the E-field probe at this position achieved the best match at a frequency of 3.2 GHz. In order to move this match down in frequency to 2.45 GHz, D was increased and the probe length and thickness was increased. This resulted in an observed return loss of -25 dB over a frequency band from 2.4 GHz to 2.5 GHz.

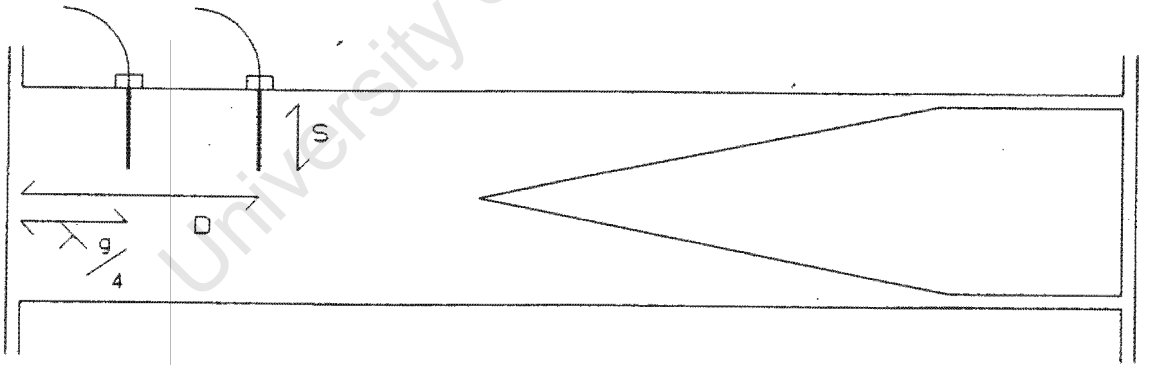

Figure 5.11: Waveguide to coaxial line transformer matching

5.5.3) Testing of the cross coupler

The cross coupler was tested on a scalar network analyser as two traces can be plotted simultaneously (channels A and B). The resistance card was removed from the terminated arm of the cross coupler and a Hewlett Pachard waveguide to coaxial line transformer (model 5281 A) was connected. This allowed the constructive and destructive waves of the cross coupler to be viewed together on the network analyser. Thus the coupling and directivity could be directly measured during the testing procedure. This experimental setup is shown in figure 5.12.

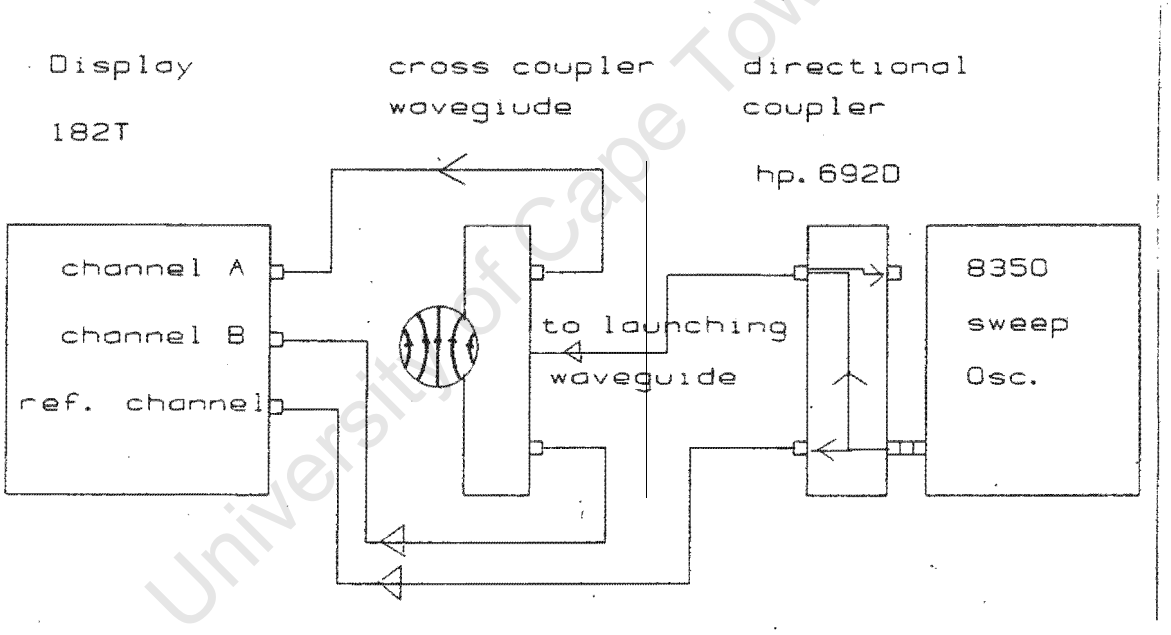

Figure 5.12: The cross coupler test setup

Figure 5.13 shows the port locations on the digestion system for the measurement of coupling and directivity.

Coupling: $C = S_{12}$ [dB]

Directivity: $D = S_{13} - S_{12}$ [dB]

Port 1 was matched with a return loss of - 26 dB. This was done with the lid of the circular cavity removed. Therefore matching the probe cancels the mismatch between the cylindrical cavity and free space.

Terminating the cylindrical cavity with a short circuit, with the lid in position, would cause a large standing wave ratio to exist down the structure which would interfere with the coupling and directivity.

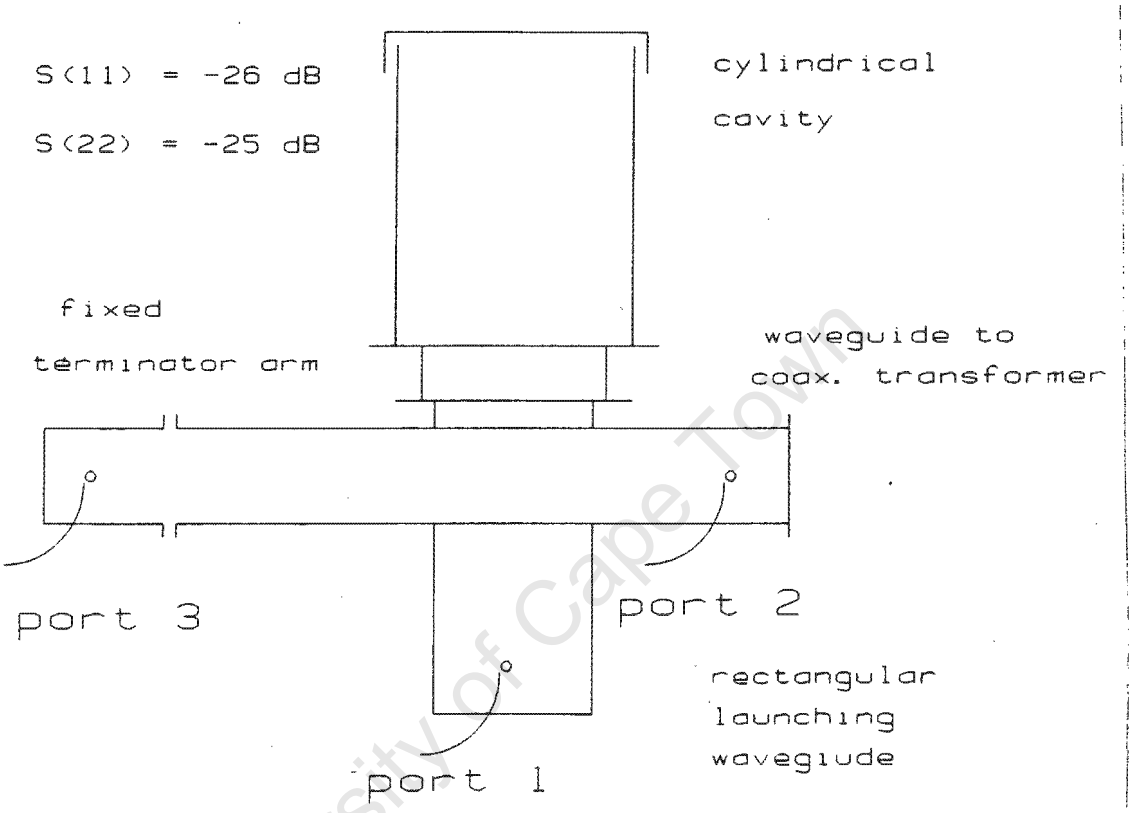

Figure 5.13: Digestion system port locations

Firstly, the coupling plate was inserted and the leakage tested using a microwave power meter connected to a horn antenna. There was no visible leakage of the signal through any possible radiating slots or cracks with the power meter set to maximum sensitivity. If this leakage was too high it would swamp the traces of coupling and directivity.

The coupling, C, required is - 40 dB. Thus with maximum reflection of the microwave power from the load, 500 W, 50 mW would be coupled to the cross coupler probe. A

directivity, D, of - 20 dB was needed. Therefore the second trace on the scalar network analyser must read - 60 dB. The directivity is important as can be seen from the coupled waves from the forward and reflected waves down the main waveguide, see figure 5.14. Thus if the directivity is very low, the forward wave will couple through to the cross coupler probe with a power of - 40 dB. This will swamp the coupled reflected wave which is to be measured. The minimum signal to the E-field probe will be 0.5 mW (- 60 dB) when the load is matched.

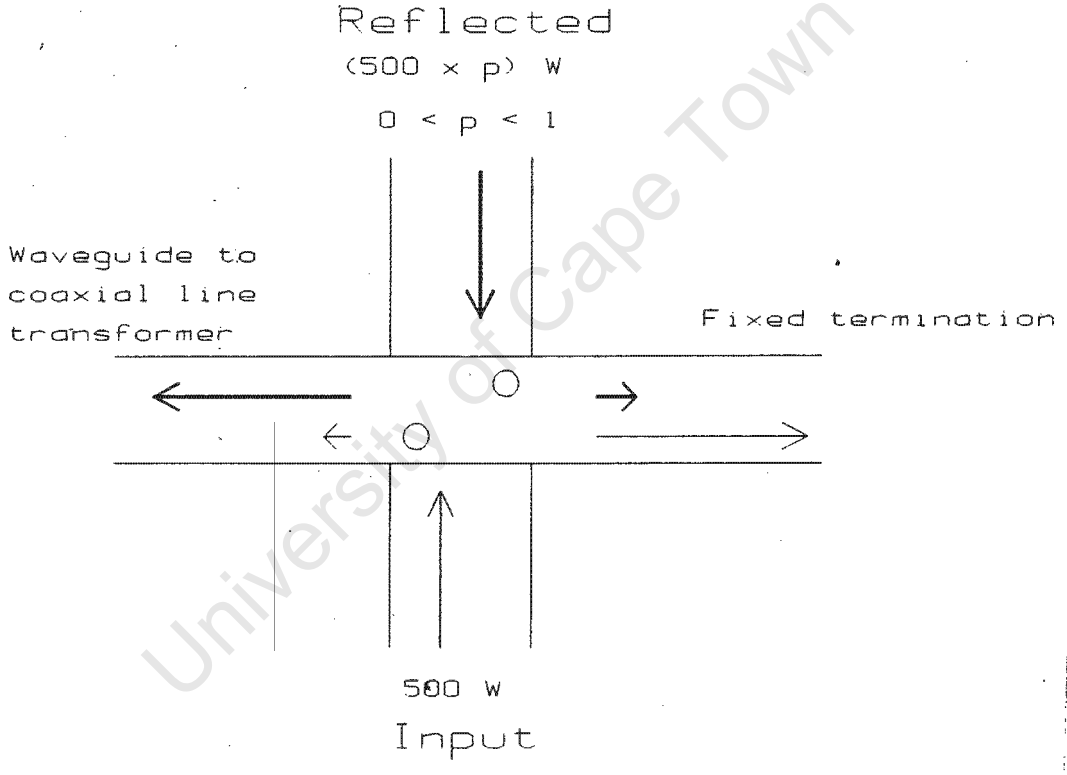

Figure 5.14: The forward and reflected coupled waves in the cross coupler

Small coupling holes were drilled in the coupling plate. The coupling plate was then placed in position between the cross coupler and rectangular launching waveguides. The holes were steadily increased in size, which increases the coupling, C, until the two traces were observable between - 40 dB and - 60 dB. Figure 5.15 shows a diagram of the observed traces with a hole

diameter of 11.7 mm. A suitable trace can be seen at a frequency of 2.59 GHz, giving the required values of coupling and directivity. Decreasing the quarter wavelength distance between the coupling holes will increase the frequency of operation of the cross coupler.

$f_0/f'_0 = \tau'_0/\tau_0 = 0.946$

Therefore: $\tau'_0 = 11.58$ cm

$\tau'_g = \tau'_0/(\sqrt{(1 - (\tau'_0/2.a)^2)}) = 16.8$ cm

Therefore $\tau'_g/4 = 4.2$ cm

A new coupling plate was used with the coupling holes separated vertically and horizontally by this new distance. This resulted in a similar trace to that shown in figure 5.15. There was no downward shift of the trace at 2.59 GHz to 2.45 GHz. The separation distance between the two coupling holes was reduced further but with no effect on the received traces. It was noticed that the two traces shown in figure 5.15 over lapped and crossed each other over the swept frequency range. This indicates that while the coupling to one of the cross coupler arms is good at one frequency, it is bad at another, where the other arm will enjoy the good coupling factor. Transferring the cylindrical cavity termination from an open circuit to a short circuit by slowly lowering the cavity lid, the traces of channels A and B were seen to cross over and assume alternate positions. This was explained as follows. A large standing wave exists down the cavity structure, with large wave peaks. As the cavity lid was lowered to short circuit the cavity, the standing wave pattern shifts relative to the coupling holes. The peaks of the standing wave, being large, may cause an uneven electric field distribution to exist across the coupling holes aperture. Thus, as the load impedance varies and the standing wave moves over the coupling holes, the

coupling mechanism of the electromagnetic wave through the coupling holes will squint, causing the coupling, C, to alternate between the arms of the cross coupler.

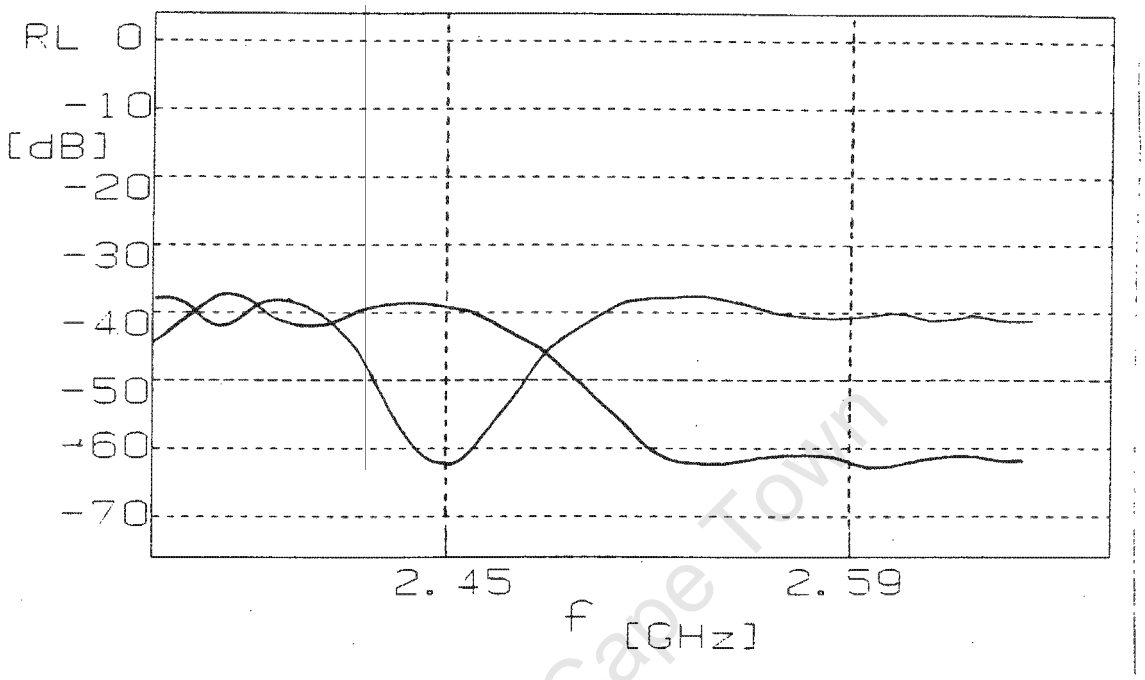

Figure 5.15: Network analyser testing of the cross coupler

Therefore the two hole cross coupler only works for a transmission line with a fixed load. It is not suitable for use in the digestion system where the load is continually variable. The cross coupler was removed from the digestion system and the coupler window was sealed with a brass plate. It was decided, that for experimental digestion procedures where a particular experiment was only needed to be proved feasible, a measure of the reflected power was not necessary. The match achieved for large loads was extremely wide band which would result in a good energy transfer efficiency over the digestion process. Although the match for smaller loads would be more narrow band and more sensitive to a change in the load over the heating process, a lower energy transfer efficiency was needed as smaller loads require less microwave power to reach a set temperature.

5.6) The temperature measurement system

A system was required to measure the load temperature in the cavity up to a maximum of 300°C. Fibre-optical and infra-red temperature sensors proved to be too expensive to purchase. Although these methods are the more accurate and convenient, and do not interact with the microwave field, the building and testing of such a temperature measuring system would be outside the scope of this project. The integrated circuit chip LM35 was considered but it does not have sufficient temperature range. A thermocouple temperature measuring system was then chosen. Thermocouples can be used over a range of temperatures, and optimized for various atmospheres. They are the most rugged and versatile temperature transducers available. A type J (iron-constantan) thermocouple was acquired which has a temperature range of 0°C to 700°C. The excited electromagnetic mode in the cylindrical cavity will have no component of electric field parallel to the thermocouple, thus avoiding any surface currents being formed in the thermocouple, which can cause erroneous reading. However the formation of higher order modes in the dielectric load could cause problems. Some problems in thermocouple operation are discussed below.

5.6.1) Practical thermocouple operation

When two wires, composed of dissimilar metals, are joined at both ends and one end is heated, a continuous current flows in the thermoelectric circuit. If one end is broken, then the net open circuit voltage is a function of junction temperature and the composition of the two metals. This is known as the Seebeck voltage and is given by:

instrumentation amplifier and thermocouple cold junction compensator on a monolithic chip. It uses an ice point reference with a precalibrated amplifier to produce a high level output (10 mV/°C) directly from a thermocouple signal. It includes a thermocouple failure alarm which indicates if the thermocouple leads become open circuit. This alarm output is TTL compatible. The AD594 is precalibrated by laser wafer trimming to match the characteristics of a type J thermocouple to 1% accuracy. The AD594 also has a differential input which rejects common mode noise voltage on the thermocouple leads.

Using a +5 volt supply, the chip configuration is shown in figure 5.16, which will provide a direct output from a type J thermocouple measuring from 0°C to 300°C. The failure alarm was tested as it would be used to detect a break in the thermocouple. The circuit was built to test the linearity of the thermocouple amplifier. A heating test was performed by heating ethylene glycol, which has a boiling point of 200°C, on a hot plate. Comparing the AD594 output voltage with the recorded temperature, using a fluke digital multimeter unit with a type J thermocouple, the chips output transfer function was calculated. A graph of the recorded results is shown in figure 5.17. The AD594 thermocouple linearised the J type thermocouple signal giving an output signal of 7.805 mV/°C.

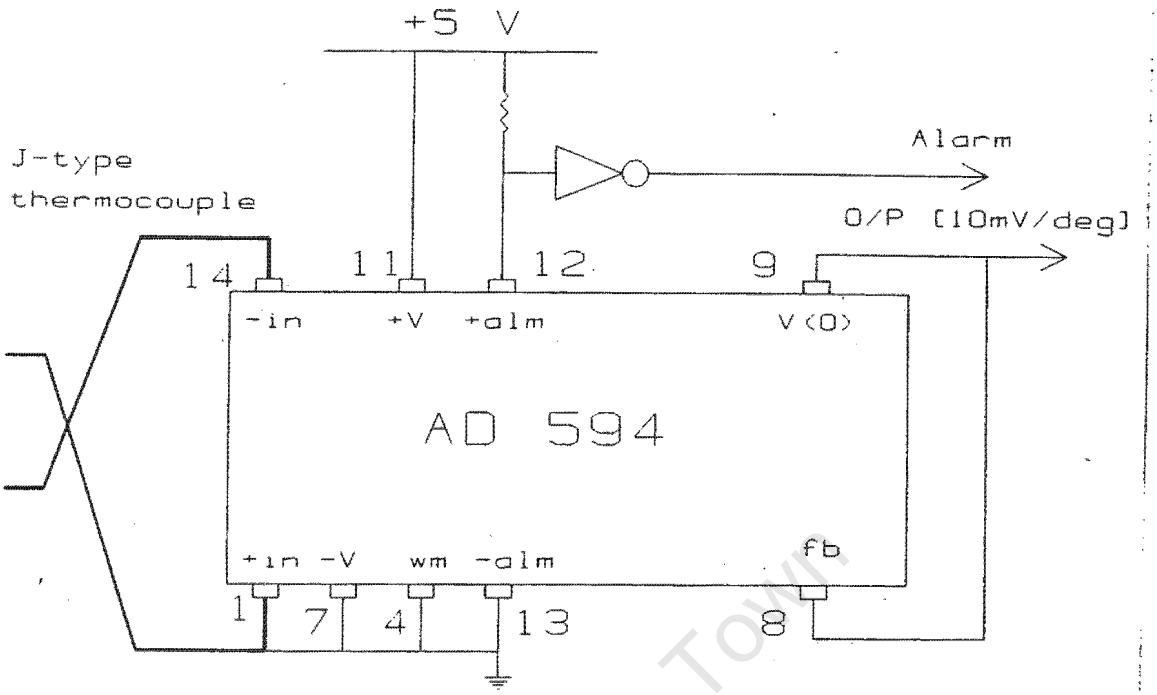

Figure 5.16: AD594 thermocouple amplifier

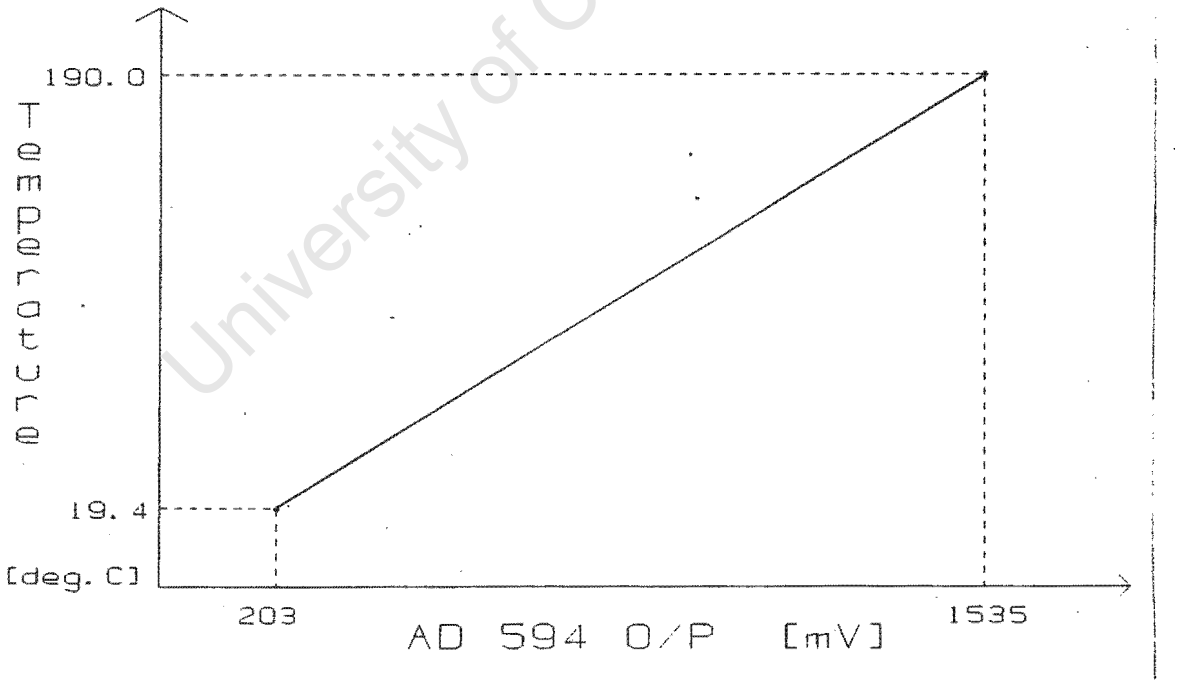

Figure 5.17: AD594 thermocouple amplifier test results

5.7) The computer control system

A microprocessor or computer control system was needed to control the digestion process over three or more heating cycles. This required the measurement of the load temperature into the computer and the time cycling of the magnetron to vary the delivered power. Two microprocessor systems were initially designed to fulfil this purpose. The first design used the 8085 COMPUTER THING developed by the digital systems division of the Electrical Engineering department, UCT. This is a single board microcomputer based on the Intel 8085 microprocessor. This has 8K EPROM and 8K ROM memory. It also contains a 8253 programmable timer which was used to monitor the time of the process, and one 8255 PPI for parallel I/O. A sixteen button keypad was used with an encoder to enter heating process information and four 7 segment LEDs were used together with display drivers for the display of the process information. An assembler program was written and tested for the control of the digestion process over three cycles. A second microprocessor system was designed using a 8052AH microcontroller, this has a complete BASIC interpreter for control programming. This system used a keypad and encoder, LED displays and decoders, RAM and EPROM memory, 8255 PPI, RS232 drivers and an analogue to digital convertor. However it was decided to use a personal computer (PC) to control the digestion process. This is a more versatile system as the control program can easily be accessed for modification. An on-line graphical display of the process can be observed.

5.7.1) Description of the control system

A control program was written in Turbo Pascal 5 for an IBM compatible PC. The PC uses an analogue to digital

converter board (PC-26) to read in the thermocouple voltage via the AD594 thermocouple amplifier. Two thermocouple channels are used, the two data and failure alarm lines are multiplexed to the analogue to digital converter in the PC-26 board. These signals are amplified further to utilize the full dynamic range of the analogue to digital converter. An 8255 PPI board was used to time cycle the magnetron output power via a relay inserted in the magnetron power circuitry. A block diagram of this system is shown in figure 5.18.

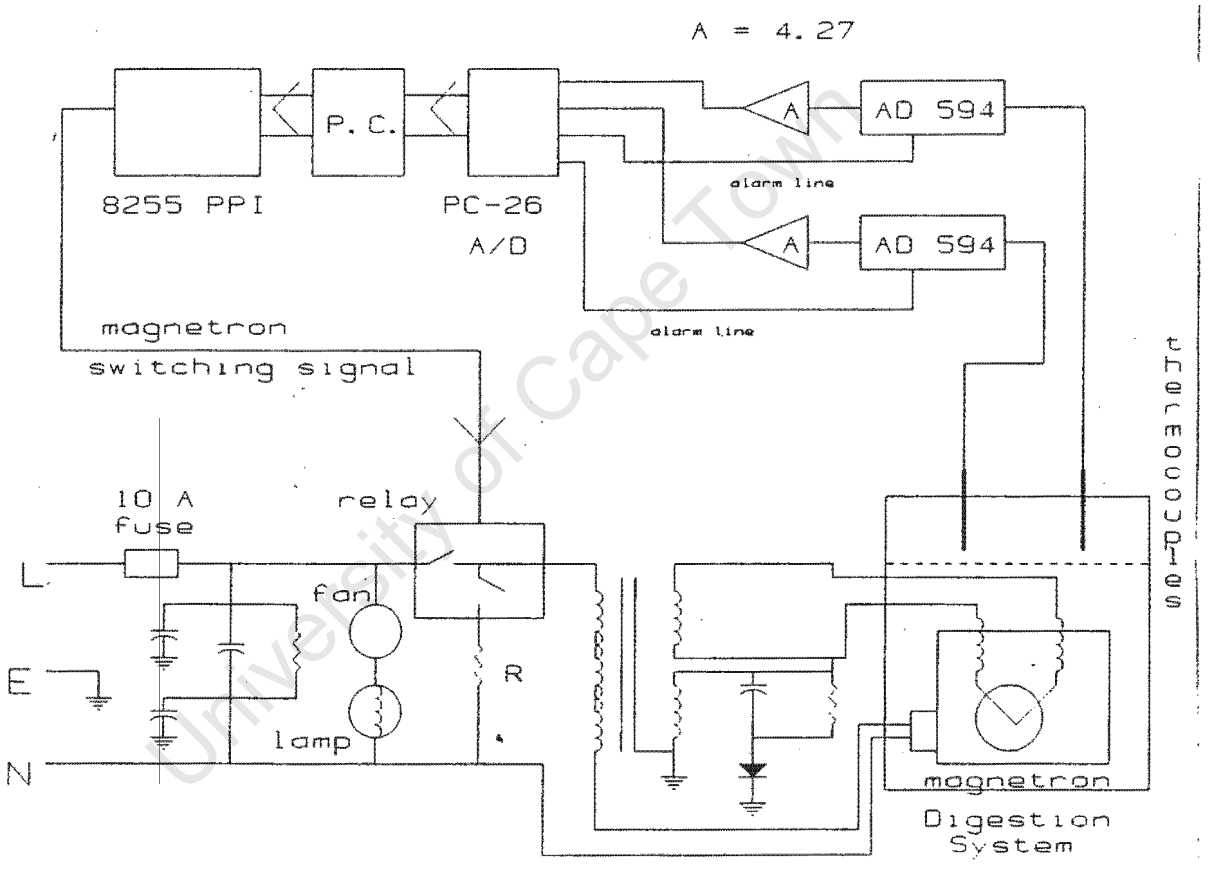

Figure 5.18: The control system block diagram

Figure 5.19 shows the complete circuit diagram of the control system.

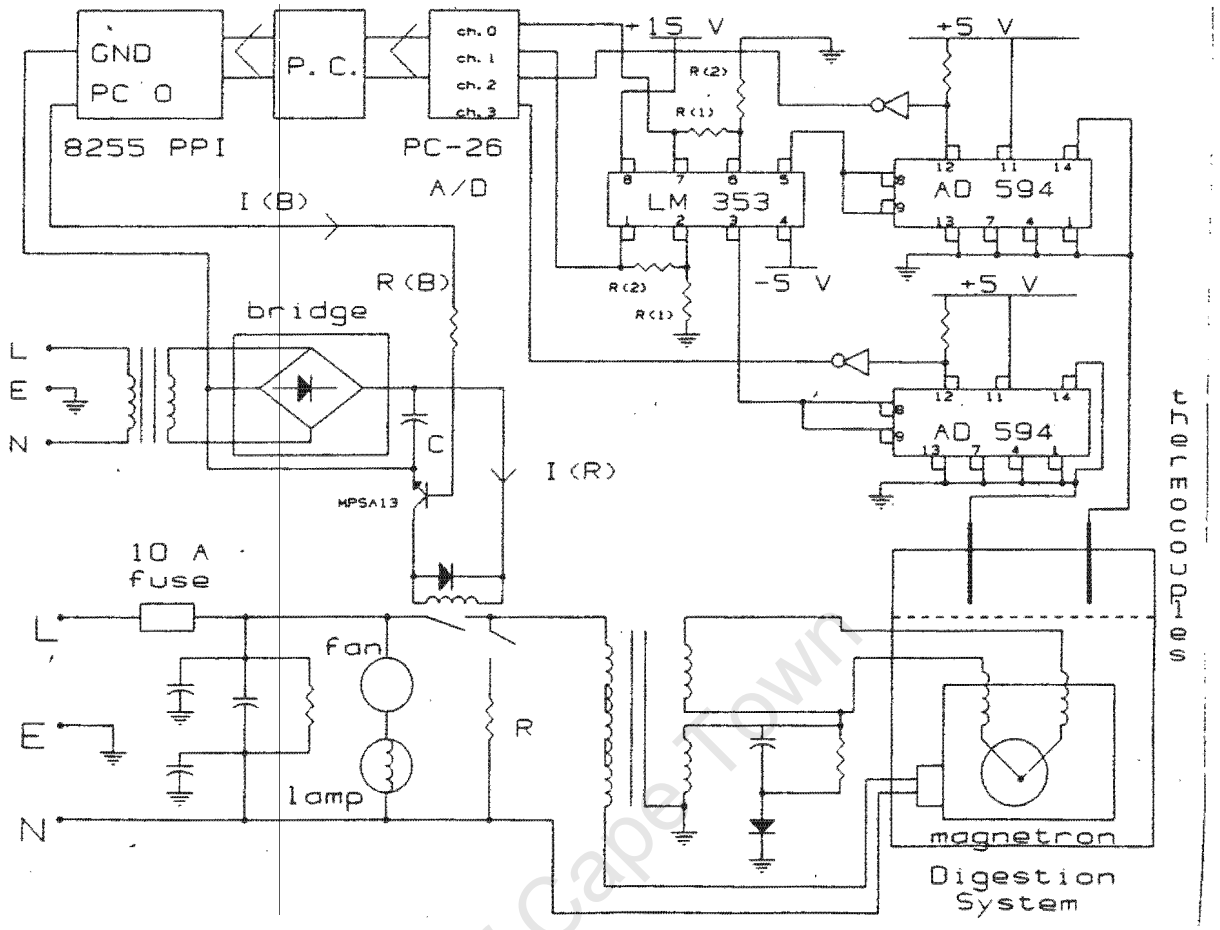

Figure 5.19: The control system circuit diagram

5.7.2) The PC-26 analogue to digital converter board

The PC-26 is a plug in data acquisition board for the IBM and compatible PCs. It includes the A/D converter (AD 574), with a typical conversion time of 25 µs, and a 16 channel multiplexer. The sample rate can be determine by software (using a software clock) or by an inboard programmable timer.

The AD 574 is a 12 bit successive approximation A/D converter. The PC-26 board allows the selection of single unipolar or bipolar input ranges to the A/D converter. The unipolar range (0 V to +10 V) was selected. Zero volts gives a digital output 0, and 10 V gives the digital output 4095 ($2^{12} - 1$) after A/D conversion. Thus a change of 2.441 mV (10/4096) in the

input voltage changes the digital output of the converter by one bit.

The three ports of the 8255 PPI are set to the correct modes by sending the control word 92 Hex to the PPI (Port 703 Hex). This sets up port A and four bits of port B (B0 to B3) as input ports for the A/D output. Port C is programmed as an 8 bit output port for multiplexer channel selection and the software clock control lines.

The turbo pascal conversion sequence for A/D conversion is shown below in FUNCTION ADSAMPLE. This function is called with the multiplexer channel number as its argument, and returns the value of the selected channel to the variable ADSAMPLE.

```
FUNCTION ADSAMPLE(channel:integer):Integer;
  VAR I: Integer;
BEGIN
  Port[$702] := (channel SHL 4) + 2;
  Port[$702] := (channel SHL 4) + 3;
  For I := 1 to 3 do
     Begin      {wait 40 µs for the end of conversion}
     End;
  ADSAMPLE := (Port[$701] AND $0F)*256 + Port[$700];
END;
```

5.7.3) The thermocouple amplifier

As discussed, the output transfer function of the AD594 thermocouple amplifier is 7.805 mV/°C. A temperature range from room temperature (+/- 15°C) to 300°C maximum will yield an maximum output voltage of 2.342 volts.

This signal must be amplified to cover the full range of the successive approximation A/D converter (0V to +10V). This requires an amplifier of gain:

$$A = 10.0/2.342 = 4.27$$

A LM353 dual operational amplifier was used for this purpose. Figure 5.19 shows the two operational amplifiers in the non-inverting configuration where resistors R1 and R2 set the gain of the amplifier, A = R2/R1. Ideally, R1 = 10 kΩ and R2 = 43 kΩ. Using a 50 kΩ potentiometer, the gain can be tuned to cover the full range of the A/D converter.

5.7.4) The magnetron power circuitry

The control circuitry to power the magnetron is shown in figure 5.19. Mains power, 220V, is fed through a 10 amp fuse, across a RC smoothing circuit to the primary of the voltage doubler transformer. This also delivers power to a magnetron cooling fan and a lamp which remain on over the whole process. A heat switch is included in the return path of this circuit which open circuits when the magnetron overheats. Time cycling of the magnetron power is accomplished using a relay inserted on the primary side of the magnetron power circuit. This requires 24 volts d.c. on its switching coils to operate. A step down transformer was used to reduce the 220V mains line voltage to 25V a.c. This was followed by a bridge rectifier and a shunt capacitor to obtain 24V d.c. The resistance of the relay was measured to be 433 Ω, thus the relay current is:

$$I_R = 24/433 = 55 \text{ mA}$$

The maximum ripple on the 24V d.c line determines the capacitor size of the rectifier circuit. A 550 μF (24V) capacitor was used which produced a smooth 24V d.c. An

MPSA13 high power darlington pair transistor was used to switch the relay, as seen in figure 5.19. This transistor has a gain of 5000, thus a collector current of 55 mA requires a base current:

$$I_B = 55x10^{-3}/5000 = 11\ \mu A$$

The transistor is switched by a 5V signal from the 8255 PPI. Therefore the transistor base resistor is:

$$R_B = 5/11x10^{-6} = 450\ k\Omega$$

5.7.5) The 8255 parallel peripheral interface

The 8255 PPI card was connected to the PC to switch the relay and thus the magnetron power. Only one bit of port C was needed as the switching channel, bit C0, however any channel can be used depending on the control word written to the control register. The 8255 PPI was used in mode 0 which is a basic input/output mode. The least significant bits of port C (C0 to C3) were set as output ports by writing 80 Hex to the control register.

```
PORT[$263] := $80
```

Now bit C0 can be set and reset by writing to port C:

```
Reset: PORT[$262] := $0
Set: PORT[$262] := $1
```

5.7.6) The turbo pascal control program

A listing of the turbo pascal control program is shown in appendix G. As the digestion system only required one thermocouple for temperature measurement, one channel and one failure alarm line was read. This can easily be updated if two temperature readings are needed or the second channel can be used to cover a higher temperature

range. The program is a three cycle temperature controller, each cycle is specified by the time of sample irradiation, the amount of power delivered to the load and the final temperature to be reached. Power is cycled to the magnetron in 10 second duty cycles and is specified in the percentage of total magnetron power. The program uses the standard units CRT, DOS and GRAPH. The CRT unit uses the full power of the PCs display and keyboard. The DOS unit supports many DOS functions for time control, file-handling routines and program execution. The GRAPH unit is a powerful graphics package which implements a complete library of more than 50 graphics routines which are used for an on-line display of the digestion process. The process data is also written to a file, Fi, for a more detailed study of the completed process. The program was written in modular form which consists of a number of heating process and graphics procedures which are called from the main program. A description of the control program procedures and the most important program variables is given in appendix F.

5.7.7) The controlled digestion system operation.

The control system was set up as designed, and the magnetron switching mechanism was seen to work correctly for the four stages of a heating cycle. The magnetron was fitted to the launching rectangular waveguide of the digestion system and the control system was connected. A small hole was made in the cylindrical cavity lid for the insertion of the thermocouple. The cavity was loaded with a water sample, and the control process was run to determine any operating problems. Initially, the thermocouple temperature measurement was totally distorted due to microwaves coupling onto the thermocouple. Using the microwave power meter and horn antenna, microwave leakage was detected down the thermocouple lead. This was prevented by using a

microwave choke positioned on the lid over the thermocouple insertion hole. Now, a clean temperature reading was measured and the final heating tests were performed on the control system.

Controlled heating tests were performed on the microwave digestion system using medium water and ethylene glycol loads. Heating step tests were carried out to test the control systems ability to reach a set point temperature and maintain that set point. All the tests were done at 100% power. The data from each test was stored on file and the following results, shown in appendix H, were produced using a Harvard graphics package. The first test process heated a 50 ml water sample stabilized at a room temperature of 21.9°C, see figure H1. Power was first applied at 10 seconds, however the first noticeable rise in the temperature was at 11.2 seconds. The set point temperature of 100°C and a process time of 60 seconds were specified. A temperature of 100.6°C was reached at 51.1 seconds. Using equation 1.1, the power delivered to the 50 ml water load was calculated to be 415.0 watts. The set point temperature was maintained over the rest of the process, however super heating occurred in the water load and temperatures of 104°C were reached. A second 50 ml water load test was performed to study the reproducibility of these heating procedures. The same parameters were used as in the first water test but the process time was extended to 110 seconds. The initial room temperature of the water sample was 21.4°C. Power was applied at 10 seconds with the first noticeable rise in the temperature at 11.1 seconds, see figure H2. A temperature of 101.6°C was reached at a time of 50.7 seconds, which specifies 425.0 watts delivered to the water load. The set point was then maintained over the rest of the process. These results show that the two experiments are reproducible, the power absorbed by the 50 ml water load was the same for both experiments.

A second set of tests were done using 50 ml ethylene glycol loads. Ethylene glycol has a boiling point of 200°C and a specific heat capacity of 0.561 $cal.°C^{-1}.g^{-1}$. The first step test performed heated the 50 ml sample from a room temperature of 23.9°C to a set point temperature of 200°C, in a process time of 100 seconds. Figure H3 shows the result of this step test. Power was first applied at 10 seconds with a first noticeable rise in the temperature at 12.6 seconds. The sample load reached a temperature of 202.2°C at 75.5 seconds. Thus 332.6 watts was delivered to the load. After this set point was reached, maintaining of the set point temperature was achieved with a maximum and minimum deviation of 202.8°C and 198.4°C respectively. A second step test was done on the 50 ml ethylene glycol load. The load was maintained at 60°C and stepped up to a set point temperature of 140°C, with a process time of 130 seconds. Figure H4 shows the result of this test. The step was applied at 10 seconds with a temperature rise being observed at 11.86 seconds. the load attained a temperature of 141.4°C at 42.3 seconds. This corresponds to 318.0 watts being delivered to the sample load. The set point temperature was maintained for the following 100 seconds of the process with a maximum and minimum deviation of 144.4°C and 139.9°C respectively. Again good reproducibility of the test results was indicated with the loads of both ethylene glycol tests absorbing similar microwave power.

These results show the ability of the control system to heat a sample load to a set point temperature with accurate maintaining of that set point over the duration of the process. Tests performed on identical loads, produced very similar results in each case, which indicates the reproducibility of the digestion procedures.

CONCLUSION

The main requirements for the operation of a microwave digestion system are:

1) A high microwave energy transfer efficiency for all loads to digested.
2) A uniform microwave field for equal heating of all the loads applied to the system.
3) Microprocessor or computer control of the digestion system.

A commercial microwave oven was studied and tested to evaluate its use in a digestion system. After testing, the microwave oven was found unsuitable for the digestion process and exhibited the following qualities:

1) The microwave oven is a multimoded cavity, adaptable for many types of loads.
2) It has a low energy transfer efficiency and is thus not an optimal heating process.
3) It is not ideal for process control.
4) For uniform heating to be possible for all the loads, the loads have to be rotated on a turntable or a stirrer must be used.

A cylindrical resonant cavity was designed and tested to satisfy the digestion system requirements. Following microwave testing of the cylindrical cavity it was concluded:

1) The cylindrical cavity has a good symmetrical field structure distributing equal microwave power to all the applied loads without the requirement for load rotation or a stirrer.

2) The cylindrical cavity match was found to be very narrow band for the small loads applied and did not have a high energy transfer efficiency for all these loads.
3) This cavity is suited to the digestion of large sample loads.

The resonant horn cavity was designed for a better coupling mechanism between the sample loads and the microwave field. This cavity satisfied the requirements for use in a digestion system and displayed the following characteristics:

1) A good match was achieved for all the loads applied to the cavity thus yielding a high energy transfer efficiency.
2) Microwave heating tests produced linear heating of all the samples applied to the horn cavity.
3) The loads did not require rotation in the microwave field and a stirrer was not needed.

An experimental microwave digestion system was designed for use in the evaluation of other industrial digestion processes. In a theoretical analysis, the critical factors affecting the efficiency of microwave energy transfer were found to be:

1) The variety of material loads used.
2) The range of sizes of loads used.
3) The loads position in the cavity and its size and shape relative to the size and shape of the cavity.
4) The load temperature.
5) The excitation frequency.

The experimental digestion system was constructed as designed and connected to a computer control system to heat the applied load over three specified heating cycles. The following conclusions were drawn:

1) The cross directional coupler is only appropriate for use in a fixed loaded system.
2) A high energy transfer efficiency was achieved for small loads. A good wide band match was obtained for larger loads.
3) The control system operated correctly for three heating cycles. The heating of the load to a set point temperature was achieved with accurate maintaining of that set point.
4) Tests performed on identical loads indicated the reproducibility of the digestion process.

RECOMMENDATIONS

Based on the conclusions of this dissertation, the following recommendations were drawn:

1) The experimental microwave digestion system is ready for use with an operating control system.
2) For further development of this project an accurate model of the heating process must be established or monitoring of the material loads dielectric constant must be achieved in order to optimize the heating process.

LIST OF REFERENCES

1) Kingston, H.M., and Jassie, L.B., "Microwave sample preparation", American Chemical Society, 1988.
2) Pougnet, M.A.B., "Microwaves ovens in the Chemical Laboratory", Department of Analytical Science, UCT, 1989.
3) Hesek, J.A., and Wilson, R.C., "The use of microwave ovens for sample drying in the chemical laboratory", Anal. Chem., 46(8), 1160, 1974.
4) Kruesi, P., "Microwave heating of minerals and chemical compounds", Chemical Engineering, Nov. 12, 18, 1984.
5) Walkiwicz, J.W., Kazonich, G., and McGill, S.L., "Microwave heating characteristics of selected minerals and compounds", Minerals and Metalurgical processing, 39-42, Feb. 1988.
6) Beary, E.S., "Applications of thermopads for drying chemical laboratory samples", Anal. Chem., 60(8), 742-746, 1988.
7) Kingston, M.H., and Jassie, L.B., "Microwave dissolution", Anal. Chem., 58(14), 1424-1428, Dec. 1986.
8) Abu-Samra, A., Morris, J.S., and Koirtyohann, S.R., "Routine sample digestion using microwave ovens", Anal. Chem., 47(8), 1475-1477, 1975.
9) Matthes, S.A., Farrel, R.F., and Mackie, A.T., Tech. Proj. Rep-US, Bur. Mines, No. 120, 1983.
10) Kingston, H.M., and Jassie, L.B., "Microwave energy for acid decomposition at elivated temperatures and pressures using biological and botanical samples", Anal. Chem., 58, 2534-2541, 1986.
11) ICP Newsletter, "Microwave disolution in closed vessels under elevated temperatures and pressures", Volume 14, Number 1, 66 Jun. 1988.
12) Asmussen, J., Lin, H.H., Manring, B., and Fritz, R., "Single-moded or controlled multimoded microwave cavity applicators for precision materials processing", Rev. Sci. Instrum., 58(8), Aug. 1987.
13) Gerling, E.E., "Power output measurement of microwave ovens", Microwave power symposium, 20-29, May 1977.
14) Copson, D.A., "Microwave heating", 2nd edition, Avi.

pub., Westport, C.T., 1975.
15) Liao, S.Y., "Microwave devices and circuits", Prentis-Hall, N.J., 1980.
16) Marcuvitz, N., "Waveguide handbook", McGraw-Hill,N.Y., 1951.
17) Yokumitsu, Y., Saito, T., Okubo, N., and Kaneko, Y., "A 6 GHz 80 W GaAs FET Amplifier with a TM-mode cavity power combiner", IEEE Trans. on microwave theory, Vol.
18) Dydyk, M., "Efficient power combining", IEEE Trans. on microwave theory, Vol. MTT-28, no. 7, July 1980.
19) Puschner, H., "Heating with microwaves", Philips, Gloeilampenfabrieken, Netherlands, 1966.
20) Montgomery, G.C., "Principles of microwave circuits", Radiation laboratory series, McGraw-Hill, N.Y., 1948.
21) Debye, P., "Polar molecules", Chemical catalogue, 1929.
22) Cole, K.S., Cole, R.H., "A model of the dipole molecules complex dielectic constant", Journal of chemical phisics, 9.341, 1941.
23) Marcuvitz, N., "Microwave handbook", Radiation laboratory series, McGraw-Hill, 351-362,1951.
24) Kyhl, R.L., "Technique of microwave measurements", Radiation laboratory series, McGraw-Hill, 589, 1947.
25) Slater, J.C., "Microwave transmission", McGraw-Hill, N.Y., Chaper 7, 1942.

BIBLIOGRAPHY

Abu-Samra, A, Morris, JS, and Koirtyohann, SR, Anal. Chem., 47(8), 1475-1477, 1975.

Asmussen, J., Lin, H.H., Manring, B. and Fritz, R., "Single-moded or controlled multimoded microwave cavity applicators for precision materials processing", Rev. Sci. Instrum., 58(8), August 1987.

Beary, ES, Anal. Chem., 60(8), 742-746, 1988.

Bradlow, Prof. H.E., and Effemey, H.G., "Propagation characteristics of low-loss tubular waveguides", Proceedings I.E.E., p254 - p260, Paper no. 2326 R, May 1957.

Carr-Brion, K., "Radio and microwave frequency techniques for on-line analysis", Trans. Inst. MC, vol. 9, Jan. - Mar. 1987.

Cheung, W.S., "Microwaves made simple; principles and applications", Artech House, Dedham, 1985.

Cole, K.S., Cole, R.H., Journal of chemical physics, 9.341, 1941.

Collin, R.E., and Zucker, F.J., "Antenna theory", McGraw-Hill, p632, N.Y., 1969.

Copson, D.A., "Microwave heating", 2nd edition, Avi pub., Westport, C.T., 1975.

Debye, P., "Polar molecules", Chemical catalogue, 1929.

Dydyk, M., "efficient power combining", IEEE trans. on microwave theory, vol. MTT-28, no. 7, July 1980.

Gerling, E.E., "Power output measurement of microwave ovens", Microwave power symposium, p 20-29, May 1977.

Hesek, JA, and Wilson, RC, Anal. Chem., 46(8), 1160, 1974.

ICP Newsletter, Volume 14, Number 1, 66, Jun 1988.

Kingston, HM, and Jassie, LB, "Microwave sample preparation", American Chemical Society, 1988.

Kingston, HM, and Jassie, LB, Anal. Chem., 58, 2534-2541, 1986.

Kingston, HM, and Jassie, LB, Anal. Chem., 58(14), 1424-1428,Dec. 1986.

Kinzie, P.A., "Thermocouple temperature measurement", Wiley-interscience, 1973.
Kruesi, p, Chemical Engineering, Nov. 12, 18, 1984.
Kyhl, R.L., "Technique of microwave measurements", Radiation laborarory series, McGraw-Hill, p 589, 1947.
Liao, S.Y., "Microwave devices and circuits", Prentis-Hall, N.J., 1980.
Marcuvitz, N., "Microwave handbook", Radiation laboratory series, McGraw-Hill, 1951.
Matthes, SA, Farrel, RF, and Mackie, AT, Tech. Prog. Rep-US, Bur. Mines, No. 120, 1983
Montgomery, G.C., "Principles of microwave circuits", Radiation laboratory series, McGraw-Hill, N.Y., 1948.
Phillips coporation, "Infrared detectors and their applications".
Pougnet, MAB, "Microwave Ovens in the Chemical Laboratory", Department of Analytical Science, UCT, 1989.
Puschner, H., "Heating with microwaves", Philips, Gloeilampenfabrieken, Netherlands, 1966.
Russel, "Microwave power combining techniques", IEEE Trans. microwave theory, vol. 32, no. 3, p301 - p308, March 1984.
Silver, S., "Microwave antenna theory and design", M.I.T., p349, McGraw-Hill, N.Y., 1949.
Slater, J.C., "Microwave transmission",McGraw -Hill, N.Y., Chapter 7, 1942.
Swift, G.W., et al., " A radial wave power combiner designed by broadband techniques", European microwave simposium, p973 - p978, 1975.
Tokumitsu, Y., Saito, T., Okubo, N. and Kaneko, Y., "A 6-Ghz 80-W GaAs FET Amplifier with a TM-mode cavity power combiner, IEEE trans. on microwave theory, vol. MTT-32, no. 3 , March 1984.
Waardebburg, T., "Low loss microwave power combiners and splitters", 1986.
Walkiwicz, JW, Kazonich, G, and McGill, SL, Minerals and Metalurgical Processing, 39-42,Feb. 1988.

ACKNOWLEDGEMENTS

Professor B.J. Downing: for supervision of this dissertation.

Mr. M.A.B. Pougnet: for his many personal interviews and assistance.

Mr. D. Kenyan: for building of the microwave cavities.

Mr. C. Shutz: for his inspiring proverb "One should not think about things one cannot see."

Mr. C. Broderick: for his help in producing this dissertation.

APPENDIX A

ELECTROMAGNETIC PLANE WAVES

1) Electric and magnetic wave equations

The electric and magnetic waves are derived from Maxwell's equations yielding the solutions:

$$\nabla^2 E = \gamma^2 E \ ,$$

$$\nabla^2 E = \gamma^2 E \ ,$$

where $\gamma = \sqrt{(jw\mu(\sigma + jw\epsilon))} = \alpha + j\beta$, is the intrinsic propagation constant ....(A.1)

α = the attenuation constant

β = the phase constant

μ = the magnetic permeability

ϵ = the dielectric permittivity

2) Uniform plane waves in free space

Electromagnetic plane waves in free space are typical uniform plane waves. The electric and magnetic fields are mutually perpendicular to each other and to the direction of propagation of the waves. This is a transverse electromagnetic wave or a TEM wave. For plane wave propagation in the z direction, in a lossless dielectric where $\sigma = 0$, the solution of the wave equations gives the electric and magnetic intensities [15]:

$$H_y = \sqrt{(\epsilon/\mu)} E_x,$$

where $v_p = 1/\sqrt{(\mu_o \epsilon)} = c/\sqrt{\epsilon_r}$, is the phase velocity

$\alpha = 0$,

$$\beta = w\sqrt{(\mu_o \epsilon)} \qquad \ldots.(A.2)$$

$n = \sqrt{(\mu_o/\epsilon)} = n_o/\sqrt{\epsilon_r}$, is the intrinsic impedance

$\ldots.(A.3)$

3) Plane wave propagation in a lossy media

3.1) Plane wave in a good conductor

A good conductor has a very large conductivity, the conduction current is much larger than the displacement current. The energy of the wave decreases as it as it travels through the medium as ohmic losses are present. For a good conductor :

$$\sigma >> w\epsilon,$$

and the propagation constant is expressed as:

$$\gamma = (1 + j)\sqrt{(w\mu\sigma/2)}.$$

As a result: $\alpha = \beta = \sqrt{(w\mu\sigma/2)}$

The skin depth, δ, is the depth at which the travelling wave is reduced to 1/e, and is given to be:

$$\delta = 1/\sqrt{(w\mu\sigma/2)} = 1/\alpha = 1/\beta.$$

The intrinsic resistance of a good conductor is given as:

$$n = (1 + j)R_s \qquad \ldots.(A.4)$$

where $R_s = \sqrt{(w\mu/2\sigma)}$, $\ldots.(A.5)$

and is known as the surface resistance per unit area of conductor.

3.2) Plane wave in a lossy dielectric

The conductivity of all dielectric materials is small, $\sigma << w\epsilon$, and the intrinsic impedance of the dielectric is :

$$n = \sqrt{(\mu/\epsilon)}[1 - j\sigma/w\epsilon]^{-1/2}$$

The loss tangent is defined as: $\tan\theta = \sigma/w\epsilon$. This results in the displacement current density leading the conduction current density by 90^{o}. The phase relationship is shown in figure A.1. If the loss tangent is small ($\sigma/w\epsilon << 1$), then the propagation constant and the intrinsic impedance can be approximated by:

$$\gamma = jw\sqrt{(\mu\epsilon)}[1 - j\sigma/2w\epsilon] \quad ....(A.6)$$

$$n = \sqrt{(\mu/\epsilon)}[1 + j\sigma/2w\epsilon] \quad ....(A.7)$$

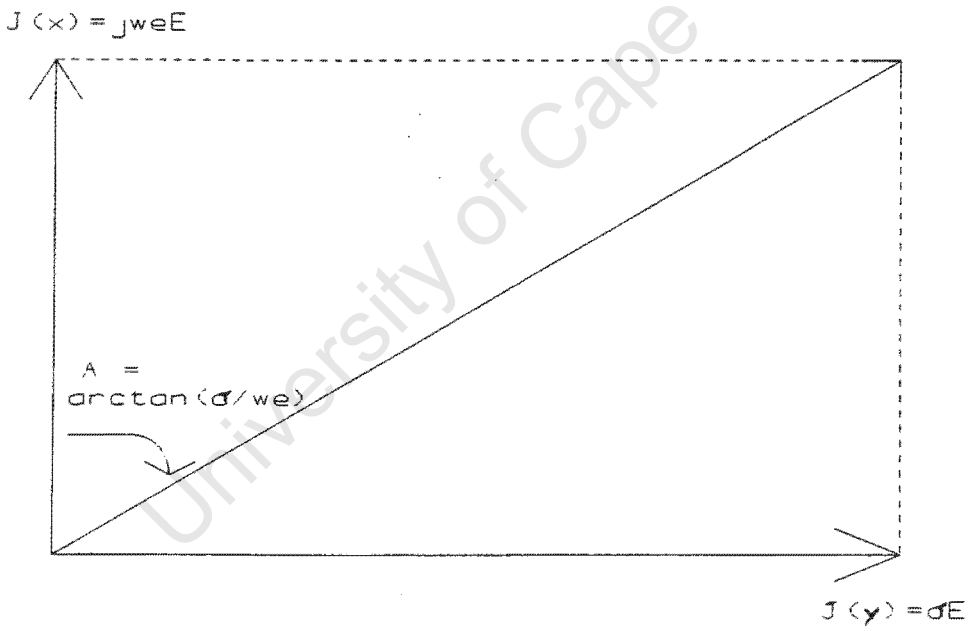

Figure A.1: The loss tangent for a lossy dielectric

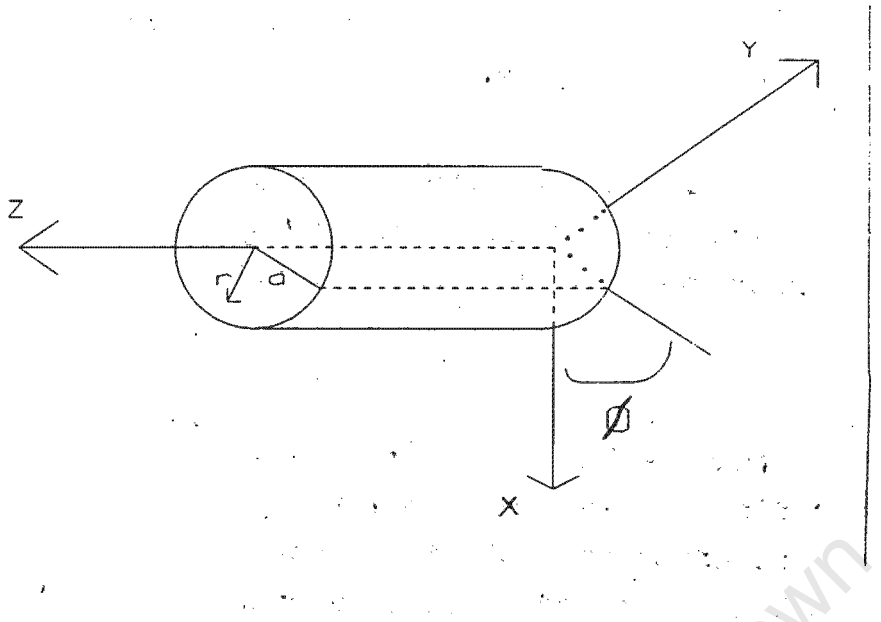

Figure B.1: Coordinates for a cylindrical waveguide.

1.1) TE modes in cylindrical waveguides

The direction of propagation is assumed to be in the z direction. TE_{np} modes are characterized by $E_z = 0$. The component of the magnetic field in this direction, H_z, must exist in order for energy to propagate. The magnetic and electric field components in the cavity are found by solving Maxwell's equations, using the solution of the Helmholtz equation for H_z, and solving for the boundary conditions. This requires that the tangential component of the electric field must be zero along a conducting surface, and the normal component of the magnetic field must be zero at a conducting surface:

$$E_{\phi} = 0 \text{ at } r = a$$

$$H_r = 0 \text{ at } r = a$$

These conditions solve to the requirement that:

$J_n'(k_c a) = 0$, where J_n' is the derivative of J_n...(B.4)

APPENDIX C

Pictures of the designed cylindrical resonant cavity

Side view:

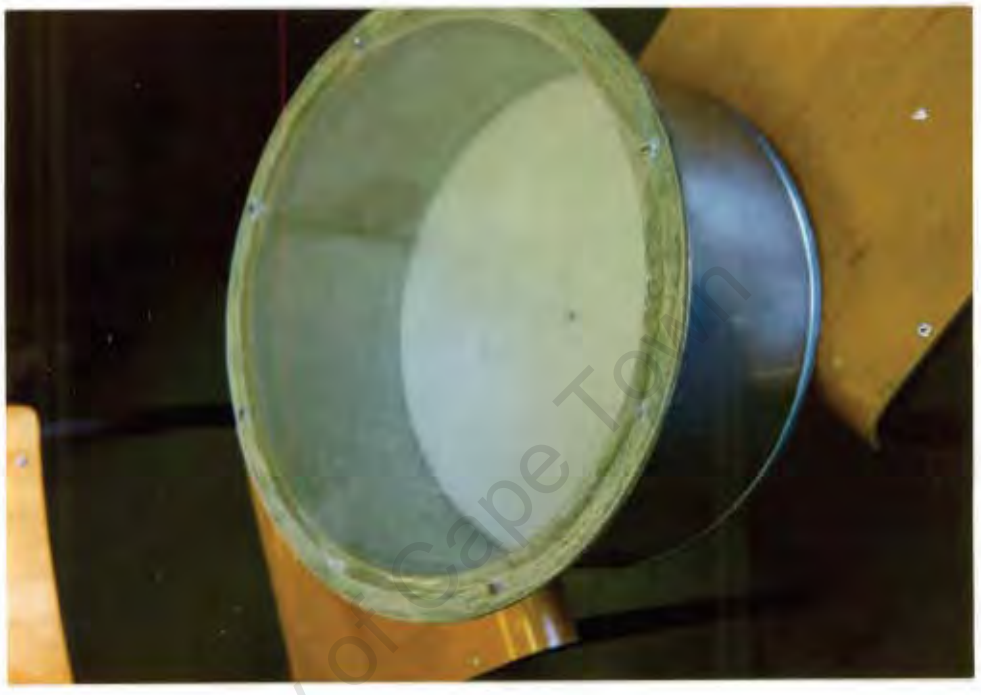

Top view:

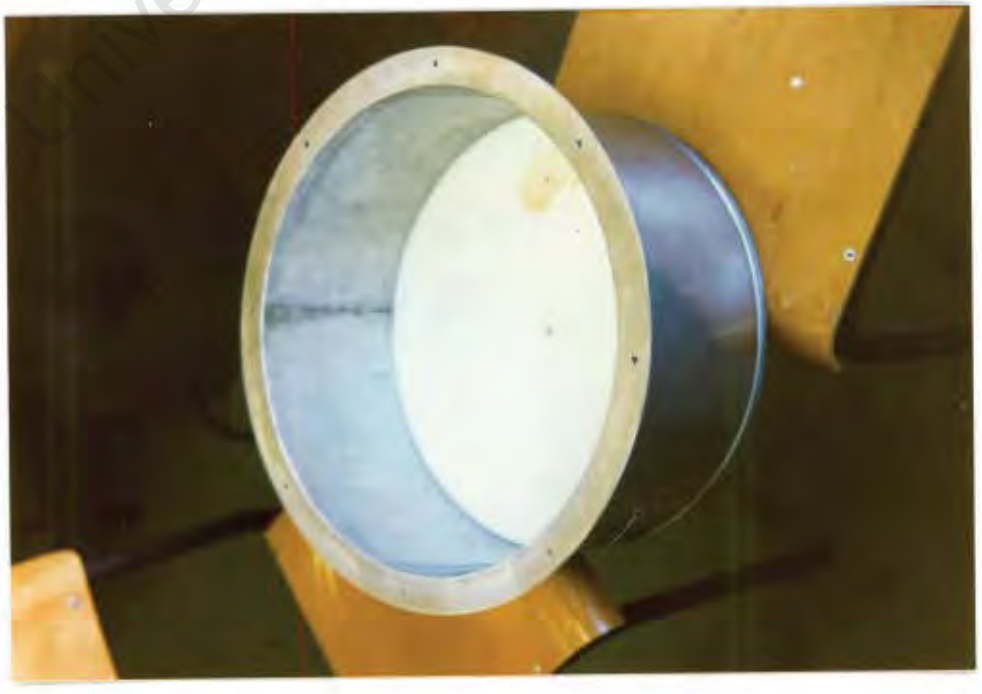

APPENDIX D

Pictures of the designed resonant horn cavity

Top view:

Side view:

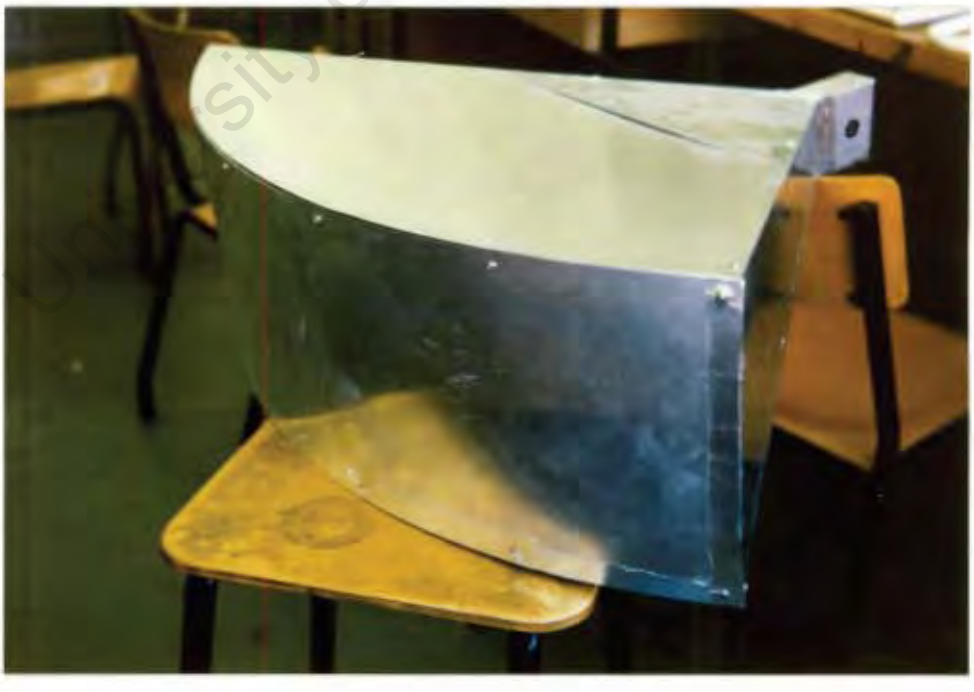

APPENDIX E

THE EXPERIMENTAL MICROWAVE DIGESTION SYSTEM DESIGN

Pictures of the experimental microwave digestion system

Front view:

Side view:

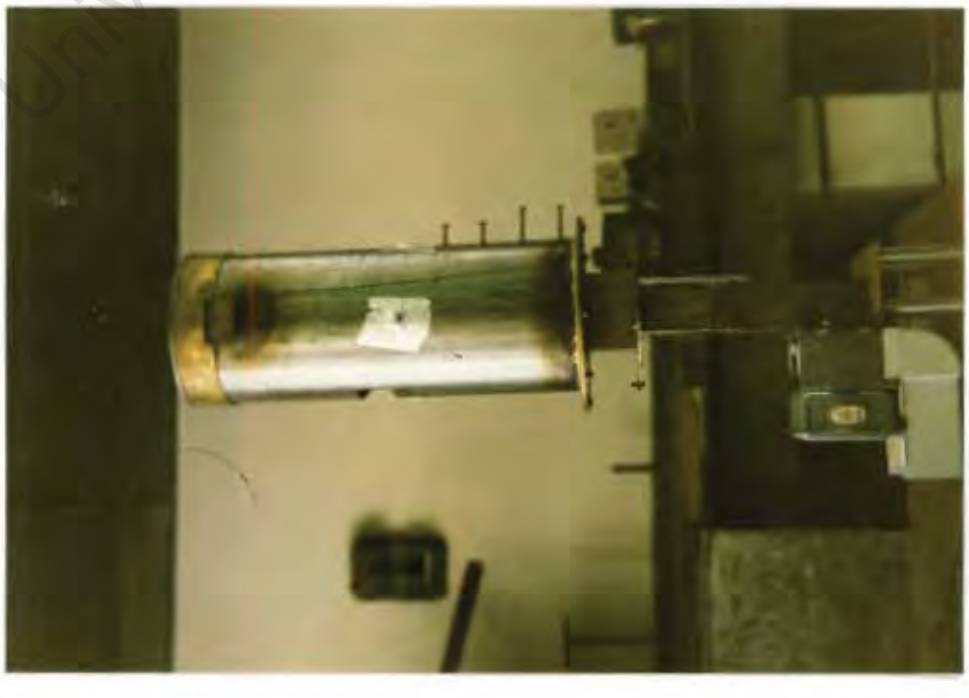

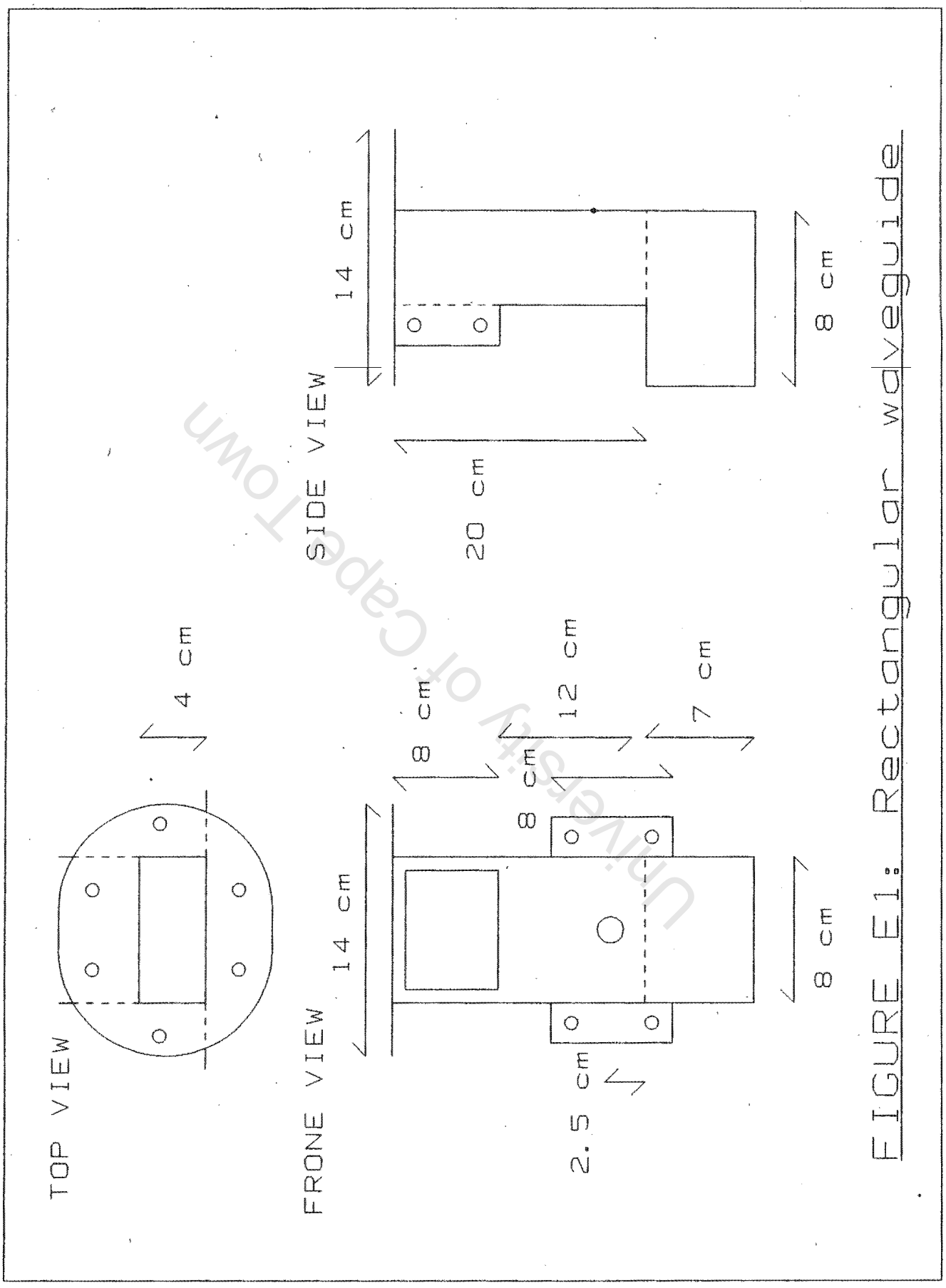

FIGURE E1. Rectangular waveguide

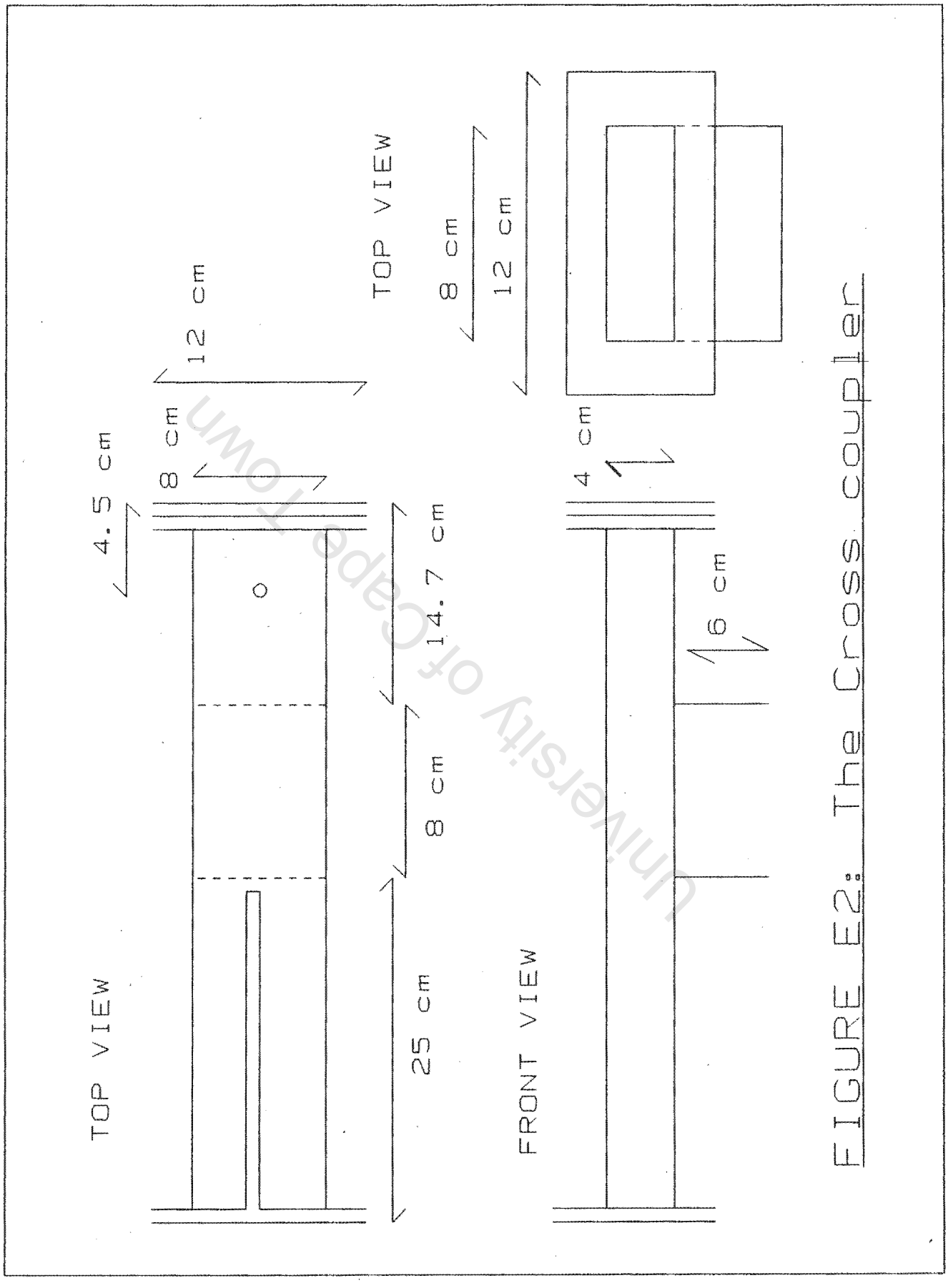

FIGURE E2: The Cross coupler

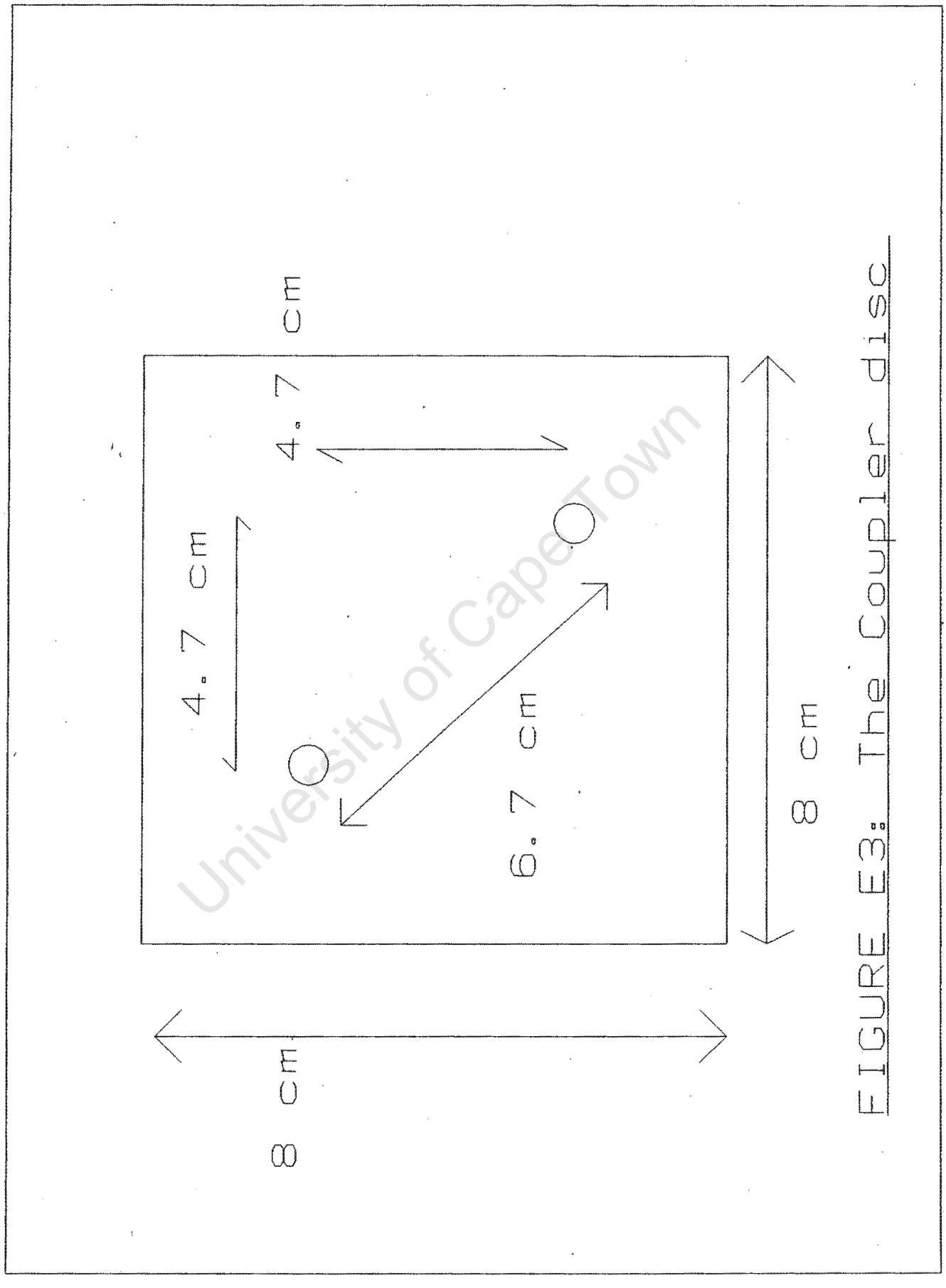

FIGURE E3. The Coupler disc

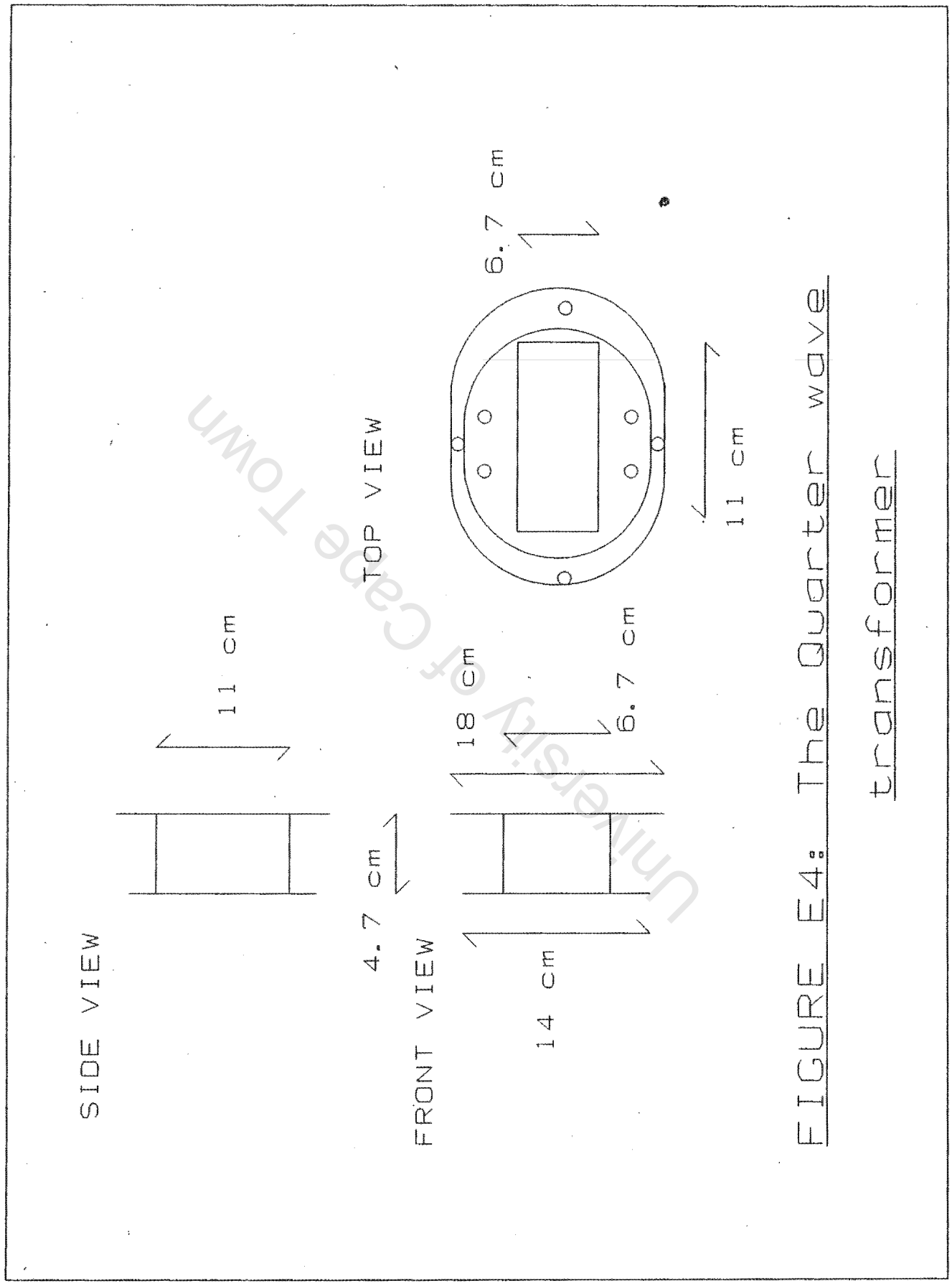

FIGURE E4: The Quarter wave transformer

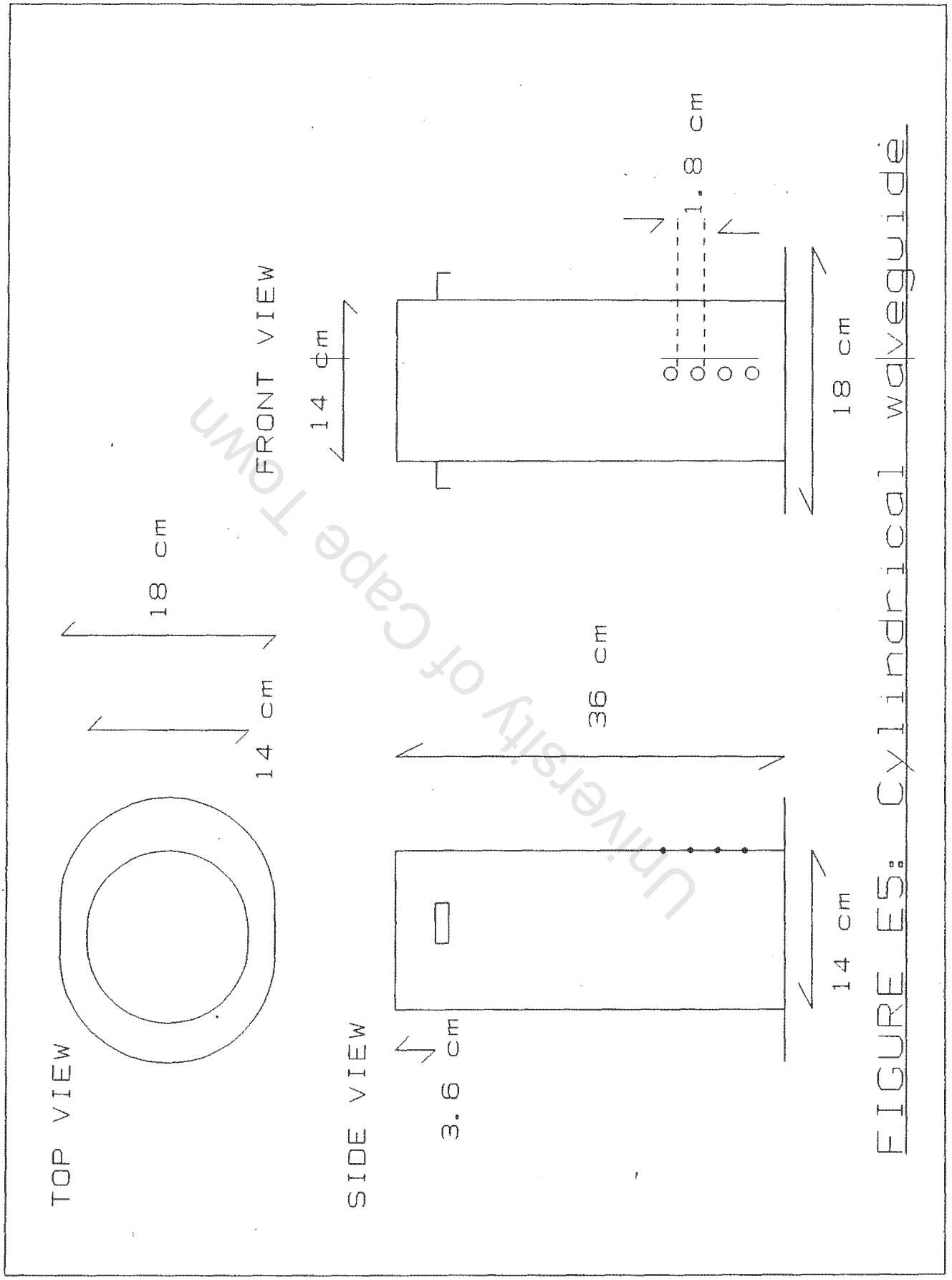

FIGURE E5: Cylindrical waveguide

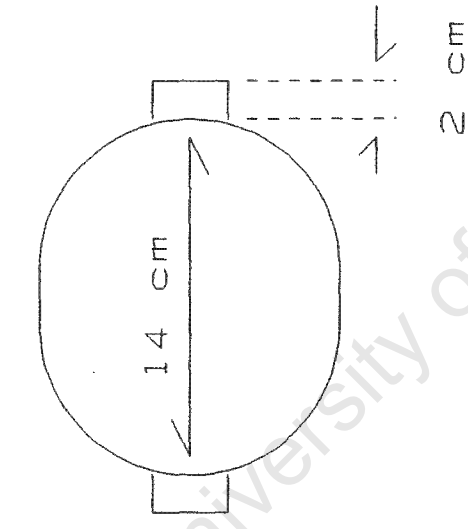

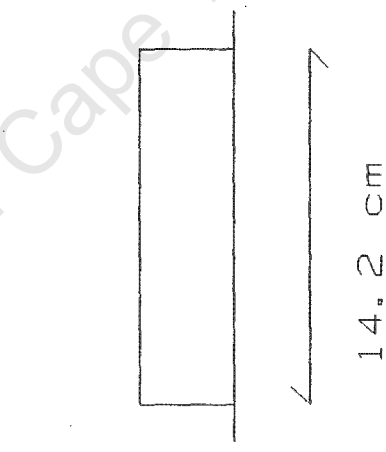

FIGURE E6: Cavity lid

APPENDIX F

A DESCRIPTION OF THE CONTROL PROGRAM

The most important variables used in the turbo pascal control program are described below:

PRESENTIME: This holds the current time set in the operating system.
STARTIME: The time of the last sample temperature reading.
USETIME: The current cycles time of completion.
CYCTIME: This is a three element array holding the time durations of the three heating cycles.
REFERENCETIME: The start time of the digestion heating process.
PLOTIME: The present time of duration of the digestion heating process.
TOTALTIME: The total time of the three heating cycles.
CYCTEMP: This is a three element array housing the set point temperatures of the three heating cycles.
ADSAMPLE: The current sample temperature is read from the PC-26 and stored in Adsample.
DIFFTEMP1: The difference in temperature between the present and last sample readings.
USETEMP: The present cycles set point temperature.
LASTEMP1: The last temperature reading of the sample.
POWER: This is a three element array holding the percentage of magnetron power delivered to the sample for the three heating cycles.
USEPOWER: The present cycles percentage delivered power.
TEST: The state of the failure alarm line

During the control process the main program calls graphics procedures to set up and update the visual display, and heating stage procedures to control the temperature of the load at the specified parameters. A

description of the control program procedures and their flow charts follow:

1) Function PRESENTIME: This uses the DOS procedure GetTime which returns the current time of the operating system in hours, minutes, seconds and hundredths of seconds. This is converted to seconds.

2)Procedure GRAPHSETUP: This procedure sets up the visual display in graphics mode. The GRAPH procedure INITGRAPH is called which initializes the graphics system and sets the hardware into graphics mode. The function GRAPHRESULT is checked to determine an error in this graphics operation. The RECTANGLE procedure is then used to draw two windows. The top, large window will hold a graphical display (temperature vs. time) of the on-line heating process. The lower, small window is used for the numerical display of sample temperature, process on time, magnetron status (on/off), the present heating cycle and the current heating stage. The maximum temperature and total process time are then used to draw the axes of the graphics display graph. Ten divisions are marked on the vertical temperature scale and horizontal time scale.

3) Procedure PLOTPT: This procedure is used to plot the latest temperature recorded from the PC-26 on the temperature vs. time graph. As the axis of this graph will be different for each digestion process, a scaling factor is needed for the correct placement of the plotted point on the time and temperature axes. This is done using the variables calculated in the main program, X and W. Procedure PLOTPT also fills the lower graphics window with the updated process data, temperature, on time, status, cycle and stage.

4) Procedure COLLECTDATA: This procedure is used to read in the digitized sample temperature from the PC-26. Figure F.1 shows a flow chart of this procedure. Data will not be read if the time since the last reading is less than 0.5 seconds. This is to prevent unnecessary over sampling of the thermocouple signal. The digitized temperature is stored in ADSAMPLE. The failure alarm line is read every ten times COLLECTDATA is called and its state is stored in TEST. If TEST is high (> 2050 > $2^{12}/2$) then the magnetron is turned off, the file Fi is closed and the program halted. As ADSAMPLE holds the digitized version of the sample temperature it must be converted to numerical form. When the sample temperature is 300°C ADSAMPLE will read 4095, therefore a scaling factor of 4095/300 = 13.65 is introduced to yield the correct degrees celsius temperature reading. The present time of duration of the heating process is then calculated, PLOTIME, and the procedure PLOTPT called.

5) Procedure DETSAMPLETEMP: This procedure is called before the heating process has begun, and is used to stabilize and determine the initial sample room temperature. A flow chart is shown in figure F.2. This is stage zero of the heating process with the magnetron turned off. Data is collected until the sample temperature has stabilized and the time of data collection has exceeded ten seconds. These values can be changed for different sample load materials. REFERENCETIME is set to PRESENTIME to indicate the begin of the heating process.

6) Procedure GETOSETPOINT: This is the first stage of a heating cycle and is used to heat the given sample load to the specified temperature, USETEMP, over the cycle time, USETIME, in the set percentage power, USEPOWER. Figure F.3 shows the flow chart of this procedure. Over

the ten second heating duty cycle, power is delivered to the magnetron for USEPOWER/10 seconds (Ton), the magnetron is then switched off for the following 1 - USEPOWER/10 seconds (Toff). This heating cycle is only entered if the sample temperature, ADSAMPLE, is less than the cycle set point temperature, USETEMP, and the cycle time has not been exceeded. The procedure will only be terminated on the breaking of one of these conditions. The magnetron is turned on and data collected until Ton is exceeded, this is followed by the magnetron being switched off for the remaining Toff seconds. Once Toff has been exceeded the next duty cycle Ton and Toff are calculated.

7) Procedure SETTLING: The flow chart of this second stage of a heating cycle is shown in figure F.4. This short procedure allows the sample to settle after it has been heated to the set point temperature by GETOSETPOINT. Data is collected until the difference in temperature between the present and last read temperatures is less than 0.5°C or the cycle time has been exceeded.

8) Procedure MAINTAINSETPOINT: This is the third and last stage of a heating cycle which holds the sample temperature at the set point temperature. Figure E.5a and E.5b show the flow charts of this procedure. The procedure is conditional on the cycle time not being exceeded. The magnetron is turned off until the sample temperature is less than the set point temperature. Once the sample temperature has dropped below the set point, Ton and Toff are calculated for an initial 30% power level (z = 3). The sample is now heated while the sample temperature is less than the set point and the cycle time has not been exceeded. Once again the magnetron is switched on for Ton seconds, and off for the rest of the duty cycle. After every duty cycle, if the sample

temperature has not reattained the set point temperature the percentage power is increased by 10% (z = z + 1), if the set point temperature has been attained then this percentage power is decreased 10% (z = z + 1). The new Ton and Toff at this power level for the next duty cycle is then calculated. This was done to prevent the set point from never being reattained. This method thus adjusts itself to the optimum power level for the set point to be maintained. After the set point temperature has been regained, the sample is allowed to settle and the procedure is repeated until the cycle time is exceeded.

9) The MAIN PROGRAM: A flow chart of the main program is shown in figure F.6. Here, the user must enter the time, percentage power and temperature of the three heating cycles. During this operation the total process time is calculated, TOTALTIME, and the maximum temperature determined. The control words are then written to the control registers of the PC-26 and the 8255 PPI boards. The program assigns an external file to Fi, whereupon the old file is deleted and a new file created. Next, the procedure GRAPHSETUP is called. This sets up the visual display in graphics mode. The scaling factors X and W are then calculated. These are used by the procedure PLOTPT to ensure the correct scaling of the plotted points onto the graphics display. The procedure DETSAMPLETEMP is called to allow the sample to settle and to determine the starting temperature. The three heating cycles are then executed for the specified temperature, power and time. The procedures GETOSETPOINT, SETTLING and MAINTAINSETPOINT are then called respectively to reach and maintain the cycle temperature in the given cycle time. Once completed CLOSEGRAPH is called which shuts down the graphics system and the data file, Fi, is closed.

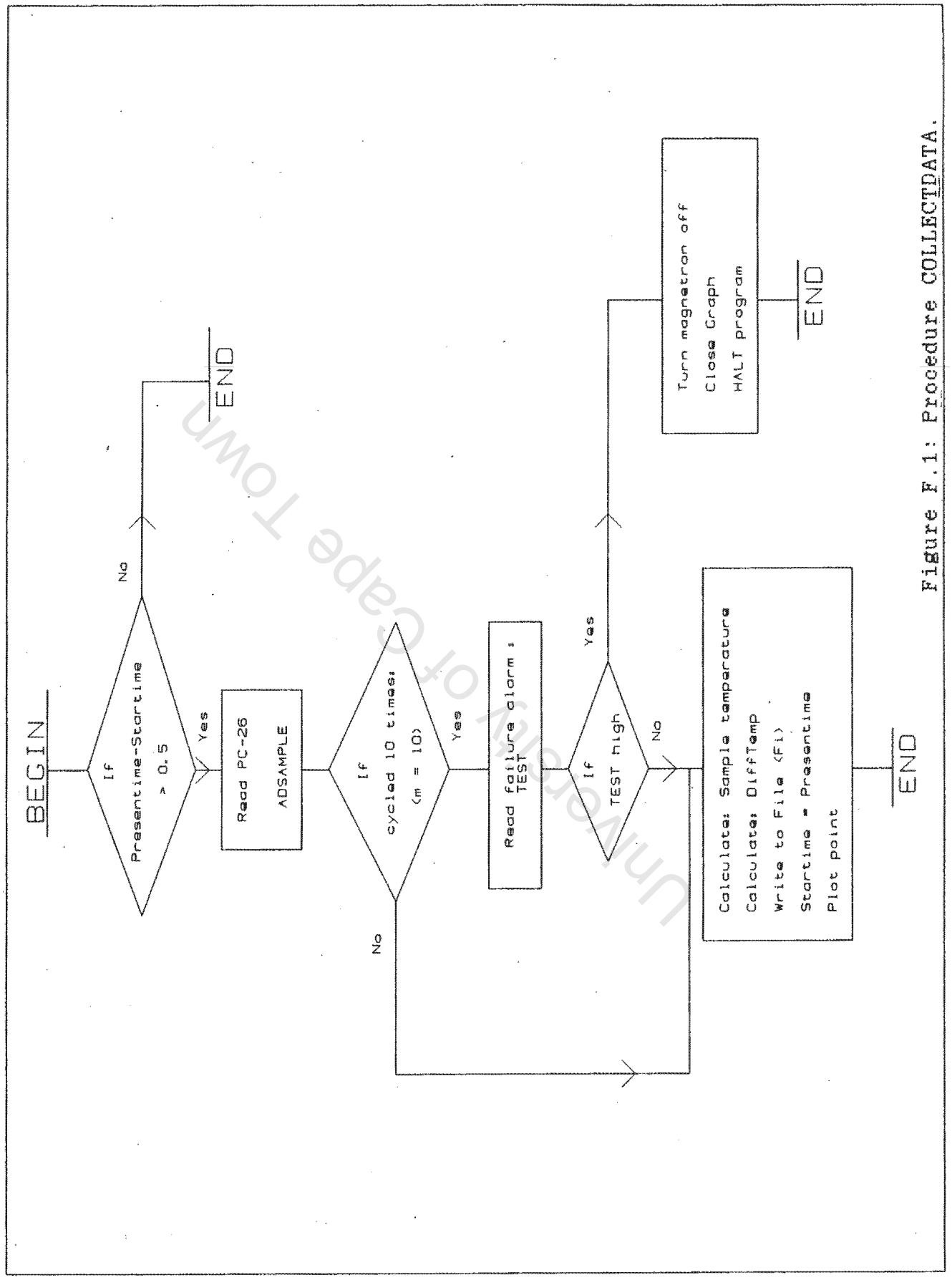

Figure F.1: Procedure COLLECTDATA.

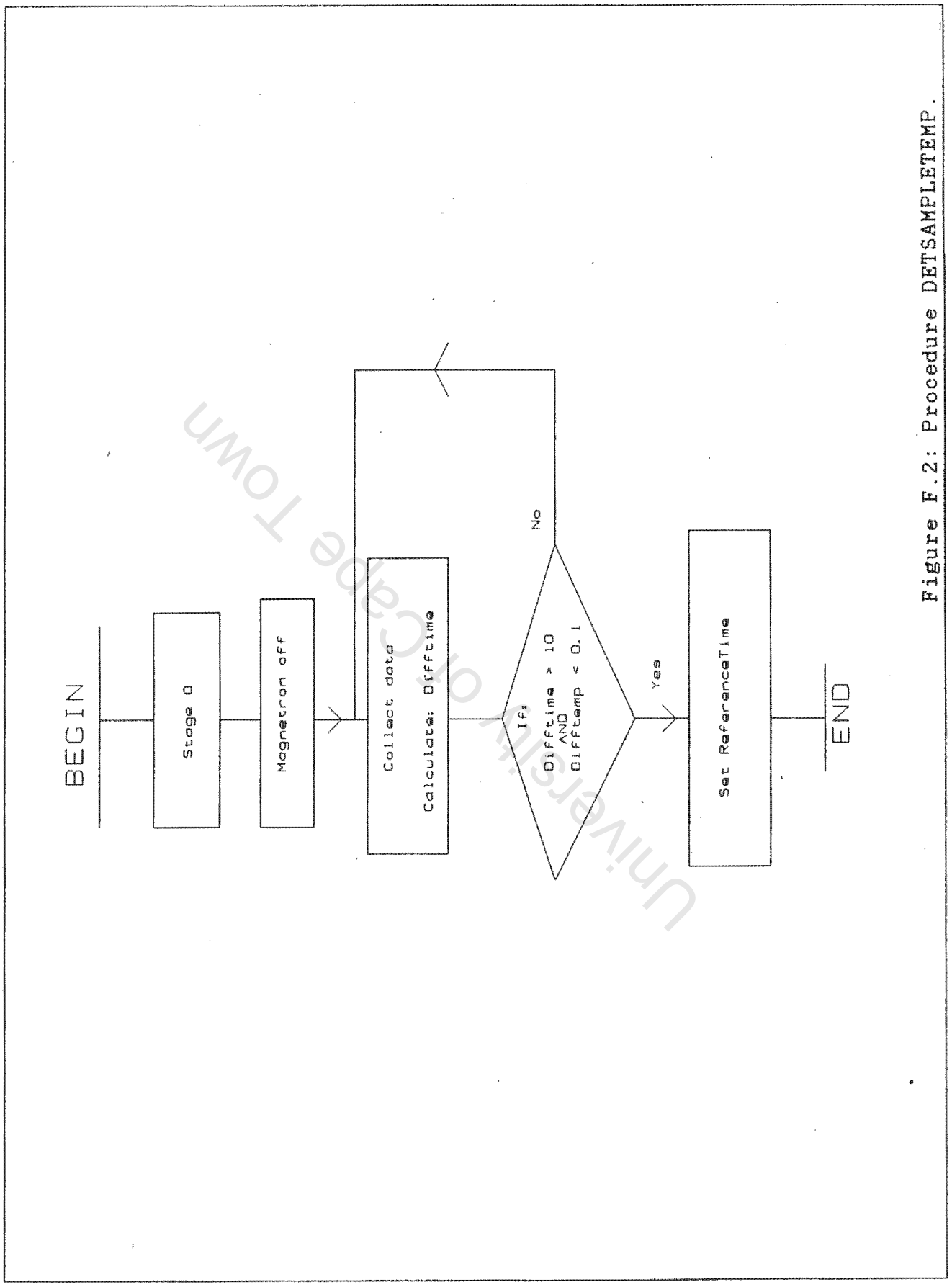

Figure F.2: Procedure DETSAMPLETEMP.

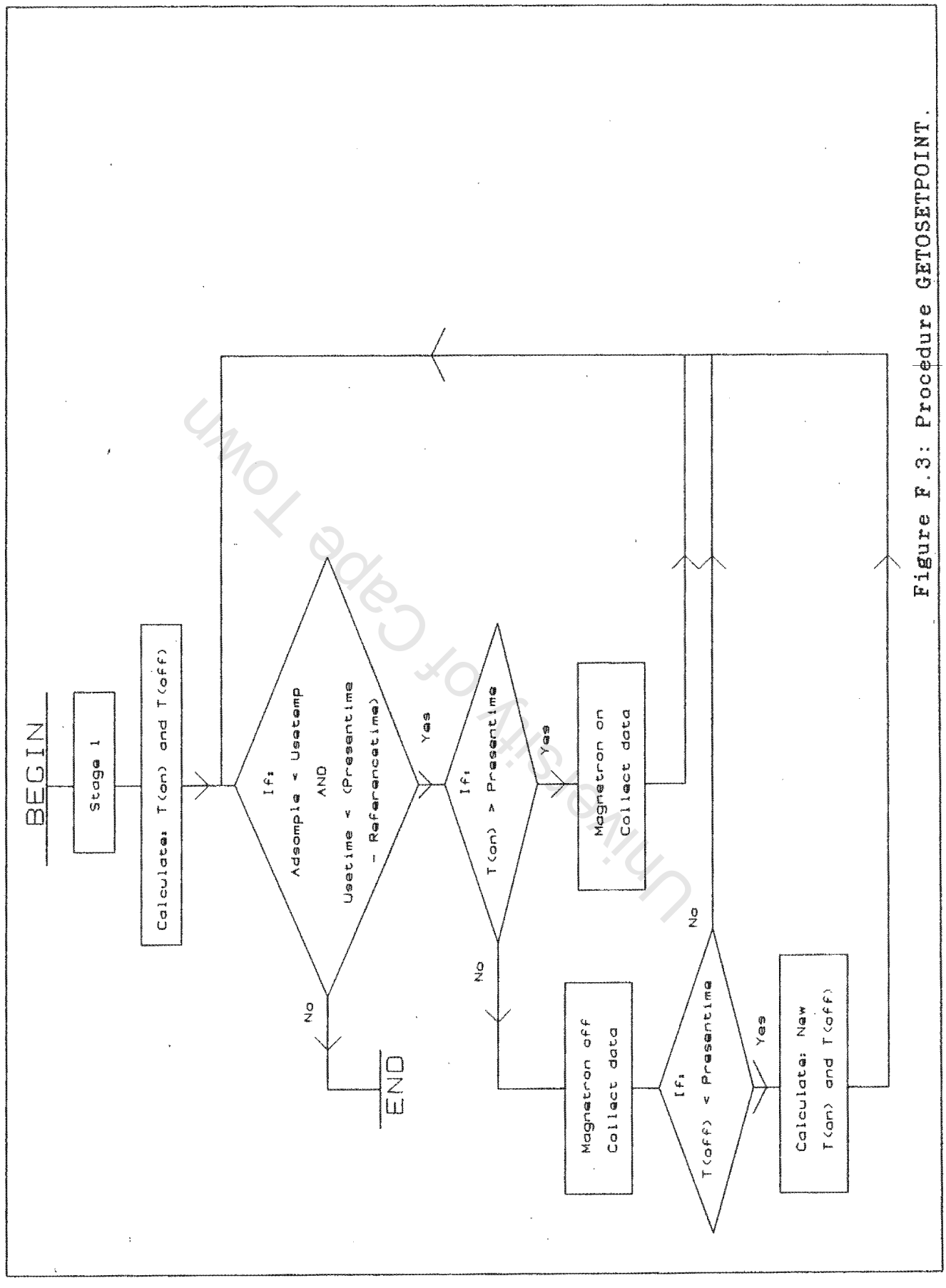

Figure F.3: Procedure GETOSETPOINT.

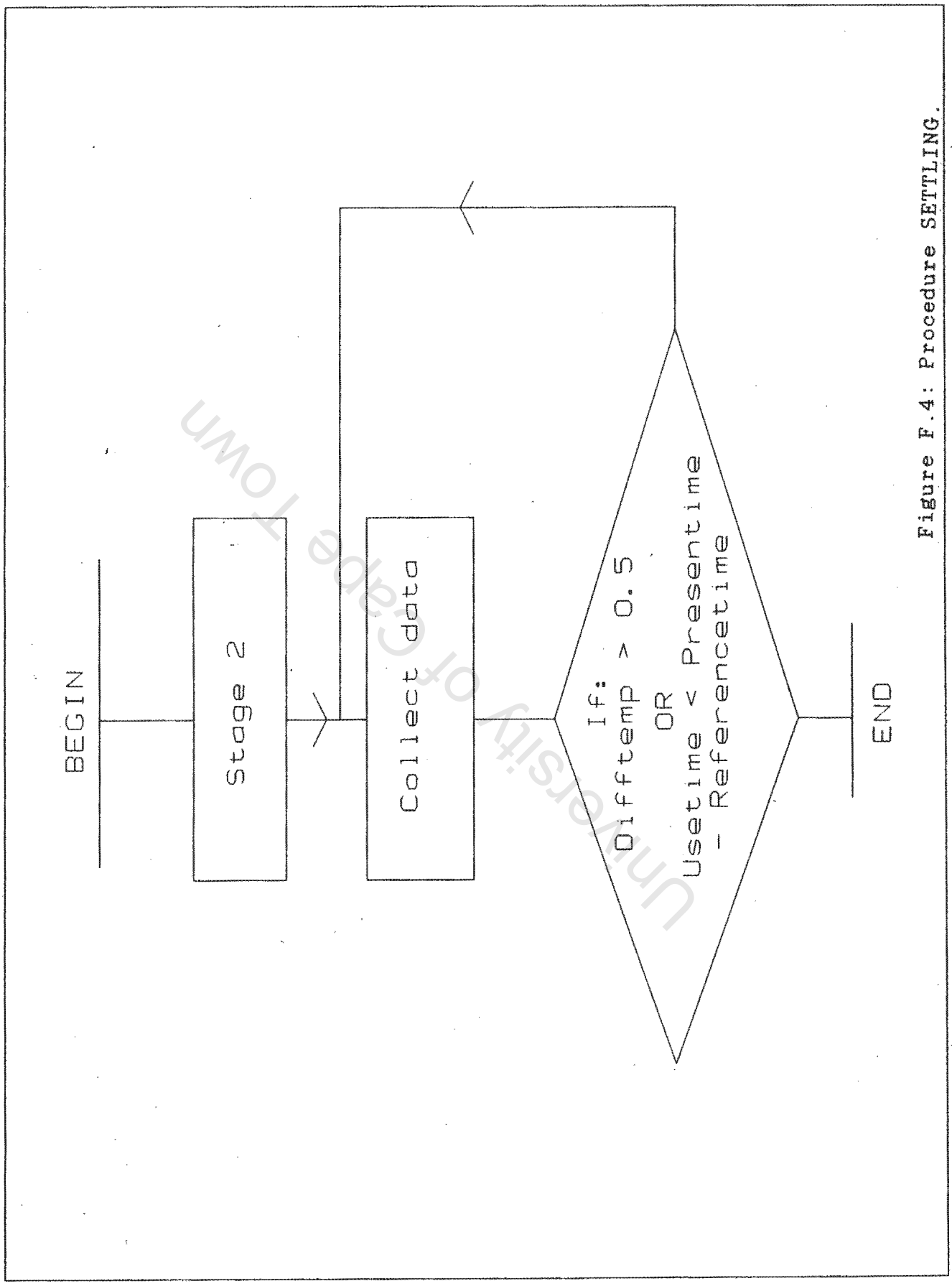

Figure F.4: Procedure SETTLING.

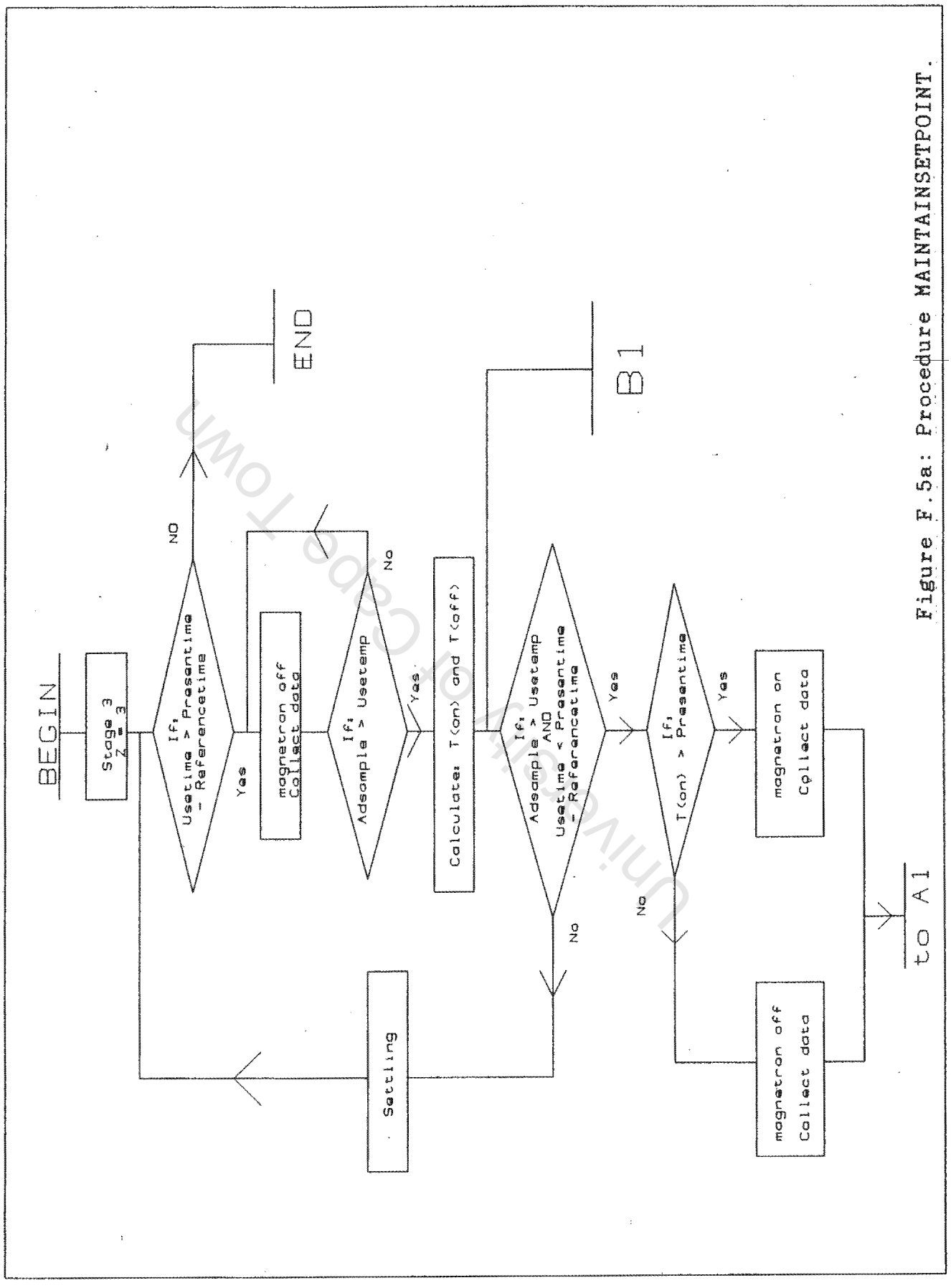

Figure F.5a: Procedure MAINTAINSETPOINT.

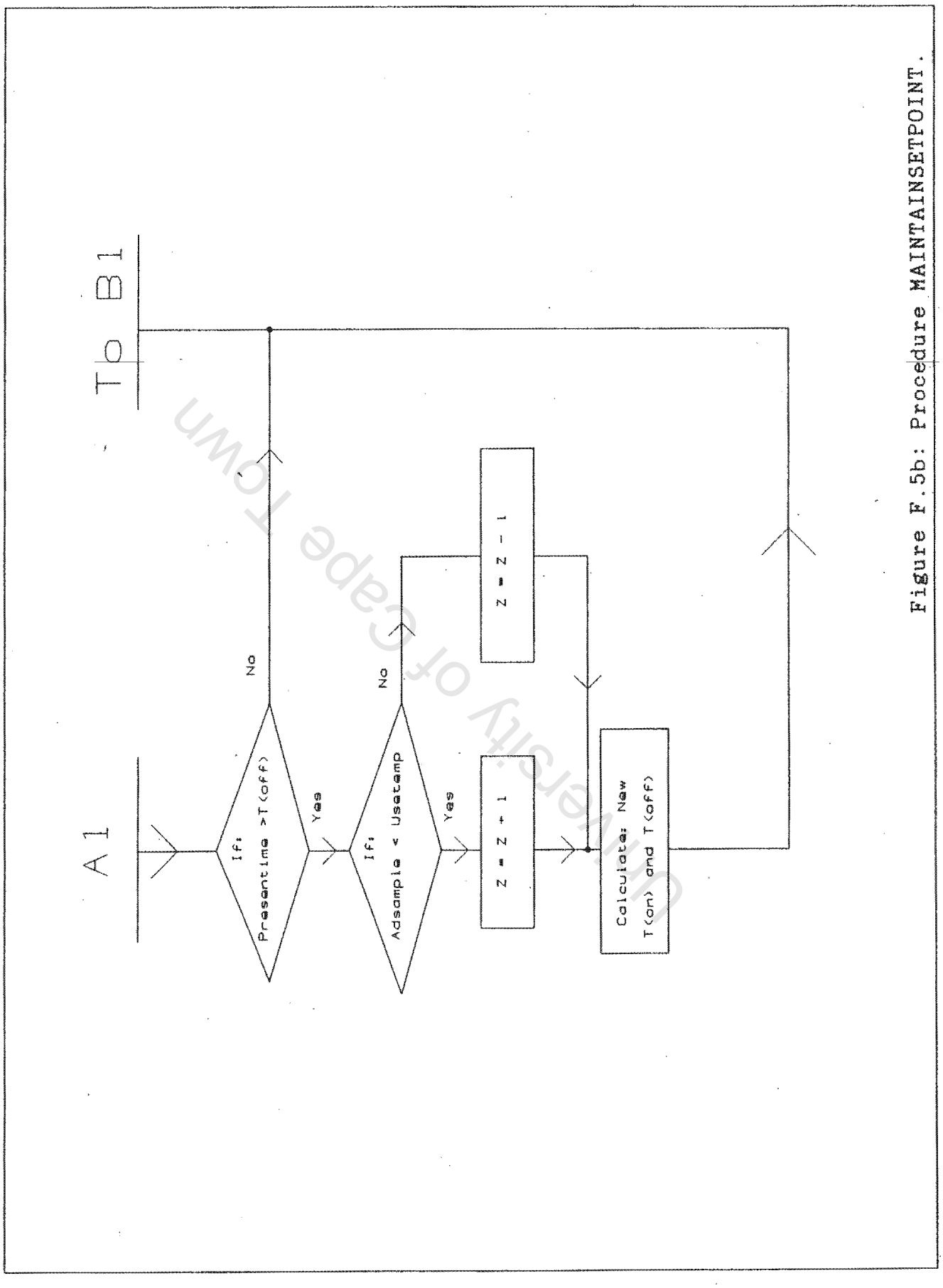

Figure F.5b: Procedure MAINTAINSETPOINT.

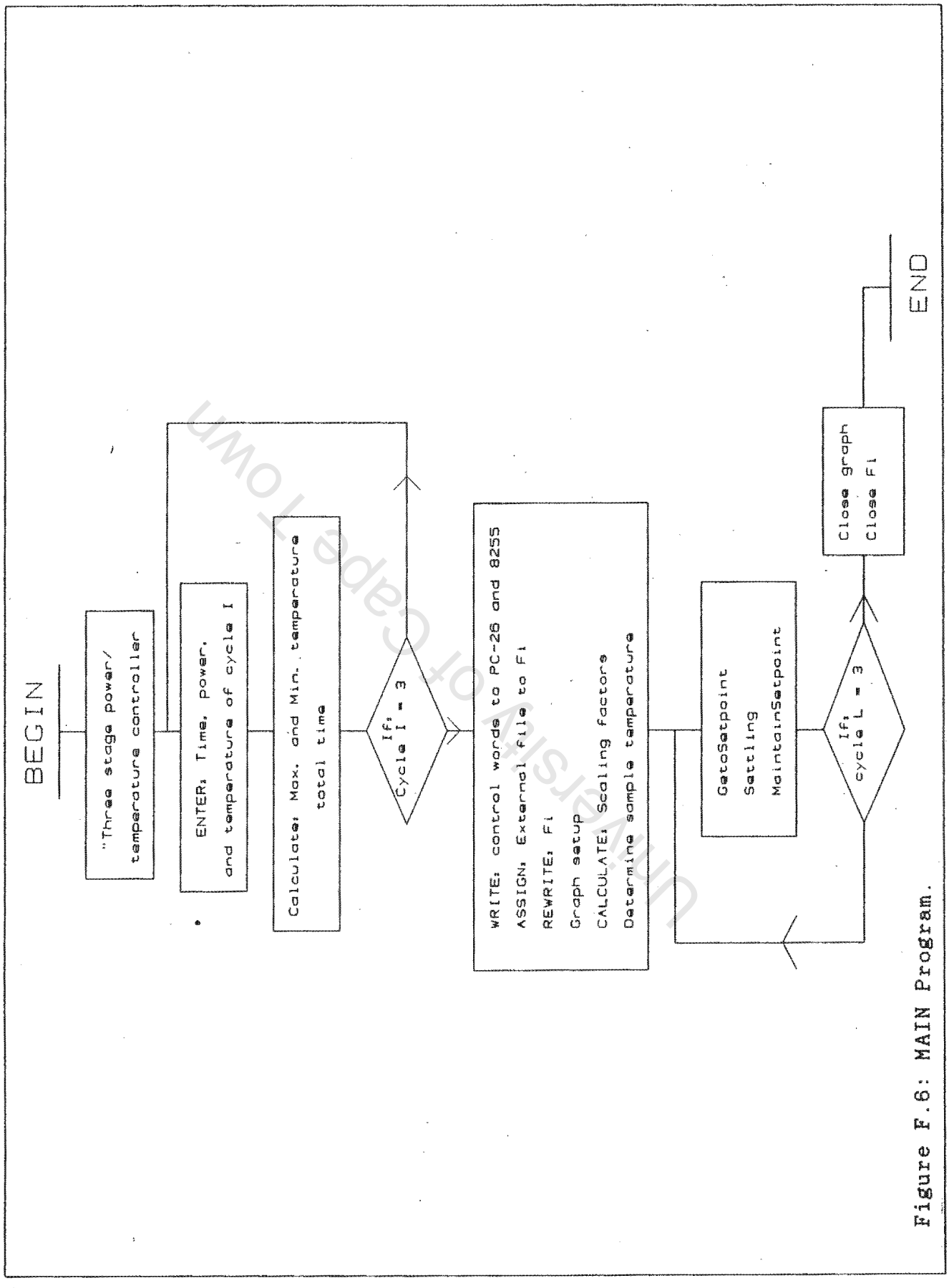

Figure F.6: MAIN Program.

APPENDIX G

THE TURBO PASCAL CONTROL PROGRAM

```
PROGRAM TEMPERATURE_CONTROLLER
{by: GRANT BROOMHALL}

VAR    CYCTEMP,CYCTIME,POWER              :ARRAY[0..2] OF REAL;
       CYCLE,STAGE                        :STRING[9];
       FI                                 :TEXT;
       PLOTIME,I,L,M                      :INTEGER;
       STATUS                             :BOOLEAN;
       STARTIME,DIFFTEMP1,TEST,ADSAMPLE,LASTEMP1,TOTALTIME,
       MAXTEMP,DIFFTIME,REFERENCETIME,USETIME,USETEMP,TON,
       USEPOWER,ROOMTEMP,TOFF,W,X,Z       :REAL;


FUNCTION PRESENTIME:REAL;
VAR HOUR,MINUTE,SECOND,SEC100:WORD;
BEGIN
  GETTIME(HOUR,MINUTE,SECOND,SEC100);
  PRESENTIME:=3600*HOUR+60*MINUTE+SECOND+SEC100/100;
END;

PROCEDURE GRAPHSETUP;
VAR ERRORCODE,GRAPHDRIVER,GRAPHMODE,J,K:INTEGER;
    S                                  :STRING[6];
BEGIN
  GRAPHDRIVER := DETECT;
  INITGRAPH(GRAPHDRIVER,GRAPHMODE,'C:\TP');
  ERRORCODE :=GRAPHRESULT;
  IF ERRORCODE <>GROK THEN
    BEGIN
      WRITELN('GRAPHICS ERROR:',GRAPHERRORMSG(ERRORCODE));
      READLN;
      HALT(1);
    END;
  SETACTIVEPAGE(0);
  SETVISUALPAGE(0);
  SETTEXTSTYLE(SANSSERIFFONT,HORIZDIR,1);
  SETTEXTJUSTIFY(CENTERTEXT,CENTERTEXT);
  OUTTEXTXY(GETMAXX DIV 2,5,'TEMPERATURE CONTROL');
  RECTANGLE(0,20,GETMAXX,285);
  RECTANGLE(0,295,GETMAXX,GETMAXY);
  LINE(49,40,49,241);
  LINE(49,241,701,241);
  SETTEXTSTYLE(SMALLFONT,HORIZDIR,4);
  SETTEXTJUSTIFY(LEFTTEXT,LEFTTEXT);
  OUTTEXTXY(50,309,'TEMPERATURE');
  OUTTEXTXY(170,309,'ON TIME');
  OUTTEXTXY(280,309,'STATUS');
  OUTTEXTXY(330,309,'CYCLE');
  OUTTEXTXY(400,310,'STAGE');
  OUTTEXTXY(45,33,'Temperature (Deg C)');
  OUTTEXTXY(335,275,'Time (s)');
  TOTALTIME :=(ROUND(TOTALTIME/10+0.5))*10;
  MAXTEMP := (ROUND(MAXTEMP/10+0.5))*10;
  FOR J :=0 TO 10 DO
    BEGIN
      LINE(49,40+J*20,53,40+J*20);
      STR((MAXTEMP-(J*MAXTEMP/10)):3:1,S);
      OUTTEXTXY(15,43+J*20,S);
    END;
```

```
  FOR K :=0 TO 65 DO
    BEGIN
      STR((K*TOTALTIME/65):5:1,S);
      IF (K MOD 5 =0) THEN
        BEGIN
          SETTEXTSTYLE(SMALLFONT,VERTDIR,5);
          LINE(50+K*10,236,50+K*10,241);
          SETTEXTSTYLE(SMALLFONT,HORIZDIR,4);
          SETTEXTJUSTIFY(CENTERTEXT,CENTERTEXT);
          OUTTEXTXY(50+K*10,250,S);
        END;
      IF (K MOD 5 <>0) THEN
        BEGIN
          SETTEXTSTYLE(SMALLFONT,VERTDIR,5);
          LINE(50+K*10,238,50+K*10,241);
        END;
    END;
  END;

 PROCEDURE PLOTPT(TIME:integer;U:REAL);
 CONST VP1          :VIEWPORTTYPE = (X1:50;Y1:40;X2:700;Y2:240;CLIP:CLIPON);
 VAR   nTime,YP,UP :LONGINT;
       T           :STRING[5];
 BEGIN
   WITH VP1 DO
   BEGIN
     SETVIEWPORT(X1,Y1,X2,Y2,CLIP);
     nTime :=ROUND(Time/w);
     UP:=200-ROUND(U*x);
     CIRCLE(NTIME,UP,2);
   { PUTPIXEL(nTIME,UP,15); }

     SETVIEWPORT(2,310,GETMAXX-2,GETMAXY-1,CLIPON);
     STR(U:3:2,T);
     SETACTIVEPAGE(0);
     OUTTEXTXY(80,20,T);
     STR(TIME,T);
     OUTTEXTXY(185,20,T);
     IF STATUS = TRUE THEN T:='ON ' ELSE T:='OFF';
     OUTTEXTXY(295,20,T);
     STR(L,T);
     OUTTEXTXY(415,20,'CYCLE '+T);
     OUTTEXTXY(550,20,Stage);
     DELAY(50);
     CLEARVIEWPORT;
     IF TIME = TOTALTIME THEN CLEARVIEWPORT;
   END;
 END;


PROCEDURE CollectData;

BEGIN
  If (Presentime-Startime)>0.5 Then
    BEGIN
          Lastemp1:=Adsample;
          PORT[$702]:=(0 SHL 4)+02;
          PORT[$702]:=(0 SHL 4)+03;
          For I:=1 To 26 Do
            BEGIN
            END;
          Adsample:=(PORT[$701] AND $0F)*256 +PORT[$700];
```

```
      If M=10 Then
        BEGIN
          M:=0;
          PORT[$702]:=(1 SHL 4) + 02;
          PORT[$702]:=(1 SHL 4) + 03;
          For I :=0 to 26 Do
            BEGIN
            END;
          Test:=(PORT[$701] AND $0F)*256 + PORT[$700];
          If Test>2050 Then
            BEGIN
              PORT[$262]:=0;
              closegraph;
              close(fi);
              HALT(1);
            END;
        END;
      M:=M+1;
      Adsample := Adsample/13.64;

      Writeln(Fi,Presentime:5:2,'   ',Adsample:3:2);
      Difftemp1:=Adsample-Lastemp1;
      Lastemp1:=Adsample;
      Delay(50);
      Startime:=Presentime;
    END;
  Plotime:=Round(Presentime-Referencetime);
  Plotpt(Plotime,Adsample);

END;

PROCEDURE DetSampleTemp;
 BEGIN
   Stage := 'Stage 0';
   PORT[$262]:=0;
   Status:=False;
   Lastemp1:=18;
   Adsample:=20;
   Difftemp1:=5;
   Startime:=Presentime;
   REPEAT
     CollectData;
     Difftime:=Presentime-Referencetime;
   UNTIL ((Difftemp1 < 0.1) AND (Difftime > 10));
   Roomtemp:=Lastemp1;
   Referencetime:=Presentime;
 END;

PROCEDURE GetoSetPoint;

BEGIN
  Stage := 'Stage 1';
  Ton:=Presentime+Usepower/10;
  Toff:=Presentime+10;

  While ((Adsample<Usetemp) AND (Usetime>(Presentime-Referencetime))) Do BEGIN
    If Ton > Presentime Then
      BEGIN
        PORT[$262]:=1;
        Status:=True;
        CollectData;
      END
      ELSE
      BEGIN
        PORT[$262]:=0;
        Status:=False;
        CollectData;
      END;
```

```
    If Presentime > Toff Then
      BEGIN
        Ton:=Presentime+Usepower/10;
        Toff:=Presentime+10;
      END;
  END;
END;

PROCEDURE Settling;

BEGIN
  Stage := 'Stage 2';
  Startime:=Presentime;
  REPEAT
    CollectData;
  UNTIL ((Difftempl <0.5) OR (Usetime<Presentime-Referencetime));
END;

PROCEDURE MaintainSetPoint;

BEGIN
  Stage := 'Stage 3';
  Startime:=Presentime;
  z := 3.0;
  WHILE (Usetime> Presentime - Referencetime) DO
  BEGIN
    Stage:='Stage 3';
    REPEAT
      PORT[$262]:=0;
      Status:=False;
      CollectData;
    UNTIL (Adsample<Usetemp);
    Startime:=Presentime;
    Ton:=Presentime+z;
    Toff:=Presentime+10;

    WHILE ((Adsample < Usetemp) and (Usetime > Presentime-Referencetime)) DO
    BEGIN
      If Ton > Presentime Then
        BEGIN
          PORT[$262]:=1;
          Status:=True;
          CollectData;
        END
      Else
        BEGIN
          PORT[$262]:=0;
          Status:=False;
          CollectData;
        END;
      If Presentime > Toff Then
        BEGIN
          IF (ADSAMPLE < USETEMP) THEN Z := Z + 1 ELSE Z := Z - 1;
          Ton := Presentime+Z;
          Toff := Presentime+10;
        END;
    END;
    Settling;
  END;
  Port[$262]:=0;
END;
```

```
{************************************************************}
{****                    MAIN PROGRAM                    ****}
{************************************************************}

BEGIN
  Maxtemp := 0;
  Usetime := 0;
  Totaltime := 0;
  M := 0;L:=0;
  for i := 1 to 3 do
    begin
      Write('ENTER TIME(SEC), POWER(%), TEMP(DEG C) OF CYCLE', i,':');
      Readln(Cyctime[i],Power[i],Cyctemp[i]);
      Totaltime := Totaltime + Cyctime[i];
      If (Cyctemp[i] > Maxtemp) Then Maxtemp := Cyctemp[I];
    end;

  PORT[$703] := $92;
  PORT[$263] := $80;
  Assign(Fi,'c:\turbo\tdat.dat');
  Rewrite(Fi);

  GraphSetUp;
  X := 200/Maxtemp;
  W := Totaltime/650;
  DetSampleTemp;
  For L := 1 To 3 Do
    BEGIN
      Usetemp := cyctemp[L];
      Usepower :=Power[L];
      Usetime := Usetime + cyctime[L];
      GetoSetPoint;
      Settling;
      MaintainSetPoint;
    END;
  repeat until keypressed;
  Closegraph;
  Close(Fi);

end;
```

APPENDIX H

Heating test results of the experimental microwave digestion system

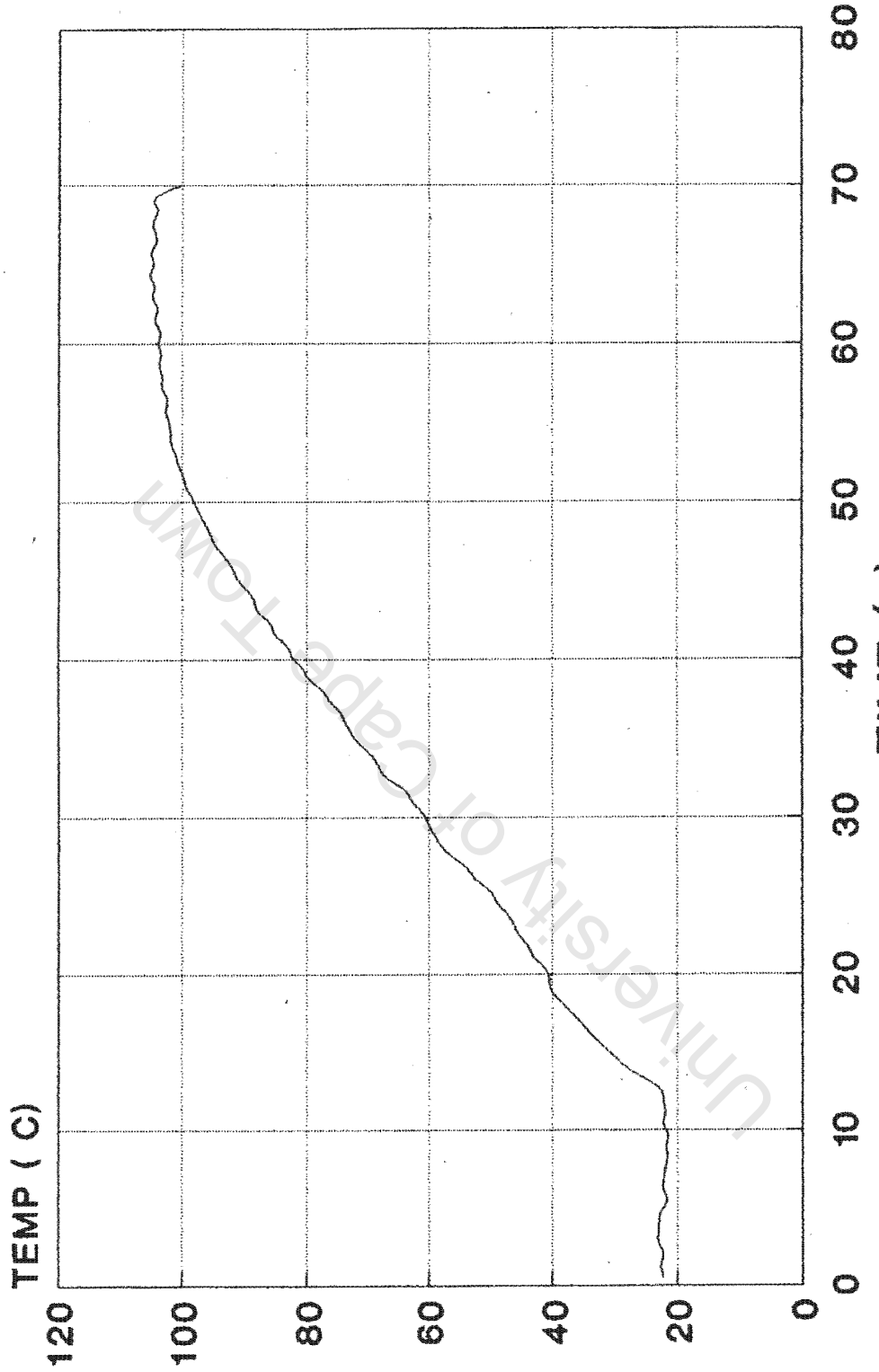

Figure H.1: Water heating test no. 1.

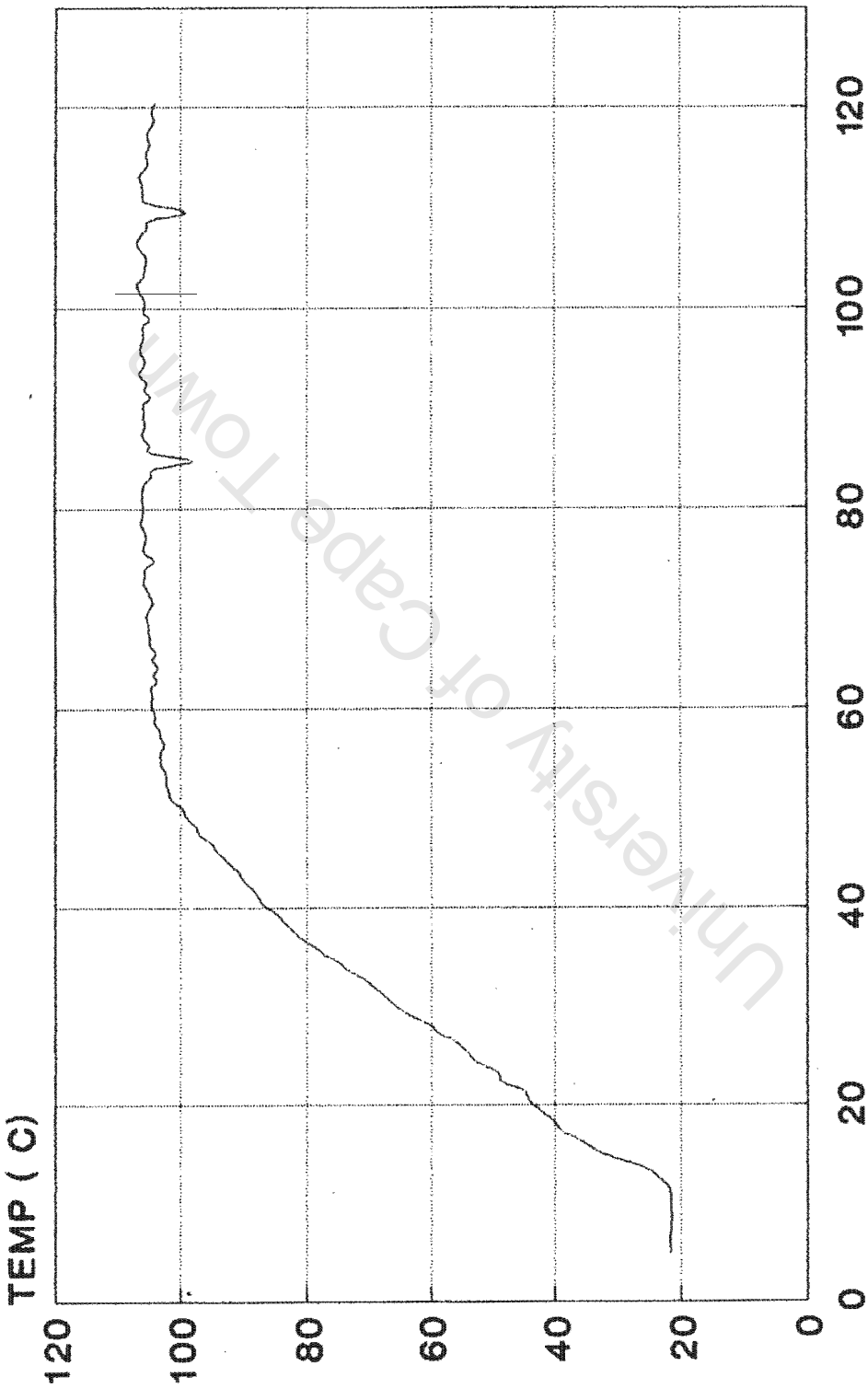

Figure H.2: Water heating test no. 2.

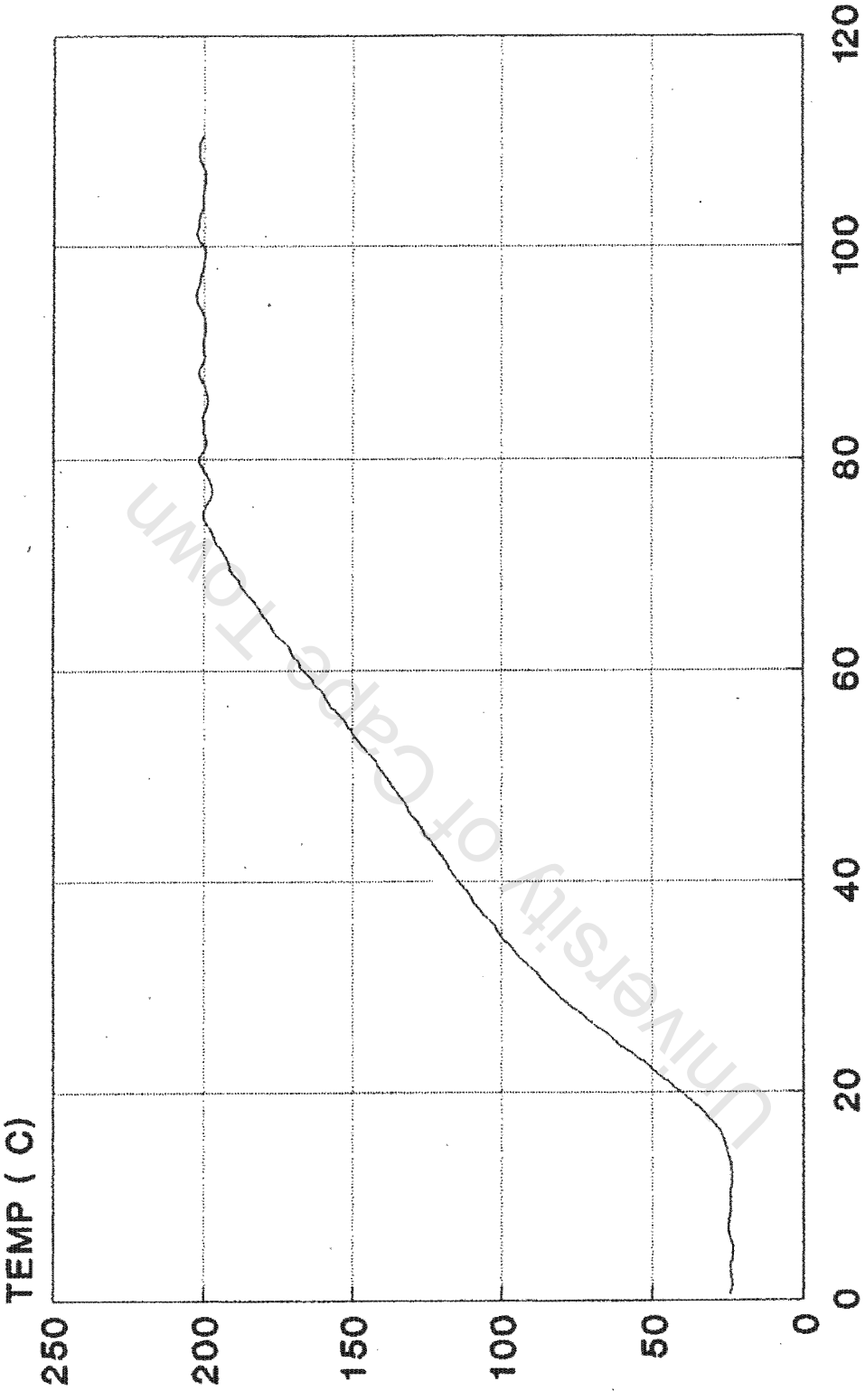

Figure H.3: Ethylene glycol heating test no. 1.

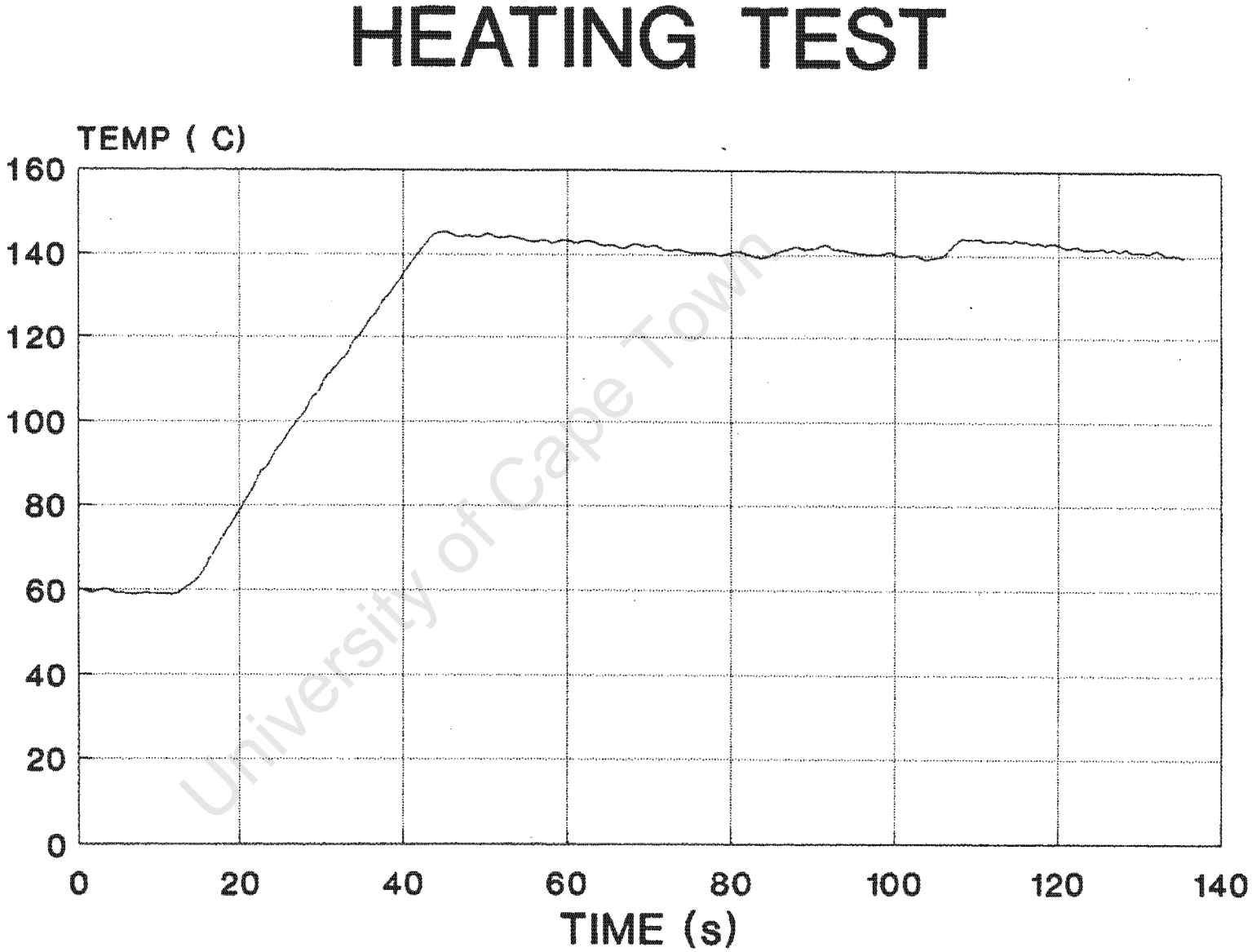

Figure H.4: Ethylene glycol heating test no. 2.

APPENDIX I

Return loss plots for 7 ml sample test loads

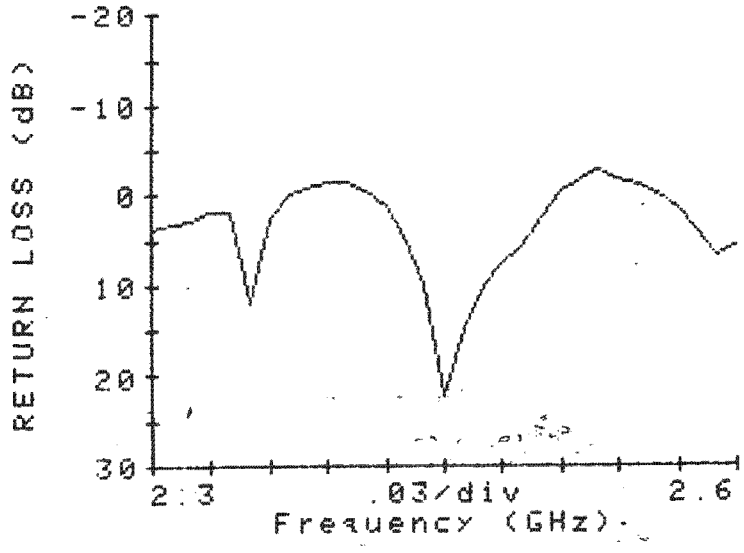

Figure I.1a: 8x7 ml

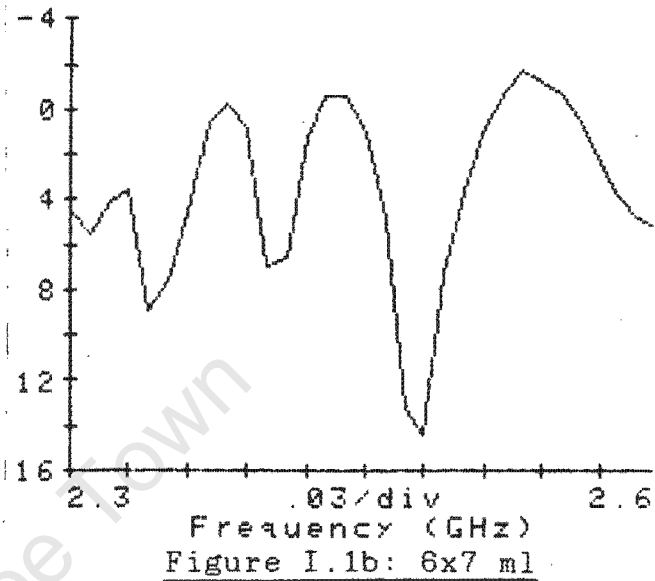

Figure I.1b: 6x7 ml

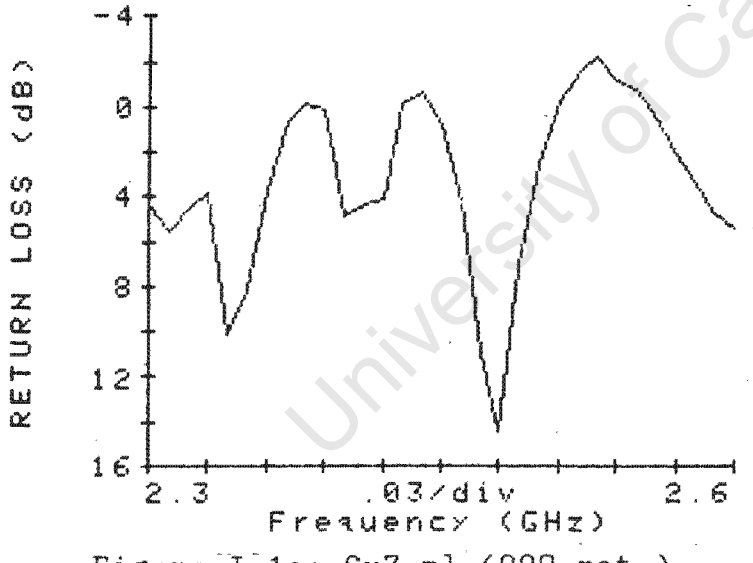

Figure I.1c: 6x7 ml (90° rot.)

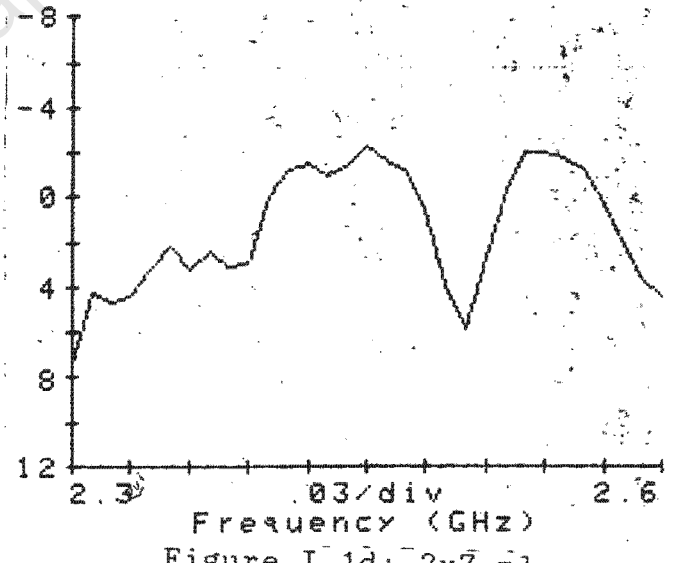

Figure I.1d: 2x7 ml

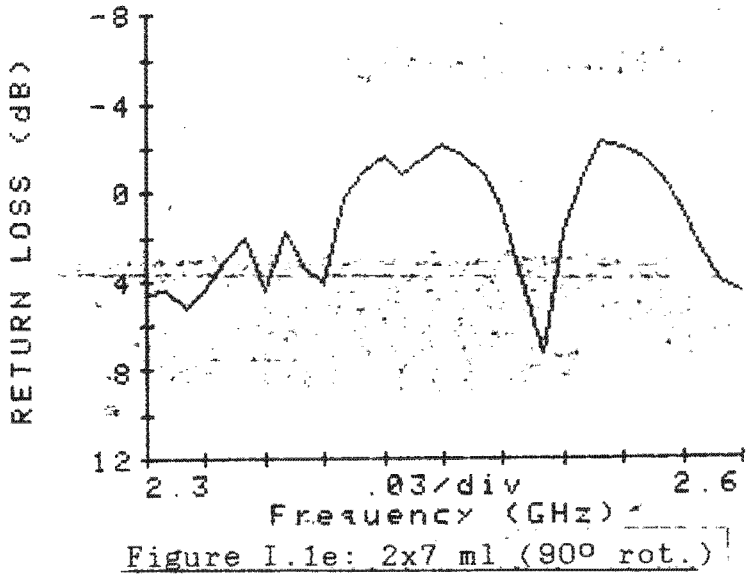

Figure I.1e: 2x7 ml (90° rot.)

Return loss plots for 5 ml saple loads

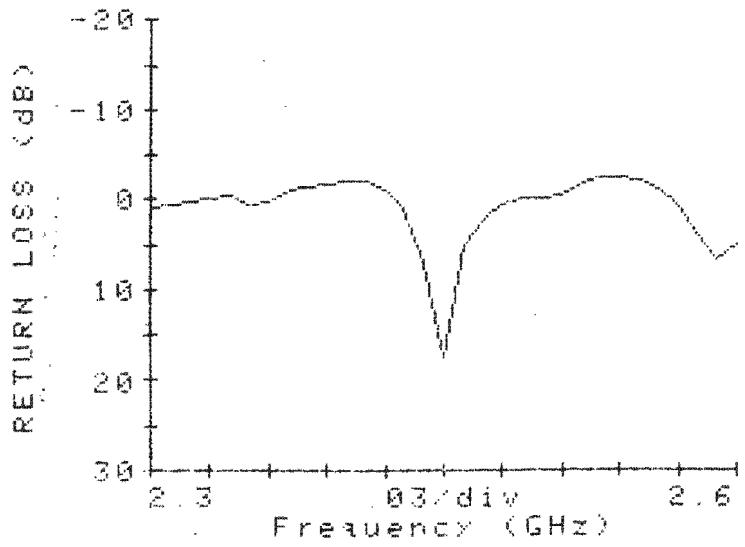

Figure I.2a: 8x5 ml

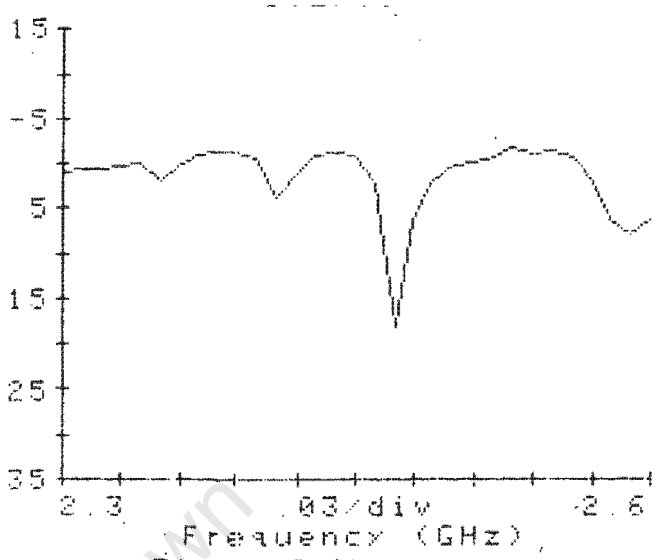

Figure I.2b: 6x5 ml

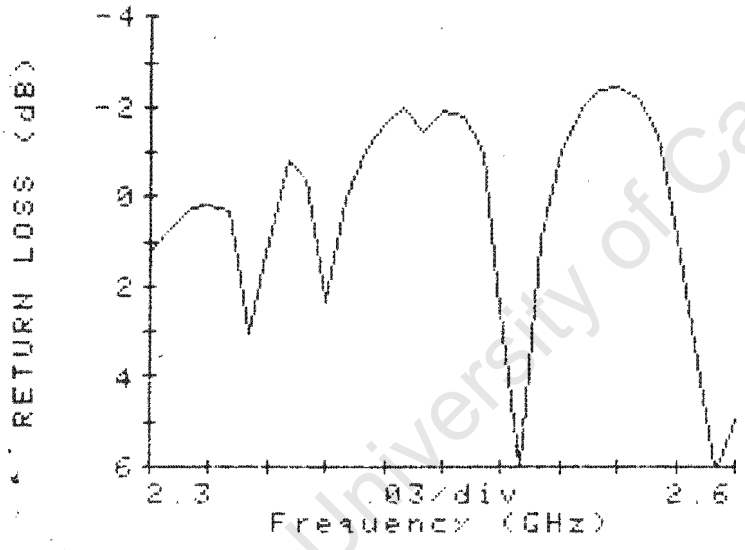

Figure I.2c: 4x5 ml

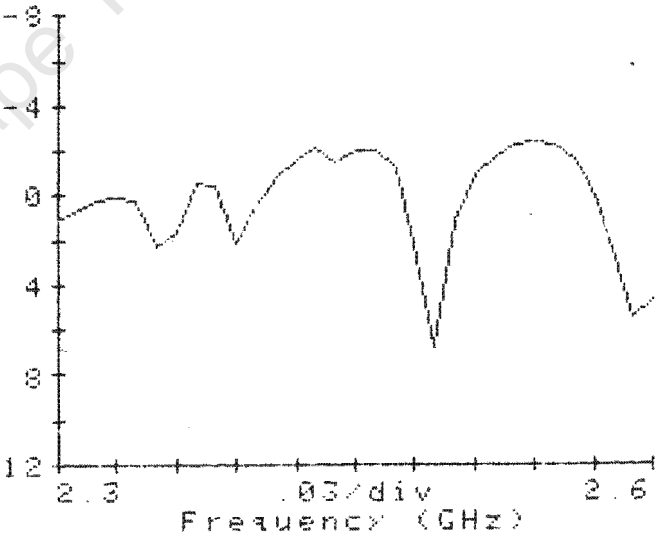

Figure I.2d: 4x5 ml (45° rot.)

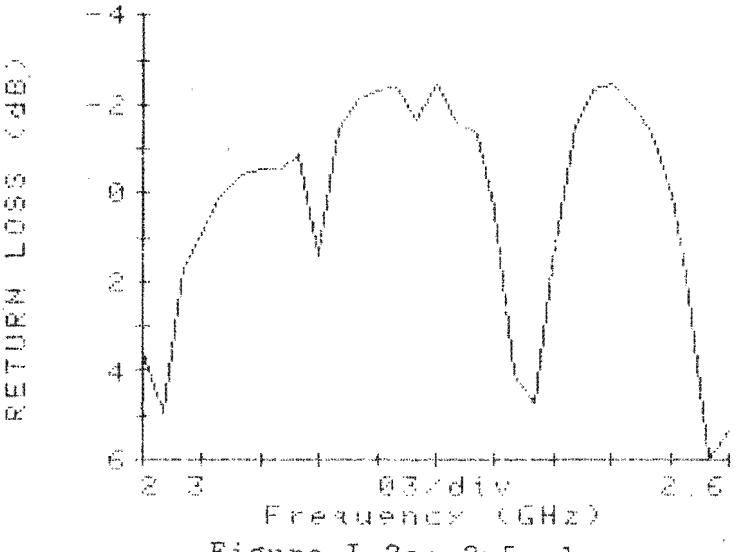

Figure I.2e: 2x5 ml

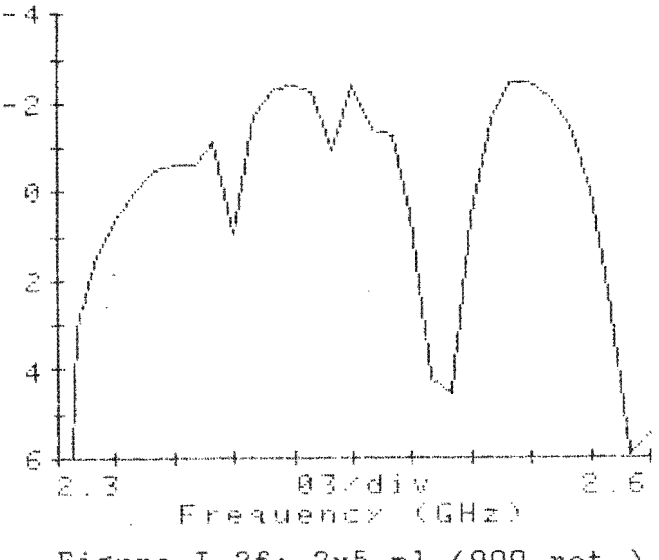

Figure I.2f: 2x5 ml (90° rot.)

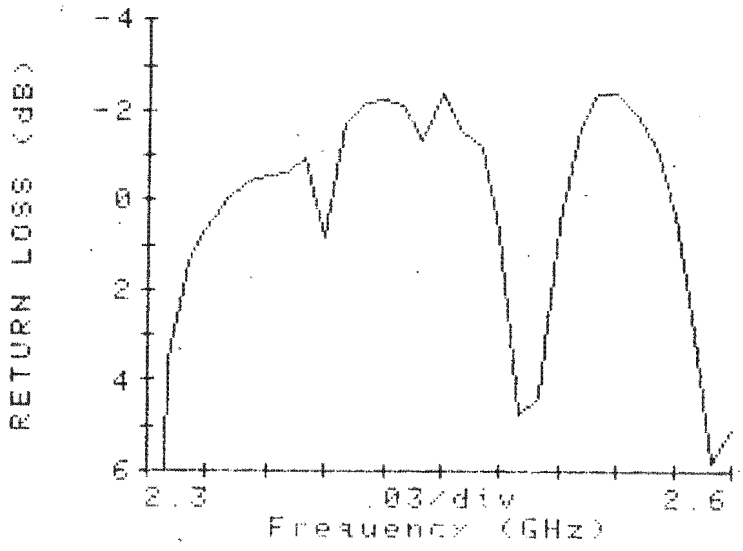

Figure I.2g: 2x5 ml (+45° rot.)

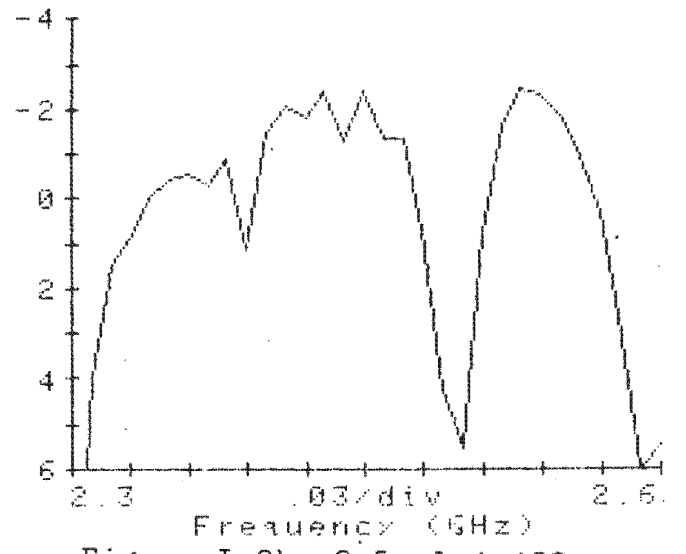

Figure I.2h: 2x5 ml (-45° rot.)

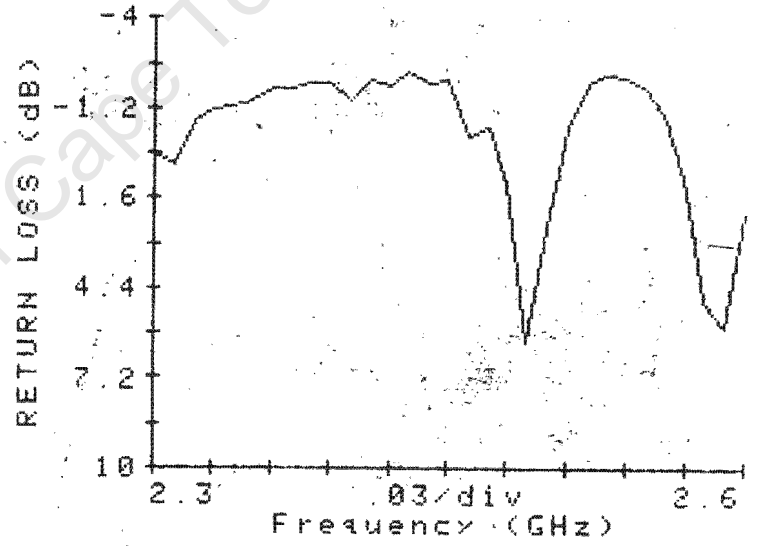

Figure I.3g: 2x3 ml (90° rot.)

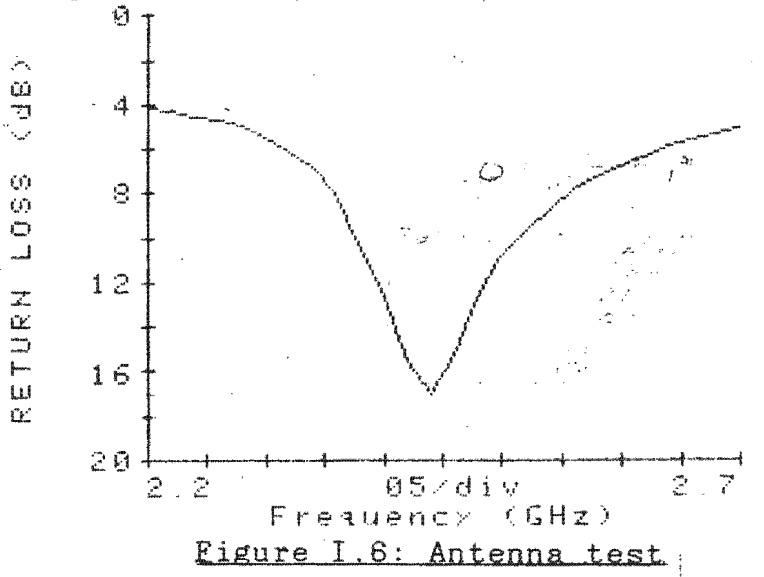

Figure I.6: Antenna test

Return loss plots for 3 ml sample test loads

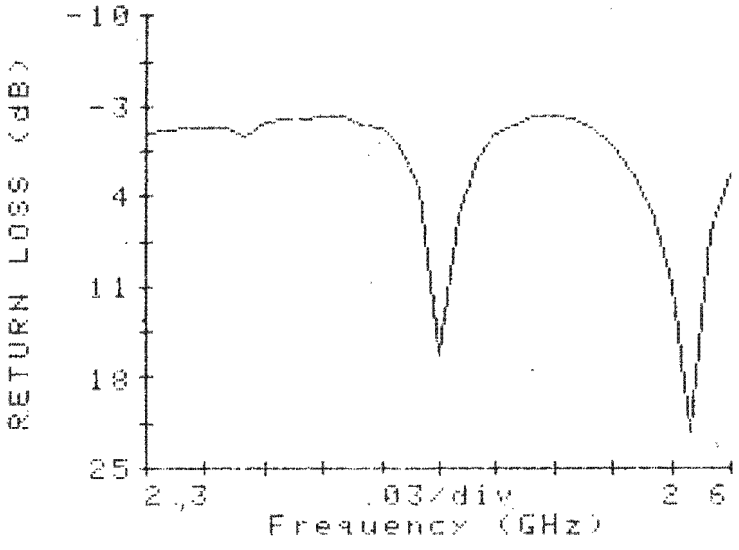

Figure I.3a: 8x3 ml

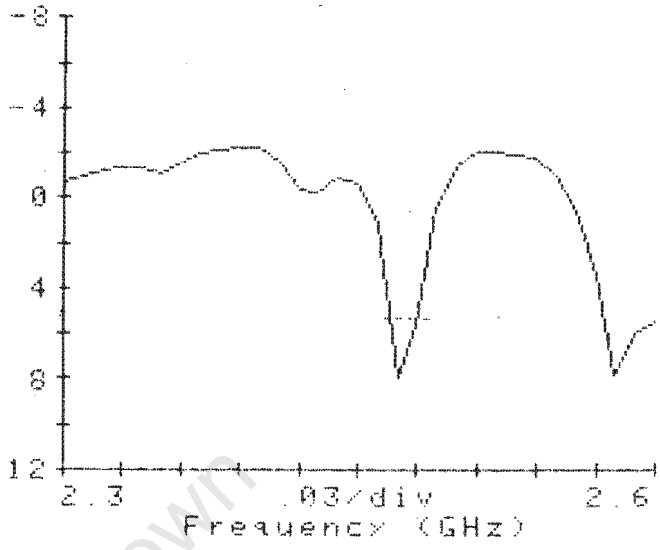

Figure I.3b: 6x3 ml

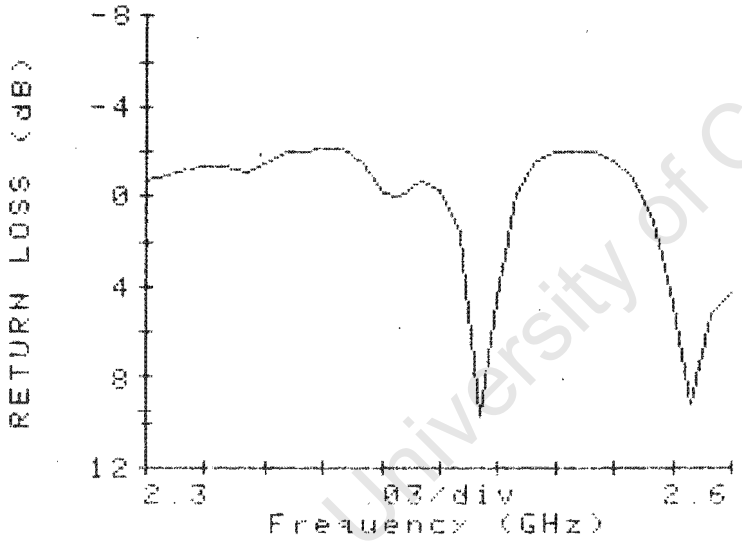

Figure I.3c: 6x3 ml (90° rot.)

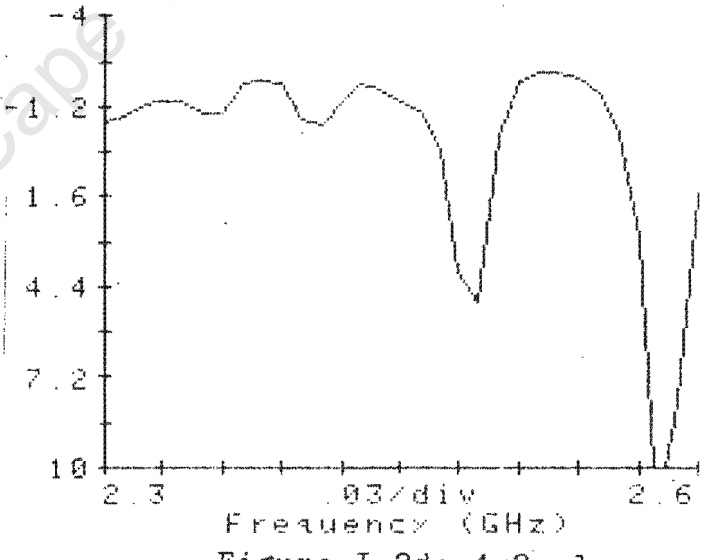

Figure I.3d: 4x3 ml

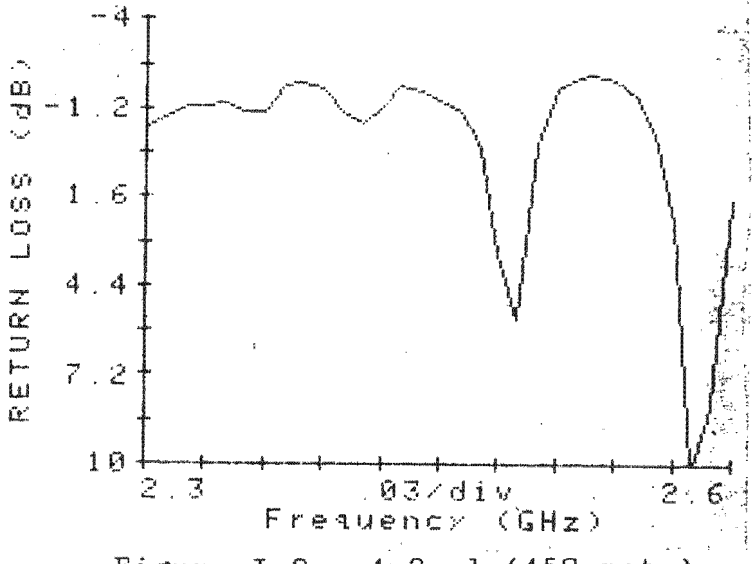

Figure I.3e: 4x3 ml (45° rot.)

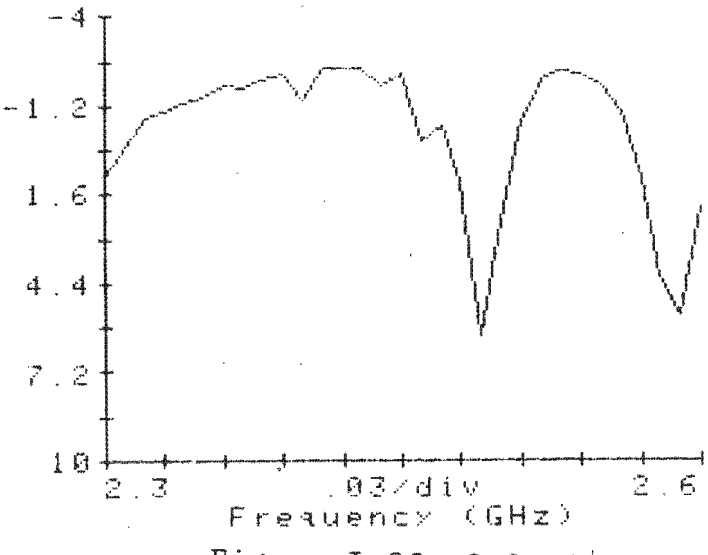

Figure I.3f: 2x3 ml

Return loss plots for the reduced height cavity

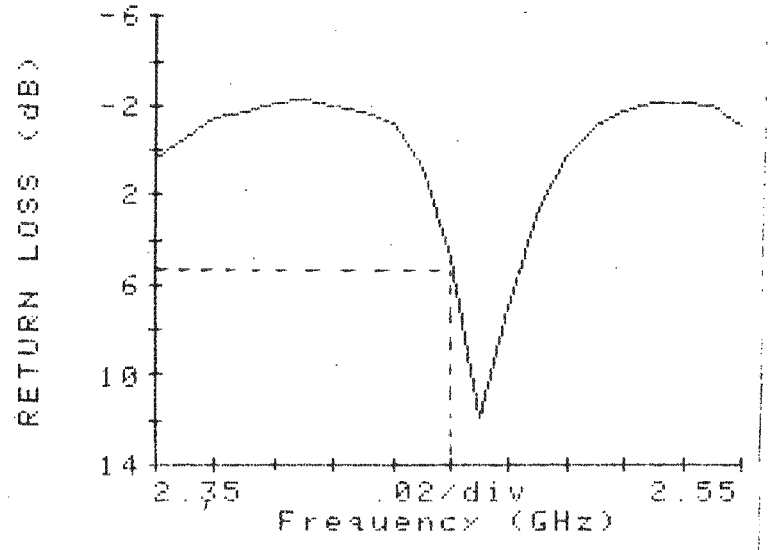

Figure I.4a: 6x3 ml

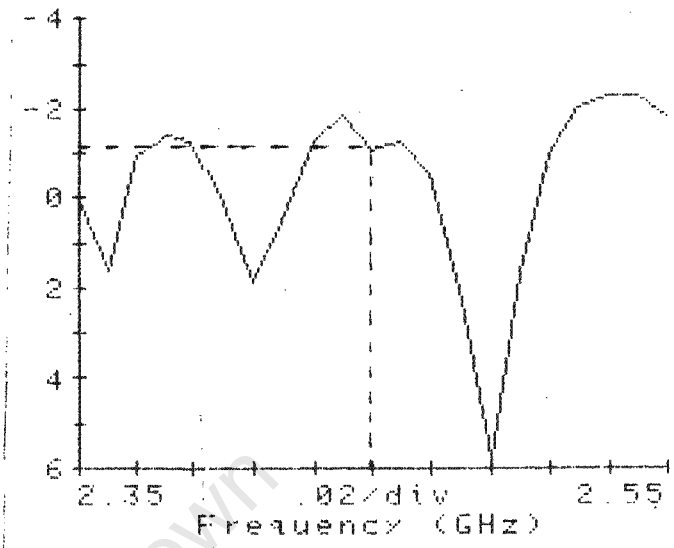

Figure I.4b: 4x3 ml

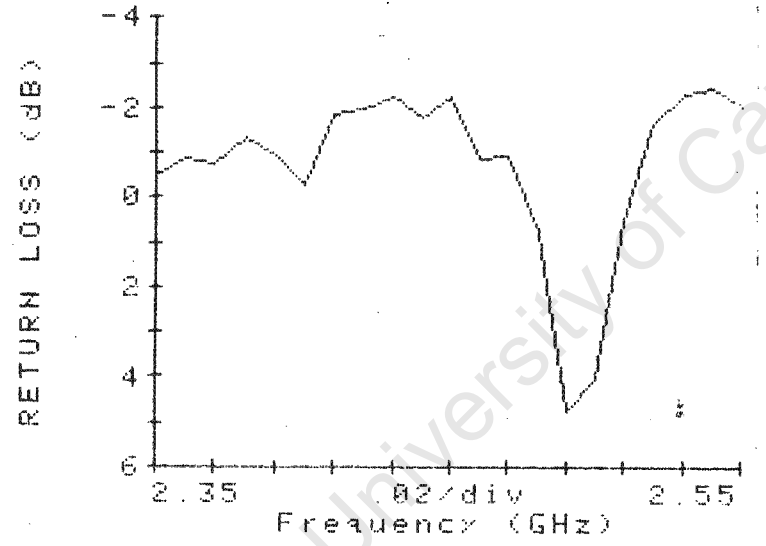

Figure I.4c: 2x3 ml

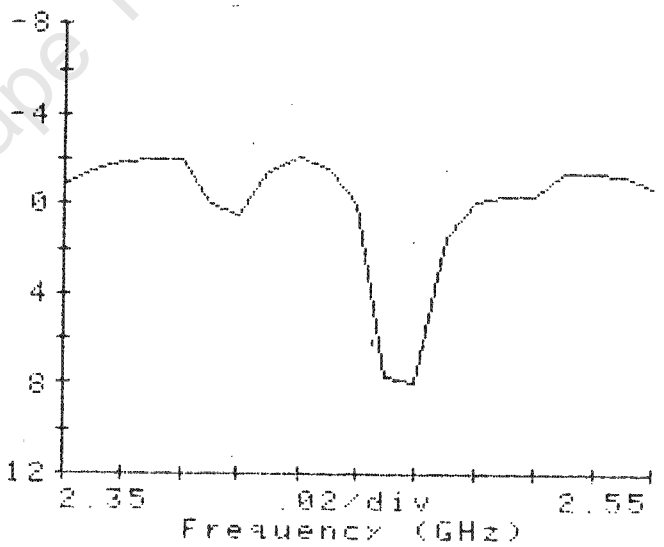

Figure I.5a: 6x5 ml

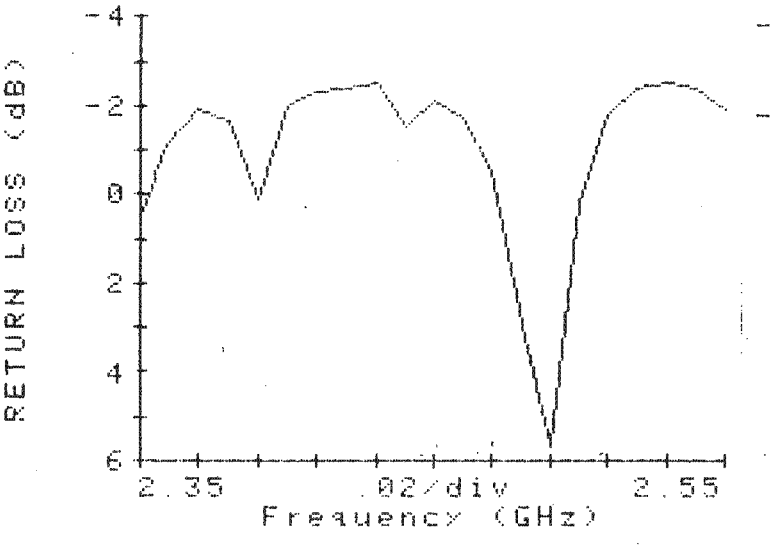

Figure I.5b: 4x5 ml

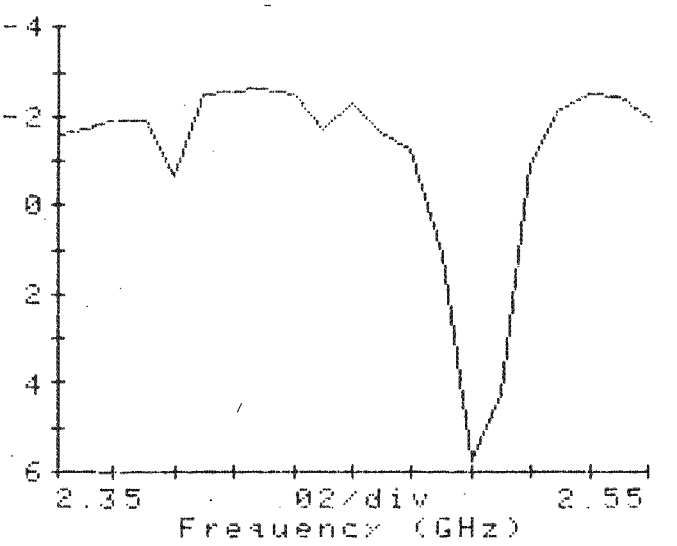

Figure I.5c: 2x5 ml

APPENDIX J

Return loss plots for the resonant horn cavity

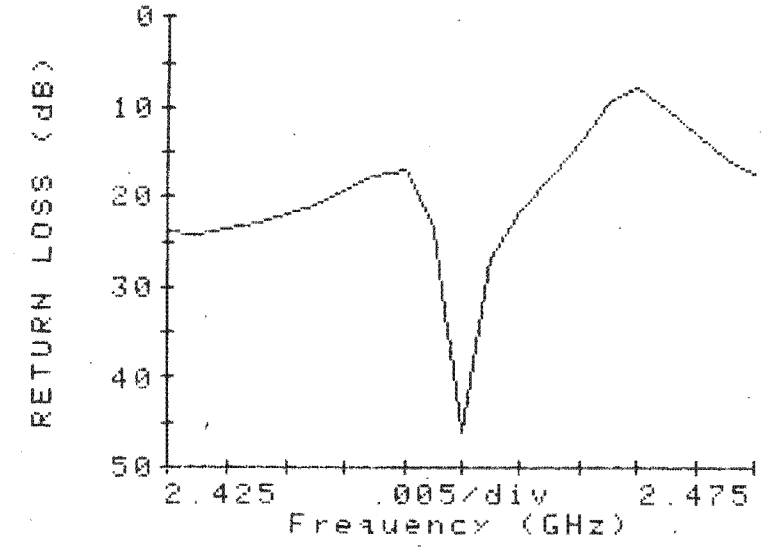

Figure J.1: no load

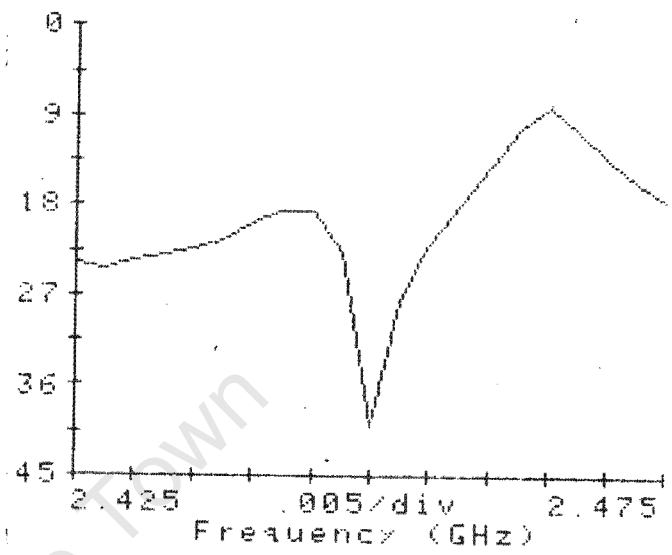

Figure J.2: 2x3 ml

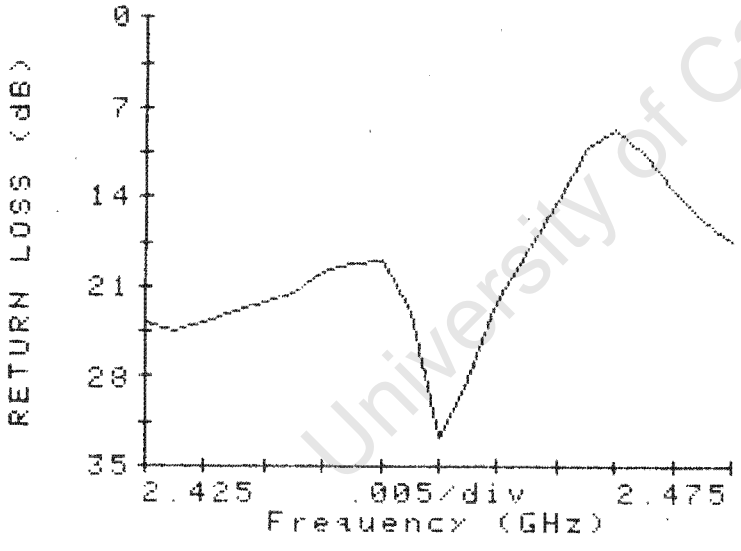

Figure J.3: 4x3 ml

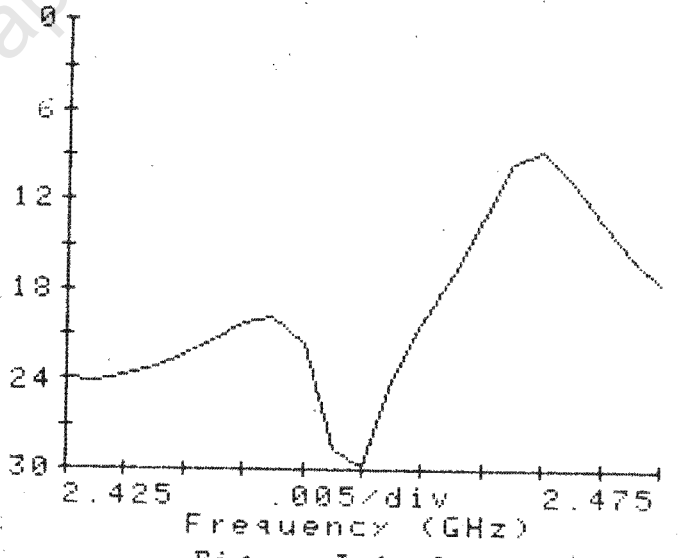

Figure J.4: 6x3 ml

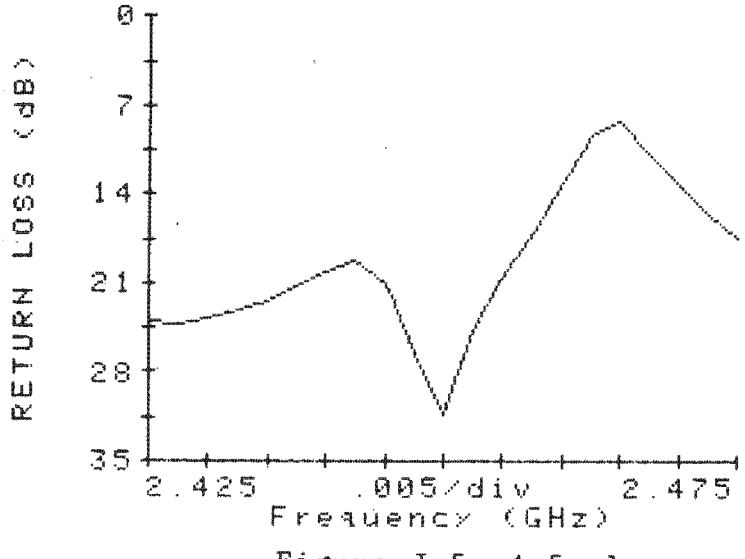

Figure J.5: 4x5 ml

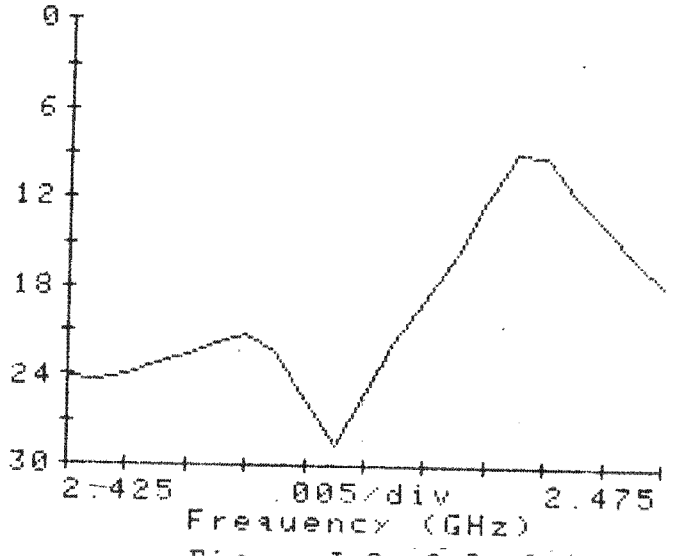

Figure J.6: 6x5 ml

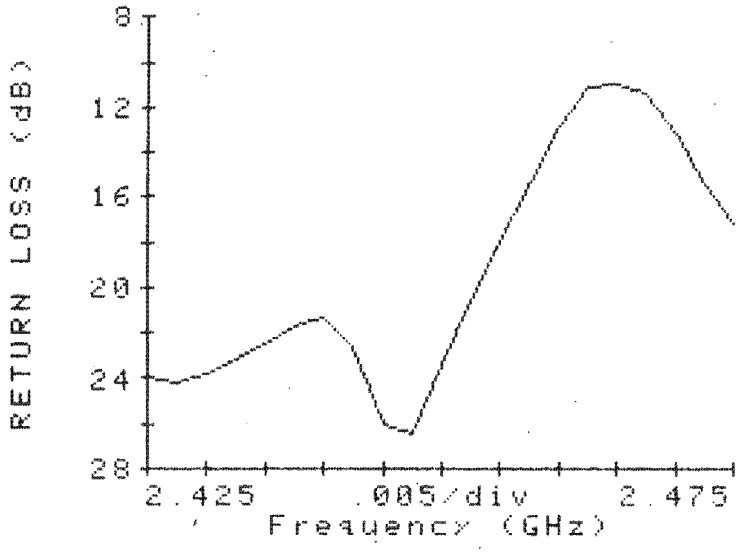

Figure J.7: 4x10 ml

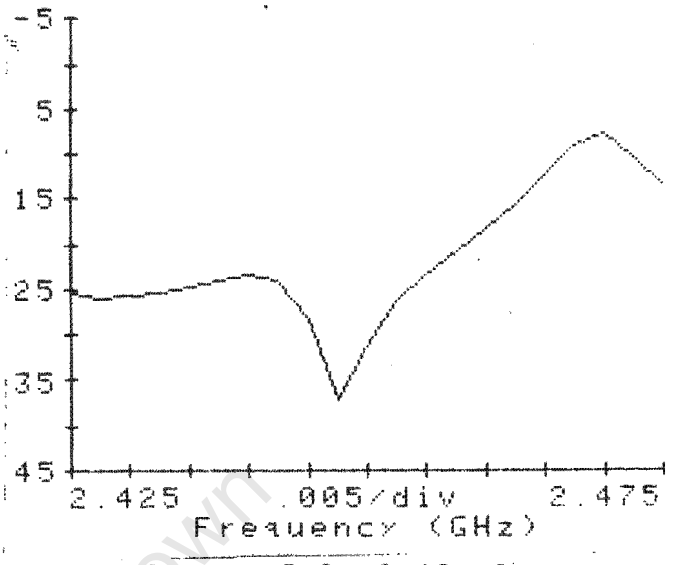

Figure J.8: 6x10 ml